



FACULTY OF INFORMATION TECHNOLOGY AND ELECTRICAL ENGINEERING  
DEGREE PROGRAMME IN ELECTRONICS AND COMMUNICATIONS ENGINEERING

## **MASTER'S THESIS**

# **PILOT SEQUENCE BASED IQ IMBALANCE ESTIMATION AND COMPENSATION**

Author	Enrique Theisen Rodrigues Pinto
Supervisor	Markku Juntti
Second examiner	Visa Tapio
Technical supervisor	Visa Tapio

April 2023

**Pinto E. T. R. (2023) Pilot Sequence Based IQ Imbalance Estimation and Compensation**  
Faculty of Information Technology and Electrical Engineering, Degree Programme in Electronics and Communications Engineering, 82 pages.

## **ABSTRACT**

As modern radio access technologies strive to achieve progressively higher data rates and to become increasingly more reliable, minimizing the effects of hardware imperfections becomes a priority. One of those imperfections is in-phase quadrature imbalance (IQI), caused by amplitude and phase response differences between the I and Q branches of the IQ demodulation process. IQI has been shown to deteriorate bit error rates, possibly compromise positioning performance, amongst other effects. Minimizing IQI by tightening hardware manufacturing constraints is not always a commercially viable approach, thus, baseband processing for IQI compensation provides an alternative.

The thesis begins by presenting a study in IQI modeling for direct conversion receivers, we then derive a model for general imbalances and show that it reproduces the two most common models in the bibliography. We proceed by exploring some of the existing IQI compensation techniques and discussing their underlying assumptions, advantages, and possible relevant issues.

A novel pilot-sequence based approach for tackling IQI estimation and compensation is introduced in this thesis. The idea is to minimize the square Frobenius norm of the error between candidate covariance matrices, which are functions of the candidate IQI parameters, and the sample covariance matrices, obtained from measurements. This new method is first presented in a positioning context with flat fading channels, where IQI compensation is used to improve the positioning estimates mean square error. The technique is then adapted to orthogonal frequency division multiplexing (OFDM) systems, including an version that exploits the 5G New Radio reference signals to estimate the IQI coefficients. We further generalize the new approach to solve joint transmitter and receiver IQI estimation and discuss the implementation details and suggested optimization techniques.

The introduced methods are evaluated numerically in their corresponding chapters under a set of different conditions, such as varying signal-to-noise ratio, pilot sequence length, channel model, number of subcarriers, etc. Finally, the proposed compensation approach is compared to other well-established methods by evaluating the bit error rate curves of 5G transmissions. We consistently show that the proposed method is capable of outperforming these other methods if the SNR and pilot sequence length values are sufficiently high. In the positioning simulations, the proposed IQI compensation method was able to improve the root mean squared error (RMSE) of the position estimates by approximately 25 cm. In the OFDM scenario, with high SNR and a long pilot sequence, the new method produced estimates with mean squared error (MSE) about a million times smaller than those from a blind estimator. In bit error rate (BER) simulations, the new method was the only compensation technique capable of producing BER curves similar to the curves without IQI in all of the studied scenarios.

**Keywords:** IQ Imbalance, Pilot Sequence, Positioning, OFDM.

# CONTENTS

ABSTRACT	
CONTENTS	
PREFACE	
LIST OF SYMBOLS AND ABBREVIATIONS	
<b>1 INTRODUCTION</b>	7
<b>2 IQ IMBALANCE MODELING</b>	10
2.1 Ideal IQ modulation and demodulation	10
2.2 Imbalanced IQ modulation and demodulation	11
2.3 Dependence on frequency	15
<b>3 REVIEW OF IQI COMPENSATION METHODS</b>	17
3.1 Blind estimators	17
3.2 MMSE and WL-MMSE equalizers	18
3.3 Other estimators	19
3.4 Joint transmitter and receiver IQI compensation	21
<b>4 IQI AND POSITIONING</b>	23
4.1 Introduction to positioning	23
4.2 System model	23
4.3 Equivalent channel estimation	25
4.4 IQI parameter and signal estimation	27
4.5 Analysis of the objective function	29
4.6 Numerical results	31
<b>5 5G NEW RADIO COMPLIANT IQI COMPENSATION</b>	37
5.1 Estimating over pilot slots	37
5.2 Analysis of the objective function	40
5.3 Low SNR or signal-less IQI estimation	41
5.4 Using the demodulation and phase tracking reference signals to estimate IQI	42
5.5 Analysis on subcarrier spacing and channel coherence time	44
5.6 Numerical Results	45
<b>6 JOINT TRANSMITTER AND RECEIVER IQI ESTIMATION</b>	53
6.1 System model	53
6.2 IQI estimation	55
6.3 Discussion on optimization issues	55
6.4 Optimizing the objective function	56
6.5 IQI compensation	57
6.6 Numerical results	58
<b>7 COMPARING COMPENSATION METHODS</b>	64
7.1 WL frequency domain equalization	64
7.2 Simulation setup	65
7.3 Results	66
<b>8 CONCLUSION</b>	70
<b>9 BIBLIOGRAPHY</b>	72
<b>10 APPENDICES</b>	76

## **PREFACE**

This work is the culmination of the research started in 2021 when I received a University of Oulu Encouragement Scholarship upon applying for the Master's Degree program at the Centre for Wireless Communications. The theory and numerical results that we present in this thesis are a consequence of two years of diligent exploration and frequent discussions between me and my supervisors: Markku Juntti and Visa Tapio. This research was also made possible by the Summer Internship Scholarship and MSc Thesis Grant offered by the University of Oulu, which played a vital role in providing the financial means for the development of this work.

Oulu, April 27, 2023

Enrique Theisen Rodrigues Pinto

## LIST OF SYMBOLS AND ABBREVIATIONS

5G	Fifth Generation
5G NR	Fifth Generation New Radio
6G	Sixth Generation
ADC	Analog-to-Digital Converter
AEVD	Augmented Eigenvalue Decomposition
ALS	Alternating Least Squares
AoA	Angle of Arrival
AWGN	Additive White Gaussian Noise
BER	Bit Error Rate
BPSK	Binary Phase Shift Keying
BS	Base Station
CDL	Cluster Delay Line
CP-OFDM	Cyclic Prefix Orthogonal Frequency Division Multiplexing
CRC	Cyclic Redundancy Check
CSI	Channel State Information
CVE	Channel Variation Energy
DAC	Digital-to-Analog Converter
DC	Direct Current
DFT	Discrete Fourier Transform
DLS-RNP	Direct Least Squares - Reduced Number of Parameters
DM-RS	Demodulation Reference Signal
DoA	Direction of Arrival
DVB-T	Digital Video Broadcast - Terrestrial
E-CID	Enhanced Cell ID
ESPRIT	Estimation of Signal Parameters via Rotational Invariant Techniques
EVD	Eigenvalue Decomposition
FCC	Federal Communications Commission
FDE	Frequency Domain Equalization
FIR	Finite Impulse Response
GNSS	Global Navigation Satellite System
HARQ	Hybrid Automatic Repeat reQuest
HiperLAN/2	High Performance Radio Local Area Network 2
IBDFE	Iterative Block Decision Feedback Equalization
ICI	Inter-Carrier Interference
IF	Intermediate Frequency
IQI	IQ Imbalance
ISI	Inter-Symbol Interference
ITS	Intelligent Traffic System
LAN	Local Area Network
LDPC	Low Density Parity Check
LMS	Least Mean Squares
LNA	Low Noise Amplifier
LO	Local Oscillator
LOS	Line-of-Sight
LPF	Low Pass Filter
LS	Least Squares
LTE	Long Term Evolution

LTS	Long Training Sequence
MIMO	Multiple Input Multiple Output
ML	Maximum Likelihood
MMSE	Minimum Mean Square Error
mmWave	Millimeter Wave
M-QAM	M-ary Quadrature Amplitude Modulation
MSE	Mean Square Error
MUSIC	Multiple Signal Classification
NLN	Network Localization and Navigation
NLOS	Non-Line-of-Sight
NM	Nelder-Mead
NMSE	Normalized Mean Square Error
OFDM	Orthogonal Frequency Division Multiplexing
PAN	Personal Area Network
PDF	Probability Density Function
PDSCH	Physical Downlink Shared Channel
PRACH	Physical Random Access Channel
PS	Particle Swarm
PSS	Primary Synchronization Signal
PT-RS	Phase Tracking Reference Signal
PUSCH	Physical Uplink Shared Channel
QAM	Quadrature Amplitude Modulation
QPSK	Quadriphase Phase Shift Keying
RB	Resource Block
RedCap	Reduced Capability
RF	Radio Frequency
RIM-RS	Remote Interference Management Reference Signal
RMSE	Root Mean Square Error
RSS	Received Signal Strength
Rx	Receive(r)
SA	Simulated Annealing
SC-FDE	Single Carrier Frequency Domain Equalization
SER	Symbol Error Rate
SISO	Single Input Single Output
SNR	Signal to Noise Ratio
TDL	Tapped Delay Line
TDoA	Time Difference of Arrival
ToA	Time of Arrival
ToF	Time of Flight
TR	Technical Report
TS	Technical Specification
Tx	Transmit(er)
UE	User Equipment
UDN	Ultra Dense Network
WCDMA	Wideband Code Division Multiple Access
WL	Widely Linear
WSN	Wireless Sensor Networks
WSS	Wide Sense Stationary
ZF	Zero Forcing

# 1 INTRODUCTION

With the higher need for intense miniaturization of antennas and subsequent radio frequency (RF) chain elements, homodyne receivers (also called zero intermediate frequency (IF) or direct conversion receivers) are becoming an increasingly more attractive option in radio transceiver design. Their appeal comes from the smaller physical size and possibly cheaper costs achieved by eliminating the expensive IF stage, requiring no image-rejection filters and only a single set of mixers. These benefits, naturally, come at the cost of having to generate a local oscillator (LO) signal at carrier frequency. This causes a range of implementation related issues [1] such as direct current (DC) offset, i.e., an oscillator signal with non-zero mean, and in-phase quadrature imbalance (IQI), i.e., the in-phase and quadrature branches of the in-phase quadrature (IQ) demodulator experiencing different amplitude and imperfect quadrature. Compared to lower frequency systems, millimeter wave (mmWave) and sub-terahertz systems are much more vulnerable to hardware imperfections. Some problems include higher susceptibility to phase noise and IQI, increasingly more complex compensation of power amplifier distortion, and high data processing pressure [2]. These complications make mitigating the effects of hardware non-idealities a necessity in order to achieve the best possible performance out of the available resources.

The impacts of IQI are more noticeable in mmWave systems due to higher operating frequency and larger bandwidth [2], and it has been shown that IQI can noticeably deteriorate position and orientation error bounds [3]. Besides, IQI can severely limit the throughput of radio links by making the use of higher order constellations not viable and generally increasing the symbol error rate (SER). Severe IQI can create performance floors for the SER curves [4], effectively placing a limit on the best achievable error rate unless the imbalance is properly compensated. Increasing the manufacturing precision of the components to minimize hardware related performance limiting issues is only feasible up to a certain point, beyond which the production costs become too prohibitive to ensure commercial viability. An interesting solution is the compensation of these impairments through signal processing techniques, implemented either in application specific hardware or in software. This is the principal topic of this thesis.

The effects of IQI vary depending on the system architecture. For example, in heterodyne receivers, IQI causes an *image problem* in which the frequency image interference partially mixes onto the desired signal during IF downconversion [5]. In homodyne receivers, IQI distorts the IQ branches of the wanted signal directly. This is caused by amplitude and phase impairments of the LO paths as well as mismatch between the I and Q branches after analog downconversion [6]. These mismatches occur due to a variety of practical reasons, such as temperature dependencies, material differences, design issues, hardware component tolerances, etc. In Chapter 2, we present a derivation of some of the possible mathematical models for IQI. There we show that two of the more popular models, the ideal I branch model and the symmetric imbalance model, are mathematically equivalent up to a complex scalar constant at the input. A brief discussion of frequency dependent IQI is presented in its final section.

Many methods have been proposed to tackle the IQI problem. Most of them rely on at least one of the following techniques: relaxing some constraints on the definition on the IQI coefficients to solve a system of equations, assuming IQI is small or approximately non-existent, applying the least mean squares (LMS) [7] algorithm for linear or widely linear minimum mean square error (WL-MMSE) estimation of the received signal, using a minimum mean square error (MMSE) estimator directly, or applying a blind estimator for the coefficients by assuming an underlying distribution for the received signal. It is also very common that some methods assume that some information which would be very hard to achieve in a practical situation is known, such as knowing the true channel covariance and complementary covariance matrices,

having perfect channel knowledge, or knowing some quantity which is hard to estimate directly from the data with usual methods.

Some approaches are only concerned with compensating for the IQI and not necessarily estimating its coefficients. These are certainly valid and effective at what they were designed to achieve, but lack the advantage of being able to distinguish the distortion caused by IQI from channel effects. Isolating the effects of IQI is important, for example, in a positioning context where the angle of arrival measurements rely on knowing the received waveform precisely instead of only estimating the received symbols. To contextualize the remainder of the thesis, Chapter 3 displays a survey of some of the IQI estimation or compensation procedures available in the literature. They are classified as either blind estimators, MMSE equalizers, or as another kind of estimator. The original expressions from the references are presented in order to give the reader an idea of the overall concept of the procedures, but no detailed explanation is given due to scope restrictions. Each different method is presented along with a short discussion on their possible advantages, disadvantages, and limitations.

Accurate position estimation and location awareness is becoming increasingly more important with the advent of fifth generation (5G) mmWave and the development of the future sixth generation (6G) standard. In 5G new radio (5G NR), the positioning performance requirements are defined for its massive commercial applications such as intelligent transportation, entertainment, industry automation, robotics, remote operation, healthcare, smart parking, etc. [8] [9]. Fueled by key enablers such as the use of mmWave bands which allow for wide bandwidths, dense antenna arrays, precise beamforming, as well as ultra dense networks (UDNs) with smart antenna equipped access nodes, positioning in 5G is not only used to aid in the data transfer process, but also as an use case in itself, such as intelligent traffic systems (ITSs) in the vehicle location-based communication context [10]. With this in mind, in Chapter 4, we introduce a novel, timing robust, pilot sequence based receiver IQI compensation procedure for positioning applications in a flat fading scenario. A detailed derivation of the method and its assumptions are presented, followed by an analysis section. The final section of the chapter presents numerical results, assessing the position estimate mean square error (MSE) as a function of the IQI parameter values, as well as the signal-to-noise ratio (SNR) and pilot sequence length. The method is compared to a blind estimator as a performance reference.

Chapter 5 extends the concepts of the IQI estimation method in the previous chapter to an orthogonal frequency division multiplexing (OFDM) receiver IQI scenario. A detailed analysis of the convergence properties of the method is conducted, and an in-depth discussion of the application details is presented. The derived technique is then readily extended to exploit the fifth generation new radio (5G NR) reference signals in a 5G compliant IQI compensation method. The chapter is concluded with a numerical results section evaluating the IQI estimation performance as a function of the SNR, number of training slots, and number of subcarriers. The new method is again compared to a blind estimator and 5G physical uplink shared channel (PUSCH) throughput simulations are included.

Chapter 6 further generalizes the proposed OFDM IQI estimation method to tackle the transmitter and receiver IQI case. This is a valuable result, because joint transmitter and receiver IQI compensation is a relatively little explored topic if compared to receiver IQI only. Besides, our method does not rely on knowing the signals at adjacent carriers at all, which is a requirement of some of the techniques in the bibliography. Furthermore, the data from many transmissions can be combined to further improve the quality of the estimates. After introducing the operating principle of the method, a short discussion regarding the implementation details is included, focusing on computational complexity and optimization issues. Like the other chapters, this chapter is concluded with a numerical results section, displaying and discussing the effects of the pilot sequence length, SNR, and number of subcarriers in the MSE of the IQI

parameter estimates.

To provide a reference for evaluating the performance of the proposed IQI compensation procedure, Chapter 7 compares our method to different IQI compensation techniques, verifying the effectiveness of the IQI compensation by analysing the bit error rate (BER) curves. The OFDM IQI compensation procedure from Chapter 5 is compared to a blind estimator and a widely linear least mean squares (WL-LMS) frequency domain equalizer (FDE) adaptive filter. The impacts of the training sequence length and SNR on the resulting BER curves are explored and conclusions are drawn from the presented figures.

This thesis aims to introduce a novel IQ imbalance compensation method with potential to outperform other existing techniques while still being relatively easy to apply. In doing so, we intend to provide a step towards a definitive solution for the aforementioned issue. We expect the high quality IQI estimation and compensation methods proposed in this thesis to further enable increased data rates and reliability for the 5G standard and other radio access technologies.

## 2 IQ IMBALANCE MODELING

IQI is the resulting effect of a wide range of hardware imperfections in wireless receivers and transmitters. Modeling these properties directly is not feasible or convenient in a signal processing perspective. Thus, a collection of simpler IQI models exist to model this effect at a higher level perspective. These models vary mainly in two aspects: how the mismatch is distributed between the I and Q branches, and whether any component dependence on signal frequency is taken into account. Let us first focus on IQI modeling for radio transmitters and direct conversion receivers by first giving an overview of the IQ modulation and demodulation process. After this overview, the imbalance modeling approaches will be introduced and discussed.

### 2.1 Ideal IQ modulation and demodulation

We will first analyse the ideal IQ case. Let  $x_I(t)$  and  $x_Q(t)$  be two real valued signals that we wish to transmit through IQ modulation. In the modulation scheme, these signals are assigned to the I and Q branches respectively and upconverted with the following operation

$$x_{\text{RF}}(t) = x_I(t)a_I(t) - x_Q(t)a_Q(t) \quad (2.1)$$

$$= x_I(t) \cos(\omega_0 t) - x_Q(t) \sin(\omega_0 t), \quad (2.2)$$

where  $a_I(t) = \cos(\omega_0 t)$  and  $a_Q(t) = \sin(\omega_0 t)$  are respectively the ideal I and Q branches of the transmitter LO, and  $\omega_0$  is the carrier frequency. The expression in (2.1) is obviously real valued, but  $x_{\text{RF}}$  can be expressed in complex form by defining  $x_L(t) = x_I(t) + jx_Q(t)$ , also called the baseband (or lowpass) equivalent signal [11]

$$x_{\text{RF}}(t) = \frac{1}{2} (x_L(t)e^{j\omega_0 t} + x_L^*(t)e^{-j\omega_0 t}) = \Re \{x_L(t)e^{j\omega_0 t}\}. \quad (2.3)$$

Then,  $x_{\text{RF}}(t)$  signal is amplified and transmitted. In a direct conversion wireless receiver, the received signal  $y_{\text{RF}}(t)$  is amplified with a low noise amplifier (LNA), which we will assume is ideally linear with unit gain (any amplifier gain could be absorbed by channel path-loss terms anyway, so this gain assumption comes with no loss of generality), then it is IQ demodulated directly from RF to baseband, and lowpass filtered to remove frequency components outside the desired signal range

$$y_I(t) = \text{LPF} \{y_{\text{RF}}(t)b_I(t)\} = \text{LPF} \{y_{\text{RF}}(t) \cos(\omega_0 t)\} = \Re \{y_L(t)\} \quad (2.4)$$

$$y_Q(t) = \text{LPF} \{y_{\text{RF}}(t)b_Q(t)\} = \text{LPF} \{-y_{\text{RF}}(t) \sin(\omega_0 t)\} = \Im \{y_L(t)\}, \quad (2.5)$$

where  $b_I(t) = \cos(\omega_0 t)$  and  $b_Q(t) = -\sin(\omega_0 t)$  are respectively the ideal I and Q branches of the receiver LO, LPF denotes ideal lowpass filtering, and  $y_L(t) = y_I(t) + jy_Q(t)$  is the baseband equivalent of the received signal such that  $y_{\text{RF}} = 2\Re \{y_L(t)e^{j\omega_0 t}\}$ . In the ideal down-conversion, no residual images centered at  $-\omega_0$  are present in the final signal. We will see that this does not happen if the I and Q branches have any amplitude or phase mismatch. To assist the reader in visualizing the modulation and demodulation structures in the common receiver and transmitter topologies, Figures 2.1 and 2.2 present block diagrams of imbalanced direct conversion and heterodyne receivers, respectively. Similarly, Figures 2.3 and 2.4 depict imbalanced direct conversion and heterodyne transmitters.

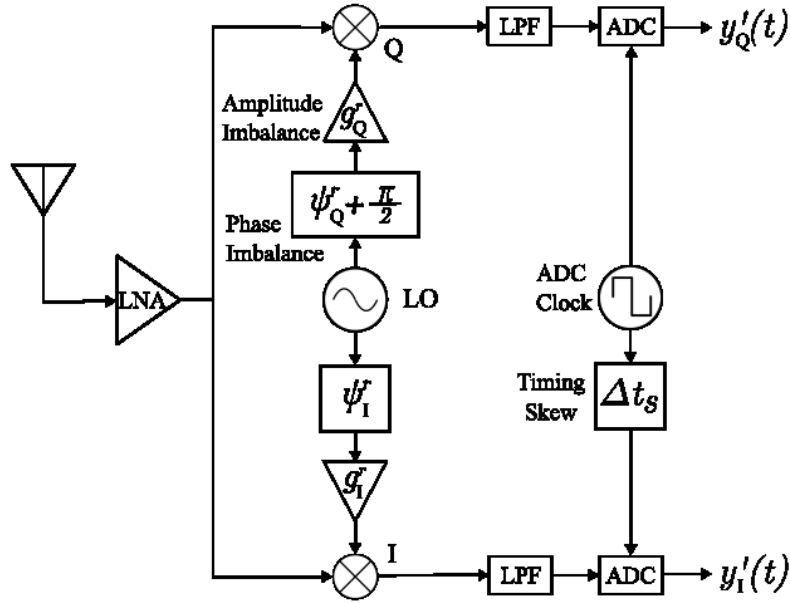


Figure 2.1. Block diagram representation of a direct conversion receiver affected by general IQI.

## 2.2 Imbalanced IQ modulation and demodulation

In this section, we will first analyse IQ imbalanced demodulation. We will show that any arbitrary linear imbalance may be expressed as a symmetric imbalance across the I and Q branches or as an ideal I branch with imbalanced Q branch. The complex equivalent signal of a receiver's LO under arbitrary imbalance may be written as [6]

$$s_{LO}^r(t) = g_I^r \cos(\omega_0 t + \phi_I^r) - j g_Q^r \sin(\omega_0 t + \phi_Q^r) \quad (2.6)$$

such that  $y_L(t) = 2\text{LPF}\{y_{\text{RF}}(t)s_{LO}^r(t)\}$ . The I and Q components of the received signal are now

$$\begin{bmatrix} y_I'(t) \\ y_Q'(t) \end{bmatrix} = \begin{bmatrix} g_I^r \cos(\phi_I^r) & g_I^r \sin(\phi_I^r) \\ -g_Q^r \sin(\phi_Q^r) & g_Q^r \cos(\phi_Q^r) \end{bmatrix} \begin{bmatrix} y_I \\ y_Q \end{bmatrix}. \quad (2.7)$$

A vector with the real and imaginary parts of a complex number is related to a vector of the complex number itself and its conjugate by the relations

$$\begin{bmatrix} x \\ x^* \end{bmatrix} = \begin{bmatrix} 1 & j \\ 1 & -j \end{bmatrix} \begin{bmatrix} \Re\{x\} \\ \Im\{x\} \end{bmatrix} \longleftrightarrow \frac{1}{2} \begin{bmatrix} \Re\{x\} \\ \Im\{x\} \end{bmatrix} = \begin{bmatrix} 1 & 1 \\ -j & j \end{bmatrix} \begin{bmatrix} x \\ x^* \end{bmatrix} \quad (2.8)$$

Thus, denoting by  $y_L'(t) = y_I'(t) + jy_Q'(t)$  the lowpass equivalent of the imbalanced received signal we get

$$\begin{bmatrix} y'(t) \\ y'^*(t) \end{bmatrix} = \begin{bmatrix} 1 & j \\ 1 & -j \end{bmatrix} \begin{bmatrix} y_I'(t) \\ y_Q'(t) \end{bmatrix} = \frac{1}{2} \begin{bmatrix} 1 & j \\ 1 & -j \end{bmatrix} \begin{bmatrix} g_I^r \cos(\phi_I^r) & g_I^r \sin(\phi_I^r) \\ -g_Q^r \sin(\phi_Q^r) & g_Q^r \cos(\phi_Q^r) \end{bmatrix} \begin{bmatrix} 1 & 1 \\ -j & j \end{bmatrix} \begin{bmatrix} y_L(t) \\ y_L^*(t) \end{bmatrix} \quad (2.9)$$

$$= \frac{1}{2} \begin{bmatrix} m_{11} & m_{12} \\ m_{21} & m_{22} \end{bmatrix} \begin{bmatrix} y_L(t) \\ y_L^*(t) \end{bmatrix}, \quad (2.10)$$

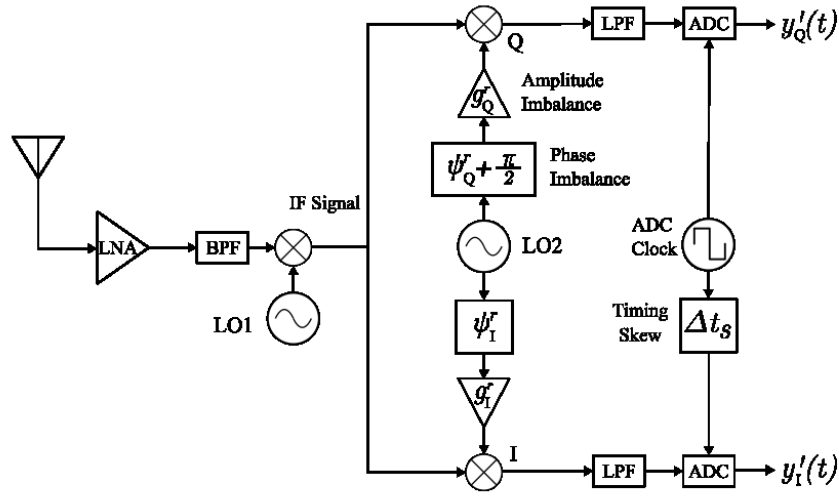


Figure 2.2. Block diagram representation of a heterodyne receiver affected by general IQI, where BPF denotes bandpass filtering.

where the elements of the imbalance matrix are

$$m_{11} = g_I^r(\cos(\phi_I^r) - j \sin(\phi_I^r)) + g_Q^r(\cos(\phi_Q^r) - j \sin(\phi_Q^r)) \quad (2.11)$$

$$m_{12} = g_I^r(\cos(\phi_I^r) + j \sin(\phi_I^r)) - g_Q^r(\cos(\phi_Q^r) + j \sin(\phi_Q^r)) \quad (2.12)$$

$$m_{21} = g_I^r(\cos(\phi_I^r) - j \sin(\phi_I^r)) - g_Q^r(\cos(\phi_Q^r) - j \sin(\phi_Q^r)) \quad (2.13)$$

$$m_{22} = g_I^r(\cos(\phi_I^r) + j \sin(\phi_I^r)) + g_Q^r(\cos(\phi_Q^r) + j \sin(\phi_Q^r)). \quad (2.14)$$

Taking only the  $y'(t)$  term and applying Euler's identity we get an expression for an arbitrary IQ imbalance

$$y'(t) = \begin{bmatrix} \frac{g_I^r e^{-j\phi_I^r} + g_Q^r e^{-j\phi_Q^r}}{2} & \frac{g_I^r e^{j\phi_I^r} - g_Q^r e^{j\phi_Q^r}}{2} \\ \frac{g_I^r e^{j\phi_I^r} - g_Q^r e^{j\phi_Q^r}}{2} & \frac{g_I^r e^{-j\phi_I^r} + g_Q^r e^{-j\phi_Q^r}}{2} \end{bmatrix} \begin{bmatrix} y_L(t) \\ y_L^*(t) \end{bmatrix} \quad (2.15)$$

To demonstrate the relation between two common IQI models, let us show that any arbitrary imbalance is mathematically equivalent to an ideal I branch with imbalanced Q branch or to a symmetric imbalance across the I and Q branches. Say that the received signal is subjected to a complex gain equal to  $\gamma_a = \frac{1}{g_I^r} e^{j\phi_I^r}$ , then

$$y'_a(t) = \frac{1 + \frac{g_Q^r}{g_I^r} e^{j(\phi_I^r - \phi_Q^r)}}{2} y_L(t) + \frac{1 - \frac{g_Q^r}{g_I^r} e^{-j(\phi_I^r - \phi_Q^r)}}{2} y_L^*(t) \quad (2.16)$$

which is equivalent to the case where  $g_I^r = 1$  and  $\phi_I^r = 0$ , with  $g_Q^r$  and  $\phi_Q^r$  being imbalanced. We can call  $m_r = \frac{g_Q^r}{g_I^r}$  and  $\psi_r = (\phi_Q^r - \phi_I^r)$  and we get the IQI coefficients for this model

$$\alpha_r = \frac{1 + m_r e^{-j\psi_r}}{2} \quad (2.17)$$

$$\beta_r = \frac{1 - m_r e^{j\psi_r}}{2} \quad (2.18)$$

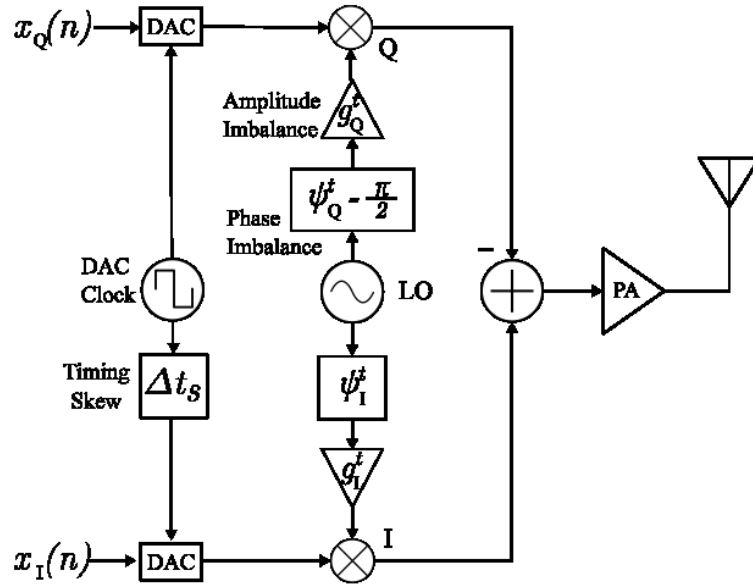


Figure 2.3. Block diagram representation of a direct conversion transmitter affected by general IQI. PA denotes the power amplifier.

such that  $y' = \alpha_r y + \beta_r y^*$ . These are the expressions for the coefficients that will be used throughout the rest of this work, they are also considered in [12] [3] [4]. Define  $m_r \triangleq 1 + \epsilon_r$ , then  $\epsilon_r$  and  $\psi_r$  are real numbers which will be respectively referred to as the receiver amplitude and receiver phase IQI parameters. Now consider the case where the complex gain is equal to  $\gamma_b = \frac{2}{g_I^r + g_Q^r} e^{j \frac{\phi_I^r + \phi_Q^r}{2}}$ , then

$$y'_b = \left( \frac{g_I^r}{g_I^r + g_Q^r} e^{j \frac{\phi_Q^r - \phi_I^r}{2}} + \frac{g_Q^r}{g_I^r + g_Q^r} e^{-j \frac{\phi_Q^r - \phi_I^r}{2}} \right) y_L + \left( \frac{g_I^r}{g_I^r + g_Q^r} e^{-j \frac{\phi_Q^r - \phi_I^r}{2}} - \frac{g_Q^r}{g_I^r + g_Q^r} e^{j \frac{\phi_Q^r - \phi_I^r}{2}} \right) y_L^*, \quad (2.19)$$

where the dependence on time has been suppressed, applying Euler's identity yields

$$y'_b = \left( \cos \left( \frac{\phi_Q^r - \phi_I^r}{2} \right) + j \frac{g_I^r - g_Q^r}{g_I^r + g_Q^r} \sin \left( \frac{\phi_Q^r - \phi_I^r}{2} \right) \right) y_L + \left( \frac{g_I^r - g_Q^r}{g_I^r + g_Q^r} \cos \left( \frac{\phi_Q^r - \phi_I^r}{2} \right) - j \sin \left( \frac{\phi_Q^r - \phi_I^r}{2} \right) \right) y_L^*. \quad (2.20)$$

If we call  $\epsilon_r = \frac{g_I^r - g_Q^r}{g_I^r + g_Q^r}$  and  $\psi_r = \frac{\phi_Q^r - \phi_I^r}{2}$  we get

$$\alpha_r = \cos(\psi_r) + j \epsilon_r \sin(\psi_r) \quad (2.21)$$

$$\beta_r = \epsilon_r \cos(\psi_r) - j \sin(\psi_r), \quad (2.22)$$

which is one of the more commonly used models, used in works such as [8] [13] [14] [15]. Any other imbalance distribution between the I and Q branches is mathematically equivalent

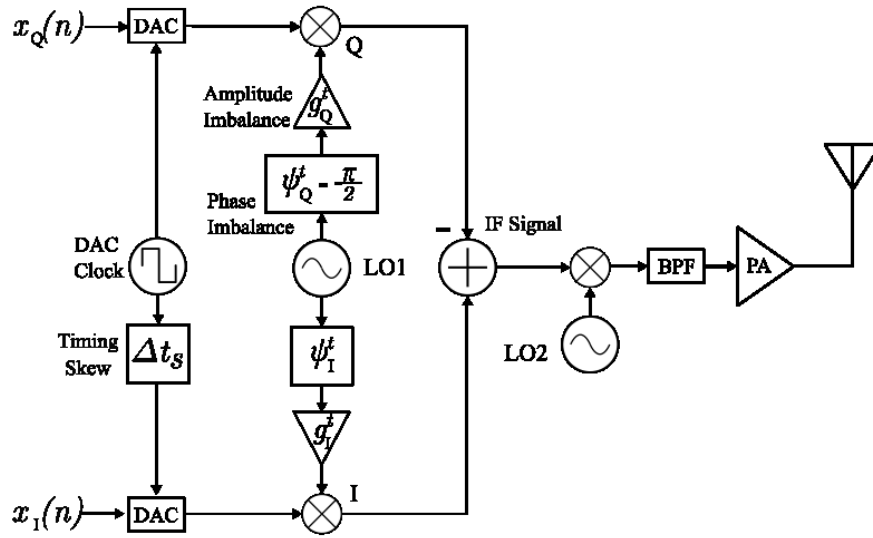


Figure 2.4. Block diagram representation of a heterodyne transmitter affected by general IQI.

to one of the two formulations that have just been presented. Choosing a particular expression for the coefficients is mostly up to convenience and personal preference. It is also important to restate that imbalance is a relative property, e.g., the signal from the Q branch can only be said to be imbalanced if its amplitude and phase differ from an expected reference signal. If we used the I branch as a reference, then it is ideal by definition, any imbalance in the Q branch will then be quantified with respect to the I branch, leading to the model in (2.17) and (2.18). On the other hand, if the reference amplitude and phase are set to the average of the I and Q branches, then both branches are imbalanced by definition, leading to the model in (2.21) and (2.22).

As previously stated, Figures 2.1 and 2.2 contain, respectively, a block diagram description of a direct conversion and a heterodyne receiver affected by general IQI in both I and Q branches. They also depict a timing skew in the analog-to-digital Converters (ADCs), which will be further explained in the next section. The figures consider that any amplitude and phase imbalances caused by the low-pass filters can be lumped in the LO path. Additionally, if the signal is sufficiently narrowband (as may be the case with individual OFDM subcarriers), then the timing offset can be treated as a frequency independent phase offset, which can also be lumped into the LO path.

Let us now consider imbalance in the modulation. Define the transmitter complex equivalent of the transmitter LO signal

$$s_{LO}^t(t) = g_I^t \cos(\omega_0 t + \phi_I^t) + j g_Q^t \sin(\omega_0 t + \phi_Q^t), \quad (2.23)$$

which satisfies the equality

$$\Re \{x_L(t) s_{LO}^t(t)\} = x_I(t) g_I^t \cos(\omega_0 t + \phi_I) - x_Q(t) g_Q^t \sin(\omega_0 t + \phi_Q). \quad (2.24)$$

We can express the above equality as

$$\begin{aligned} x_I(t)g_I^t \cos(\omega_0 t + \phi_I^t) - x_Q(t)g_Q^t \sin(\omega_0 t + \phi_Q^t) \\ = \left( x_I(t)g_I^t \cos(\phi_I^t) - x_Q(t)g_Q^t \sin(\phi_Q^t) \right) \cos(\omega_0 t) \\ - \left( x_Q(t)g_Q^t \cos(\phi_Q^t) + x_I(t)g_I^t \sin(\phi_I^t) \right) \sin(\omega_0 t) \end{aligned} \quad (2.25)$$

and rename the terms for the transmitted I and Q components in similar fashion as to what was done in the demodulation analysis

$$x'_I(t) = x_I(t)g_I^t \cos(\phi_I^t) - x_Q(t)g_Q^t \sin(\phi_Q^t) \quad (2.26)$$

$$x'_Q(t) = x_Q(t)g_Q^t \cos(\phi_Q^t) + x_I(t)g_I^t \sin(\phi_I^t). \quad (2.27)$$

Again, this can be expressed as a matrix equation

$$\begin{bmatrix} x'_I(t) \\ x'_Q(t) \end{bmatrix} = \begin{bmatrix} g_I^t \cos(\phi_I^t) & -g_Q^t \sin(\phi_Q^t) \\ g_I^t \sin(\phi_I^t) & g_Q^t \cos(\phi_Q^t) \end{bmatrix} \begin{bmatrix} x_I(t) \\ x_Q(t) \end{bmatrix} \quad (2.28)$$

Modifying this equation so that it is expressed in terms of  $x_L$  and  $x_L^*$  yields the following expression

$$x'_L(t) = \frac{g_I^t e^{-j\phi_I^t} + g_Q^t e^{j\phi_Q^t}}{2} x_L(t) + \frac{g_I^t e^{j\phi_I^t} - g_Q^t e^{j\phi_Q^t}}{2} x_L^*(t). \quad (2.29)$$

Setting  $g_I^t = 1$ ,  $g_Q^t = m_t$ ,  $\phi_I^t = 0$ , and  $\phi_Q^t = \psi_t$ , yields the coefficients

$$\alpha_t = \frac{1 + m_t e^{j\psi_t}}{2} \quad (2.30)$$

$$\beta_t = \frac{1 - m_t e^{j\psi_t}}{2} \quad (2.31)$$

that were used in [3] and will be used in this work.

Figures 2.3 and 2.4 contain, respectively, a block diagram description of a direct conversion and a heterodyne transmitter affected by general IQI in both I and Q branches. Like the previously presented receivers, they include a timing skew in the digital-to-analog Converters (DACs). Once again, if the signal is sufficiently narrowband, then the timing offset can be treated as a frequency independent phase offset, which can be lumped into the LO path.

### 2.3 Dependence on frequency

So far, only frequency independent IQI models have been considered. Nevertheless, IQ imbalance is best modeled as a frequency dependent effect due to a variety of reasons. In down-conversion, the I and Q branches are lowpass filtered after the mixing stage. These filters are naturally not perfectly matched to one another, causing imbalance that depends nonlinearly on frequency, specially on the band edge. Furthermore, any timing skew  $\Delta t_s$  between I and Q branch ADCs or DACs will generate a linear in frequency phase imbalance of  $\omega_0 \Delta t_s$ , which is comparable to a Doppler shift. Mixer related IQI is generally frequency independent [16]. In

OFDM systems, modeling frequency dependent IQI requires only assigning a different value of the IQI coefficients for each subcarrier. This is possible because, as we have shown in the previous section, IQ imbalance models are mathematically equivalent to each other and may be translated by absorbing a conversion coefficient into the complex channel gain. However, if one wants to precisely estimate the true channel and received signal before IQI this approach is not necessarily valid because the conversion coefficient would be different for each frequency, effectively distorting the channel estimate. On the other hand, for IQI compensation purposes only, modeling frequency dependent IQI as a set of coefficients associated to each subcarrier is perfectly valid. For the remainder of this work, we will mainly address frequency independent IQI compensation and estimation, while some remarks about adapting the proposed techniques to the frequency dependent case will be occasionally made.

### 3 REVIEW OF IQI COMPENSATION METHODS

We will now present a survey of IQI estimation and compensation approaches. It is important to state that the mentioned references use different IQI models, i.e., some of them consider IQI to be equally divided between the I and Q branches, while others consider the I branch to be preserved intact while all IQI is offloaded into the Q branch. As discussed in Chapter 2, both models are theoretically equivalent, we preserve the original expressions from the references nonetheless. Let us subdivide the existing methods by the fundamental technique used.

#### 3.1 Blind estimators

By assuming that the I and Q components are jointly Gaussian, independent, and that the input I and Q signals are both zero mean with the same variance, Aziz *et al.* [17] derive the probability density function (PDF) of the received signal at the I and Q branches with an additive white gaussian noise (AWGN) channel. These assumptions are grounded in the statement that OFDM signals typically exhibit Gaussian distributions [18]. The authors then show that the derived distribution closely approximates (by the Kullback-Leibler divergence and the Hellinger distance) practical distributions from the transmission of wideband code division multiple access (WCDMA) and long term evolution (LTE) signals. They also state, however, that derived and the true distributions have a significant difference at SNRs lower than approximately 12 dB. Nonetheless, the derived distribution is used for its simplicity in the estimation procedure. They state that the IQI coefficients can be estimated by solving the system of nonlinear equations

$$\frac{\beta_2}{2}(\mathbf{1}^T \mathbf{p}) - \gamma(\mathbf{p}_2 \mathbf{Q}_y) = 0 \quad (3.1)$$

$$\frac{\alpha_2}{2}(\mathbf{1}^T \mathbf{p}) - \gamma(\mathbf{p}_1 \mathbf{Q}_y) = 0 \quad (3.2)$$

$$\frac{\alpha_1}{2}(\mathbf{1}^T \mathbf{p}) - \gamma(\mathbf{p}_1 \mathbf{I}_y) = 0 \quad (3.3)$$

$$\frac{\beta_1}{2}(\mathbf{1}^T \mathbf{p}) - \gamma(\mathbf{p}_2 \mathbf{I}_y) = 0 \quad (3.4)$$

where  $\alpha_{1,2}, \beta_{1,2}, \mathbf{p}, \mathbf{p}_1, \mathbf{p}_2$ , are auxiliary variables defined in [17], and  $\mathbf{I}_y$  and  $\mathbf{Q}_y$  are vector forms of the received signals in the I and Q branches, respectively, also explicitly defined in [17].

By assuming that the received signal is circularly symmetric, Matera and Sterle [15] derive a pair of maximum likelihood (ML) blind estimators over a single input single output (SISO) channel. First they consider the transmission of an M-ary quadrature amplitude modulation (M-QAM) constellation over a flat-fading noisy channel and derive the likelihood for the transmission of  $N$  symbols

$$\Lambda(\mathbf{y}; \hat{\alpha}, \hat{\theta}, \hat{\sigma}_n^2) = \prod_{k=1}^N \Lambda(\mathbf{y}_k; \hat{\alpha}, \hat{\theta}, \hat{\sigma}_n^2) \quad (3.5)$$

$$\Lambda(\mathbf{y}_k; \hat{\alpha}, \hat{\theta}, \hat{\sigma}_n^2) = \sum_{\ell=1}^M \frac{p_\ell}{\pi \hat{\sigma}_n^2 |\mathbf{C}(\hat{\alpha}, \hat{\theta})|^{1/2}} \exp \left\{ -\frac{1}{\hat{\sigma}_n^2} (\mathbf{y}_k - \mathbf{m}_\ell(\hat{\alpha}, \hat{\theta}))^T \mathbf{C}^{-1} (\mathbf{y}_k - \mathbf{m}_\ell(\hat{\alpha}, \hat{\theta})) \right\}, \quad (3.6)$$

where

$$\mathbf{y}_k = [y_{c,k} \quad y_{s,k}]^T \quad (3.7)$$

$$\mathbf{m}_\ell(\hat{\alpha}, \hat{\theta}) = \begin{bmatrix} (1 + \hat{\alpha})(\cos(\hat{\theta}/2)a_\ell - \sin(\hat{\theta}/2)b_\ell) \\ (1 - \hat{\alpha})(\cos(\hat{\theta}/2)b_\ell - \sin(\hat{\theta}/2)a_\ell) \end{bmatrix} \quad (3.8)$$

$$\mathbf{C}(\hat{\alpha}, \hat{\theta}) = \begin{bmatrix} (1 + \hat{\alpha})^2 & (\hat{\alpha}^2 - 1) \sin(\hat{\theta}) \\ (\hat{\alpha}^2 - 1) \sin(\hat{\theta}) & (1 - \hat{\alpha})^2 \end{bmatrix}, \quad (3.9)$$

in which  $p_\ell$  is the probability of transmitting the  $\ell$ th symbol of the M-QAM alphabet  $x_\ell = a_\ell + jb_\ell$ ,  $\mathbf{y}_k$  is the  $k$ th received symbol,  $\hat{\alpha}_r$  and  $\hat{\theta}$  are the trial values of the IQ imbalance coefficients and  $\hat{\sigma}_n^2$  is trial value for the noise variance. They recognize that, due to the summation in (3.6) over the  $M$  constellation symbols and due to the nonlinear nature of ML estimation, this derived estimator has a high computational complexity. They follow this up by presenting a Gaussian ML estimation approach, which assumes that the transmitted I and Q symbols  $a_\ell$  and  $b_\ell$  are uncorrelated wide-sense stationary (WSS) white Gaussian random processes with variance  $\frac{1}{2}$ . Under these assumptions, the ML blind estimators for the IQI parameters can be expressed as

$$\hat{\alpha} = \frac{\sqrt{\sum_{k=1}^N y_{c,k}^2} - \sqrt{\sum_{k=1}^N y_{s,k}^2}}{\sqrt{\sum_{k=1}^N y_{c,k}^2} + \sqrt{\sum_{k=1}^N y_{s,k}^2}} \quad (3.10)$$

$$\hat{\theta} = -\sin^{-1} \left( \frac{\sum_{k=1}^N y_{c,k} y_{s,k}}{\sqrt{\sum_{k=1}^N y_{c,k}^2} \sqrt{\sum_{k=1}^N y_{s,k}^2}} \right) \quad (3.11)$$

### 3.2 MMSE and WL-MMSE equalizers

The conventional methods of MMSE estimation can also be applied to compensate the effects of IQI. One of the earliest published attempts to use this method for IQI compensation is by Schuchert *et al.* [19]. They consider that, in an OFDM context, the received symbol in subcarrier  $k$  will have an interfering mirror image from subcarrier  $-k$  and set up an adaptive filter using signals from these subcarrier pairs. They propose what is essentially equivalent to a WL frequency domain equalizer and train it with a variation of the WL-LMS algorithm

$$\mathbf{c}_{i+1}(k) = \mathbf{c}_i(k) + \mu \mathbf{a}'_i(k) E_i^*(k) \quad (3.12)$$

$$E_i(k) = D_i(k) - Y_i(k) \quad (3.13)$$

$$Y_i(k) = \mathbf{c}_i^H(k) \mathbf{a}'_i(k), \quad (3.14)$$

where, with the subscript  $i$  denoting the index of the OFDM symbol,  $\mathbf{c}_i(k) = [c_i^*(k) \quad c_i^*(-k)]^T$  is the coefficient vector,  $\mathbf{a}'_i(k) = [a'_i(k) \quad a'_i(-k)]^T$  is the data input vector,  $D_i(k)$  is the reference signal (either a pilot subcarrier or decision directed symbols), and  $Y_i(k)$  is used as the estimate for the transmitted symbols  $a_i(k)$ . From this they are able to estimate the transmitted symbols by jointly compensating for IQI and channel effects. They verify the effectiveness of their method by simulating the transmission of a digital video broadcast - terrestrial (DVB-T) specified OFDM signal with 64-QAM constellation for both a linear channel with IQI case and an AWGN channel

with IQI. Validation is done by visual inspection of the constellations and no MSE values or are presented.

Tsui and Lin [20] propose a somewhat similar approach, but with a coupled pair of equalizers. This is necessary because they do not formulate IQI compensation as a complex-valued estimation problem, but instead consider it as a pair of simultaneous real-valued estimation problems. For compensating IQI without any channel effects, they propose the following set of equations for adapting the filter coefficients

$$W_{ii,k}(1) = W_{ii,k}(1) + \mu \varepsilon_{i,k} i_{r,k} \quad (3.15)$$

$$W_{ii,k}(2) = W_{ii,k}(2) + \mu \varepsilon_{i,k} i_{r,-k} \quad (3.16)$$

$$W_{qi,k}(1) = W_{qi,k}(1) + \mu \varepsilon_{q,k} q_{r,k} \quad (3.17)$$

$$W_{qi,k}(2) = W_{qi,k}(2) + \mu \varepsilon_{q,k} q_{r,-k} \quad (3.18)$$

$$\varepsilon_{i,k} = d_{i,k} - \hat{i}_{t,k} \quad (3.19)$$

$$\varepsilon_{q,k} = d_{q,k} - \hat{q}_{t,k} \quad (3.20)$$

$$\hat{i}_{t,k} = W_{ii,k}(1) i_{r,k} - W_{ii,k}(2) i_{r,-k} + W_{qi,k}(1) q_{r,k} + W_{qi,k}(2) q_{r,-k} \quad (3.21)$$

$$\hat{q}_{t,k} = W_{qi,k}(1) i_{r,k} + W_{qi,k}(2) i_{r,-k} + W_{ii,k}(1) q_{r,k} - W_{ii,k}(2) q_{r,-k}, \quad (3.22)$$

where  $d_{i,k}$  and  $d_{q,k}$  are decision directed outputs of the received signals in the I and Q branches at the  $k$ th subcarrier,  $i_{r,k}$  and  $q_{r,k}$ , respectively. The filter coefficients  $W$  are all constant in  $k$  if IQI is frequency independent. To address the impacts of IQI in channel estimation/correction, they state that, using the long training signal from 802.11a, two cases exist: when the symbols from the long preamble at subcarrier  $k$  and its mirror image  $-k$  have the same phase or opposite phases. They propose using two independent equalizers for each of these cases. Naturally, if we generalize to any training sequence with more than two cases, i.e., anything different from a binary phase shift keying (BPSK) equivalent constellation, then the number of equalizers needed will grow with number of existing phase differences, which may be problematic in some contexts.

By using the WL-MMSE estimator, Chen *et al.* [21] formulate the WL-MMSE channel estimation and data detection problems. They apply the known expressions in [22] [23] to the IQI equivalent channel estimation problem and arrive estimates for two cases: when the IQI coefficient matrices are known, and when the IQI coefficient matrices are unknown but the variance matrices of the equivalent channels are known as well as the complementary covariance matrix between them. Both of these cases are hard to achieve in practice. In the first case, if we already know the IQI coefficient matrices, then channel estimation is straightforward because IQI can be compensated with an WL operator directly and then the estimation can be performed as normal. The other case requires equivalent channel covariance matrices, which is notoriously difficult information to achieve, specially in fast fading channels. In this sense we may say that [21] provides more of a theoretical insight into the qualities of WL-MMSE estimation and detection applied to an IQI affected transmission.

### 3.3 Other estimators

This section includes other kinds of estimators that do not directly fit the two categories cited above. One of the most cited approaches was introduced by Tubbax *et al.* [13]. They consider that, in a decision directed or pilot sequence context where the transmitted symbol is known, in a noise free unit gain ideal channel transmission, the symbols at any carriers  $i$  and  $j$  should

satisfy the system of equations

$$(d_r)_i = \alpha(d_t)_i + \beta(d_t^*)_{m(i)} \quad (3.23)$$

$$(d_r)_j = \alpha(d_t)_j + \beta(d_t^*)_{m(j)}, \quad (3.24)$$

where  $m(i)$  denotes the mirror image carrier for carrier  $i$ , and similarly for  $m(j)$ . They relax any constraints between  $\alpha$  and  $\beta$  that would make this a nonlinear system of equations under the justification that solving this system in a mobile terminal is non-trivial. Solving this system yields

$$\alpha = \frac{(d_r)_i(d_t^*)_{m(j)} + (d_r)_j(d_t^*)_{m(i)}}{(d_t)_i(d_t^*)_{m(j)} - (d_t)_j(d_t^*)_{m(i)}} \quad (3.25)$$

$$\beta = \frac{(d_r)_i - \alpha(d_t)_i}{(d_t^*)_{m(i)}} \quad (3.26)$$

for every non-zero carrier in the current OFDM symbol. They propose averaging the estimated values over all non-zero subcarriers to achieve a final value. However, these equations are only valid in an ideal noiseless channel. They present a series of derivations for the unrealistic, but didactic, case of perfect channel state information (CSI), and then tackle the issue of practical channel estimation under IQI. Let  $\mathbf{c}$  be the vector of exact frequency domain channel coefficients, then it is stated that IQI degrades the channel estimate  $\mathbf{h}$  obtained from a long training sequence (LTS), in a high performance radio local area network 2 (HiperLAN/2) context, in the following form

$$\mathbf{h} = \alpha\mathbf{c} + \beta \cdot \mathbf{lts2} \cdot (\mathbf{c}^*)_m, \quad (3.27)$$

where the  $m$  subscript denotes frequency mirroring, and  $\mathbf{lts2} = \mathbf{lts} \cdot (\mathbf{lts})_m$ , i.e., it is the elementwise product of the LTS with its frequency mirror image. They verify that IQI indeed has a significant impact on channel estimation and propose compensating the channel estimate by applying the correction

$$\mathbf{c} = \frac{\alpha^*\mathbf{h} - \beta(\mathbf{lts2} \cdot \mathbf{h}^*)_m}{|\alpha|^2 - |\beta|^2}. \quad (3.28)$$

This, of course, requires the knowledge of the IQI coefficients. They address this by considering the system of equations formed by two adjacent carriers and assuming that  $c_i \approx c_{i+1}$  and IQI is approximately non-existent, i.e.,  $\alpha \approx 1$  and  $\beta \approx 0$ . Taking two adjacent carriers

$$h_i = \alpha c_i + \beta \cdot \mathbf{lts2}_{m(i)} \cdot (\mathbf{c}^*)_{m(i)} \quad (3.29)$$

$$h_i = \alpha c_{i+1} + \beta \cdot \mathbf{lts2}_{m(i+i)} \cdot (\mathbf{c}^*)_{m(i+i)}, \quad (3.30)$$

applying the aforementioned assumptions and solving for  $\alpha$  and  $\beta$  yields

$$\beta_{est} = \frac{h_{i+1} - h_i}{\mathbf{lts2}_{m(i)}(h_{m(i)}^* + h_{m(i+1)}^*)} \quad (3.31)$$

$$\alpha_{est} = \sqrt{1 - (\Im\{\beta_{est}\})^2} - j \frac{\Re\{\beta_{est}\} \Im\{\beta_{est}\}}{\sqrt{1 - (\Im\{\beta_{est}\})^2}}. \quad (3.32)$$

Applying these equations to all valid carrier transitions yields one estimate for each transition, these are then averaged out in a final estimate for the IQI coefficients. The resulting estimates can then also be applied in (3.28) to get an estimate for the true channel coefficients. From the assumptions we can conclude that the method in [13] is only effective if IQI effects are small, because of the  $\alpha \approx 1$  and  $\beta \approx 0$  assumptions, and if the channel has a relatively large coherence bandwidth compared to the subcarrier spacing.

### 3.4 Joint transmitter and receiver IQI compensation

So far we have only shown methods that deal exclusively with the receiver IQI compensation problem. However, some schemes also attempt joint transmitter and receiver IQI estimation/compensation. Zhang *et al.* [24] propose an iterative block decision feedback equalization (IBDFE) [25] scheme for IQI compensation. They put forward an iterative receiver to compensate for receiver and transmitter IQ imbalance in single carrier frequency domain equalization (SC-FDE) systems. They propose hard and soft detection methods to estimate the necessary parameters for updating the feedforward and feedback filters used in the proposed receiver architecture. We refer the reader directly to [24] for the detailed explanation of the procedure.

Other approach is considered by Zhang *et al.* [26] based on reduced number of parameters direct least squares (DLS-RNP) and alternating least squares (ALS) techniques. They consider a SISO system with a guard interval affected by transmitter and receiver IQI, according to the system model

$$\mathbf{y} = \mathbf{S}(\mu_r \mu_t \mathbf{h} + \nu_r \nu_t^* \mathbf{h}^*) + \mathbf{S}^*(\mu_r \nu_t \mathbf{h} + \nu_r \mu_t^* \mathbf{h}^*) + \mathbf{w}, \quad (3.33)$$

where,  $\mu$  and  $\nu$  are IQI coefficients with the subscripts  $r$  and  $t$  respectively denoting the transmitter and receiver,  $\mathbf{w} = \mu_r \mathbf{n} + \nu_r \mathbf{n}^*$  is IQI affected AWGN, and  $\mathbf{h}$  is the channel impulse response vector,  $\mathbf{S}$  is the data matrix defined in a way that the convolution of the transmitted data with the channel impulse response can be expressed as  $\mathbf{S}\mathbf{h}$  by discarding the guard interval. They state that, if the IQI coefficients are known, then IQI can be compensated in the same way as [14] at the transmitter and receiver, respectively, by applying the corrections

$$\tilde{\mathbf{s}} = \frac{\mathbf{s} - \eta_t \mathbf{s}^*}{\mu_t (1 - |\eta_t|^2)} \quad (3.34)$$

$$\tilde{\mathbf{y}} = \frac{\mathbf{y} - \eta_r \mathbf{y}^*}{\mu_r (1 - |\eta_r|^2)}, \quad (3.35)$$

where  $\eta_t = \frac{\nu_t}{\mu_t}$  and  $\eta_r = \frac{\nu_r}{\mu_r}$ . By considering the simplification that IQI is approximately non-existent, i.e.,  $\mu_r, \mu_t \approx 1$ , they suppress these terms in (3.34) and (3.35) and consider two cases: when  $\mathbf{g} = \mu_r \mu_t \mathbf{h}$  is known, and when  $\eta_r$  and  $\eta_t$  are known. It can be said that these cases are somewhat unrealistic, because both  $\eta_{r,t}$  and  $\mathbf{g}$  are hard to directly estimate. Nonetheless, they propose using equivalent channel estimates  $\hat{\mathbf{c}}_X = [\hat{\mathbf{c}}_1^T \ \hat{\mathbf{c}}_2^T]^T = (\mathbf{S}_X^H \mathbf{S}_X)^{-1} \mathbf{S}_X^H \mathbf{y}$ , where  $\mathbf{S}_X = [\mathbf{S} \ \mathbf{S}^*]$ , to estimate  $\mathbf{g}$  assuming  $\eta_r$  and  $\eta_t$  are known

$$\hat{\mathbf{g}} = \mathbf{C} \boldsymbol{\eta}_X^H (\boldsymbol{\eta}_X \boldsymbol{\eta}_X^H)^{-1}, \quad (3.36)$$

where  $\mathbf{C} = [\mathbf{c}_1 - \eta_r \mathbf{c}_2^* \ \mathbf{c}_1 - \eta_t^* \mathbf{c}_2] = \mathbf{g} \boldsymbol{\eta}_X$ , with  $\boldsymbol{\eta}_X = [1 - |\eta_r|^2 \ \ 1 - |\eta_t|^2]$ . For estimating  $\eta_r$  and  $\eta_t$  assuming  $\mathbf{g}$  is known, they propose solving the least squares optimization problem

$$\{\hat{\eta}_r, \hat{\eta}_t\} = \underset{\eta_r, \eta_t \in \mathbb{C}}{\operatorname{argmin}} \|\mathbf{c}_1 - \mathbf{g} - \eta_r \eta_t^* \mathbf{g}^*\|^2 + \|\mathbf{c}_2 - \eta_t \mathbf{g} - \eta_r \mathbf{g}^*\|^2, \quad (3.37)$$

which is not a convex problem in general. They propose solving it with an ALS technique by sequentially fixing one parameter and optimizing the other in alternating fashion. It is then shown that the proposed alternating optimization procedure converges.

One of the more innovative approaches is the one introduced by Cheng *et al.* [27] for SISO SC-FDE systems. By assuming that the coherence bandwidth of the channel is large enough that the channel variation between adjacent subcarriers should be smooth, they state that ignoring IQI in channel estimation leads to sharp fluctuation in adjacent frequency channel estimates due to mirror image frequency interference. In light of this, they define a quantity called the channel variation energy (CVE)

$$\text{CVE} \triangleq \sum_{k=0}^{N-2} |\hat{H}_{k+1} - \hat{H}_k|^2, \quad (3.38)$$

where  $\hat{H}_k$  is obtained by

$$\hat{H}_k = \frac{A_k^* Y_k - B_{N-k} Y_{N-k}^*}{|A_k|^2 - |B_{N-k}|^2} \quad (3.39)$$

$$A_k = \alpha_T \alpha_R X_k + \beta_T \alpha_R X_{\text{mod}(N-k, N)}^* \quad (3.40)$$

$$B_k = \beta_T^* \beta_R X_k + \alpha_T^* \beta_R X_{\text{mod}(N-k, N)}^*, \quad (3.41)$$

where  $\{X_k\}$  is the discrete Fourier transform (DFT) of  $\mathbf{x}$ , the ideal complex baseband signal vector, and  $\{Y_k\}$  is the DFT of  $\mathbf{y}$ , the received signal vector. They express  $\alpha_T$  and  $\alpha_R$  as functions of  $\beta_T$  and  $\beta_R$ , respectively. Then they arrive at expressions for  $\beta_T$  and  $\beta_R$  that minimize the CVE in the form:  $\beta_T = \phi_1(\beta_R, \beta_T)$  and  $\beta_R = \phi_2(\beta_R, \beta_T)$ . Defining the objective function

$$F(\beta_R, \beta_T) = \frac{1}{|f|^2} \cdot \frac{1}{|g|^2}, \quad (3.42)$$

where  $f = \beta_T - \phi_1(\beta_R, \beta_T)$  and  $g = \beta_R - \phi_2(\beta_R, \beta_T)$ , the estimation problem becomes a question of maximizing  $F$ . They state the difficulty of applying gradient-based methods to this problem and propose employing a Rosenbrock search [28]. The authors also propose a least squares (LS) compensation scheme by making the familiar *almost ideal IQI* assumptions, i.e.,  $\alpha_{R,T} \approx 1$  and  $\beta_{R,T} \approx 0$ , and neglecting some higher order terms in the expressions.

There is also the more expensive option of hardware-based IQI compensation, such as the method proposed by Aoki *et al.* [16]. They design a frequency-dependent IQI calibration module for 5G mmWave transceiver chipsets. The proposed approach uses loopback data from a known training signal to configure a complex finite impulse response (FIR) filter that is used to compensate the IQI. This approach, even if effective, requires dedicated hardware and it is not suitable to be applied in already deployed devices, once more reinforcing the flexibility of software-based IQI compensation.

This concludes our survey of IQI compensation/estimation methods. Naturally, other techniques exist in the literature, but the majority of them have reasonable similarities with the set of approaches included herein. The reader is encouraged to read in more detail the aforementioned references to get a deeper understanding of each procedure.

## 4 IQI AND POSITIONING

In this chapter, we will assess the impacts of IQI in the positioning accuracy of a single anchor line-of-sight (LOS) scenario. We will then introduce a timing robust pilot sequence based IQI compensation algorithm, which will be applied in improving the accuracy of positioning estimation in a flat fading scenario. The impacts of changing the length of the pilot sequence and the SNR are also explored, with the performance of the proposed method being compared to a blind estimator.

### 4.1 Introduction to positioning

Positioning schemes are usually classified into 3 categories: timing-based, angle-based, and hybrid. Timing-based techniques rely on estimating the time of arrival (ToA) or time difference of arrival (TDoA) of the signal between the transmitter and receivers with known position, also called anchors. Timing-based methods require some knowledge of the transmitted signal, typically of a transmission preamble such as the primary synchronization signal (PSS) in LTE and 5G NR. The performance of some TDoA positioning methods is explored in [29], while [30] proposes a TDoA based positioning algorithm for non-line-of-sight (NLOS) scenarios. Angle-based techniques utilize some combination of transmit beamforming and measuring the phase differences at the receiver antenna elements to estimate the angle of arrival (AoA) formed by the transmitter and each receiver. The densely packed antenna elements necessary for massive MIMO, enabled by mmWave frequency bands, make it possible to achieve high resolution AoA estimates using some well-established algorithms such as multiple signal classification (MUSIC) and estimation of signal parameters via rotational invariant techniques (ESPRIT). A comparison between the performance of these methods is laid out in [31]. Angle-based methods have the advantage of not requiring prior knowledge about the received signal, as well as being robust to synchronization errors. Hybrid techniques use a mixture of angle-based and timing-based methods to estimate the position of the transmitter. One notable example of a hybrid positioning method is the network localization and navigation (NLN) paradigm, introduced in [32] and extensively detailed in [33], which explores spatio-temporal cooperation between nodes allowing both angle-based and timing-based measurements to be used to compute the positional beliefs of the nodes in the network. Alternative power-based methods such as using enhanced cell ID (E-CID) in LTE networks [34], or received signal strength (RSS)-based direction of arrival estimation for wireless sensor networks (WSNs) have also been proposed [35].

For its enhanced positioning services, 5G requires sub-meter positioning accuracy in a variety of indoors and outdoors scenarios [36]. These requirements cannot be satisfied using only the traditional methods prevalent in LTE, such as global navigation satellite system (GNSS) localization and TDoA based methods, mainly because of their possible poor indoor performance and vulnerability to clock synchronization error between base stations (BSs) [37] [38]. Beyond the actual method used for positioning estimation, the quality and reliability of the hardware deployed must allow for sufficient accuracy in the necessary measurements for positioning estimation.

### 4.2 System model

Consider the case of a single receiver and transmitter with a LOS link. Let  $\mathbf{s}(t)$  be the baseband equivalent transmitted signal at time  $t$ . The baseband equivalent received signal before

downconversion is given by

$$\begin{aligned}\mathbf{x}(t) &= \gamma \mathbf{a}_R(\phi_R) \mathbf{a}_T^H(\phi_T) \mathbf{s}(t - \tau) + \mathbf{w}(t) \\ &= \mathbf{H} \mathbf{s}(t - \tau) + \mathbf{w}(t),\end{aligned}\quad (4.1)$$

where  $\gamma$  is the complex path gain,  $\mathbf{a}_R(\phi_R)$  and  $\mathbf{a}_T(\phi_T)$  are, respectively, the receiver and transmitter array response vectors as a function of the angles of arrival and departure,  $\tau$  is the propagation delay from the transmitter to the receiver, and  $\mathbf{w}(t)$  is complex circularly symmetric AWGN. The channel matrix  $\mathbf{H}$  is  $N_R \times N_T$  where  $N_R$  and  $N_T$  denote the number of receive and transmit antennas, respectively.

In a positioning context, position estimates rely on extracting the angle of arrival or departure and the distance or ranging measurements from the received signal. The angle of arrival estimates are usually performed using an algorithm such as MUSIC [39] or ESPRIT [40]. In the LOS case, ranging is usually done by measuring the time of flight (ToF)  $\tau$ .

Non-idealities of the in-phase and quadrature components of the LO signal of the converter (up or down converter) corrupt the received signal and deteriorate the quality of those estimates giving rise to IQI. From an economic and practical standpoint, it is convenient to mitigate these effects in software or baseband processing, allowing some constraints in the manufacturing process to be slightly relaxed. Let  $\Theta_A$  and  $\Theta_B$  denote the receiver IQI matrices,  $\Theta_A = \text{diag}(\alpha_1, \dots, \alpha_{N_R})$  and  $\Theta_B = \text{diag}(\beta_1, \dots, \beta_{N_R})$ , these are diagonal matrices of possibly distinct receiver IQI coefficients as defined in (2.17) and (2.18). These matrices allow us to model imbalanced IQ demodulation at each RF chain [4]. The IQI corrupted received signal is computed as

$$\mathbf{y} = \Theta_A \mathbf{x} + \Theta_B \mathbf{x}^* = \Theta \mathbf{x}_e, \quad (4.2)$$

where  $\mathbf{x}^*$  is the complex conjugate of  $\mathbf{x}$ ,  $\Theta = [\Theta_A \quad \Theta_B]$ ,  $\mathbf{x}_e = [\mathbf{x}^T \quad \mathbf{x}^H]^T$ . This is a straightforward extension of the IQI model in Section 2.2 to vector form. The receiver IQ demodulation under IQ imbalance is represented in Fig. 4.1.

The way that the equations have been defined, by using the baseband equivalent, allows us to bypass the upconversion and downconversion operations and focus only in the IQI effects. However, in a more detailed graphical representation of the IQ demodulation such as the one in Fig. 4.1,  $\mathbf{x}(t)$  must be distinguished from  $\mathbf{x}^{RF}(t)$  which is the signal that would be physically received at the antenna.

Assume that the channel propagation delay is well approximated by an integer number of samples. Then each transmitted pilot sequence sample  $\mathbf{s}(i)$ , where  $i$  denotes the discrete time sample index, has a corresponding received signal sample  $\mathbf{y}(i)$  at the appropriate sampling time accounting for channel propagation time following the relation

$$\mathbf{y}(i) = \Theta \mathbf{H}_e \mathbf{s}_e(i) + \mathbf{n}(i) = \mathbf{G} \mathbf{s}_e(i) + \mathbf{n}(i), \quad (4.3)$$

where  $\mathbf{s}_e^T(i) = [s^T(i) \quad s^H(i)]^T$ ,  $\mathbf{H}_e$  is block diagonal of the form  $\text{diag}(\mathbf{H}, \mathbf{H}^*)$ , and  $\mathbf{n} = \Theta_A \mathbf{w} + \Theta_B \mathbf{w}^*$ . From (4.3) we can write

$$\mathbf{Y} = [\mathbf{y}(0) \quad \dots \quad \mathbf{y}(N_s - 1)] = \Theta \mathbf{H}_e \mathbf{S}_e + \mathbf{N} \quad (4.4)$$

$$\mathbf{S}_e = [\mathbf{s}_e(0) \quad \dots \quad \mathbf{s}_e(N_s - 1)] \quad (4.5)$$

$$\mathbf{N} = [\mathbf{n}(0) \quad \dots \quad \mathbf{n}(N_s - 1)]. \quad (4.6)$$

Manipulating this further, using the identity

$$\text{vec}(\Theta \mathbf{H}_e \mathbf{S}_e) = (\mathbf{S}_e^T \otimes \Theta) \text{vec}(\mathbf{H}_e) \quad (4.7)$$

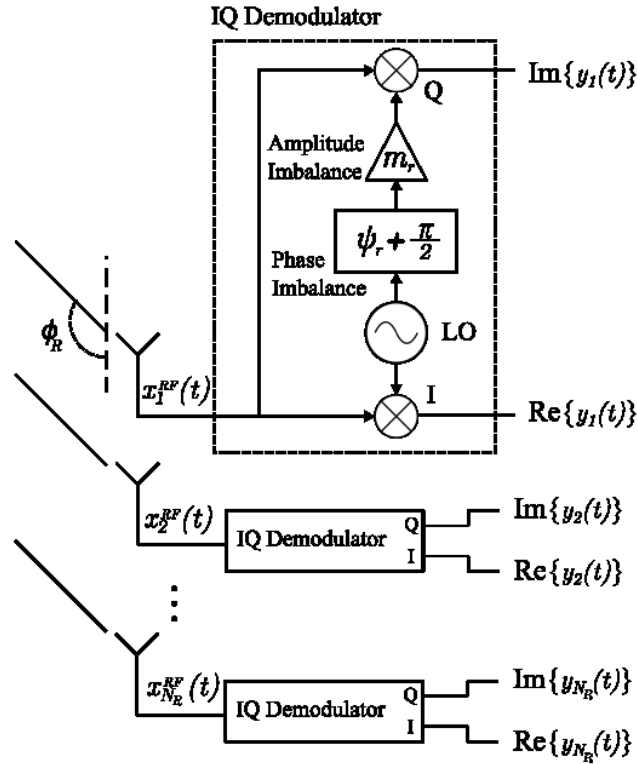


Figure 4.1. Receiver IQ demodulation scheme under IQ imbalance. Inside the IQ demodulator, the triangle block denotes an amplitude gain and the square block denotes a phase increment.

we get  $\mathbf{S}_e^T \otimes \mathbf{\Theta} = \check{\mathbf{S}}_e^T \check{\mathbf{\Theta}}$ , where  $\check{\mathbf{S}}_e = \mathbf{S}_e \otimes \mathbf{I}_{N_R}$  and  $\check{\mathbf{\Theta}} = \mathbf{I}_{2N_T} \otimes \mathbf{\Theta}$ ,  $\otimes$  denotes the Kronecker product. This yields

$$\check{\mathbf{y}} = \check{\mathbf{S}}_e^T \check{\mathbf{\Theta}} \check{\mathbf{h}}_e + \check{\mathbf{n}} = \check{\mathbf{S}}_e^T \check{\mathbf{g}} + \check{\mathbf{n}}, \quad (4.8)$$

where  $\check{\mathbf{h}}_e = \text{vec}(\mathbf{H}_e)$  and  $\check{\mathbf{n}} = \text{vec}(\mathbf{N})$ . We call  $\check{\mathbf{g}} = \check{\mathbf{\Theta}} \check{\mathbf{h}}_e$  the vectorized *equivalent channel*. By writing the equivalent channel in this vectorized form, using (4.8) we can express its covariance and complementary covariance matrix estimates as

$$\mathbf{R}_{\check{\mathbf{g}}_{\text{est}}} = (\check{\mathbf{S}}_e^T)^\dagger (\mathbb{E} \{ \check{\mathbf{y}} \check{\mathbf{y}}^H \} - \mathbf{R}_{\check{\mathbf{n}}}) (\check{\mathbf{S}}_e^*)^\dagger \quad (4.9)$$

$$\mathbf{Q}_{\check{\mathbf{g}}_{\text{est}}} = (\check{\mathbf{S}}_e^T)^\dagger (\mathbb{E} \{ \check{\mathbf{y}} \check{\mathbf{y}}^T \} - \mathbf{Q}_{\check{\mathbf{n}}}) (\check{\mathbf{S}}_e)^\dagger \quad (4.10)$$

where  $\dagger$  denotes the pseudoinverse,  $\mathbf{R}_{\check{\mathbf{n}}} = \mathbb{E} \{ \check{\mathbf{n}} \check{\mathbf{n}}^H \}$ , and  $\mathbf{Q}_{\check{\mathbf{n}}} = \mathbb{E} \{ \check{\mathbf{n}} \check{\mathbf{n}}^T \}$ .

### 4.3 Equivalent channel estimation

This section and the remainder of this thesis makes use of the concept of a widely linear (WL) operator. If the reader is unfamiliar with the basics of WL operators and WL filtering, a very brief summary of the definitions and basic concepts is presented in Appendix 1. The reader is also directed to the references [22] [23] as worthwhile introductions to the topic.

It is not generally possible to leverage the information from a known pilot sequence for improved IQI coefficient estimator performance unless the channel is precisely estimated, otherwise we cannot separate the channel effects and the IQI effects on the pilot sequence. Also the

channel cannot be estimated independently from the IQI, because every received sample is only observed after IQI. Since IQI is essentially a WL operator, to properly capture the effects of IQI in the received sequence it is necessary to estimate the channel also as a WL operator. Besides, for reasons that will be better clarified in the following section, to derive a timing-robust pilot sequence based IQI estimator in the way that we intend, it is fundamental that the estimated equivalent channel be consistent with the estimated covariance and complementary covariance matrices of the received data. Traditional least squares channel estimation by itself does not necessarily have this property and may not yield the desired results for our proposed approach.

For brevity, we will refer to the vectorized channel and equivalent channel simply as the channel and equivalent channel, respectively. Assume that the equivalent channel  $\check{\mathbf{g}}$  is constant and we only observe one single realization during the transmission of the whole sequence. Thus, we cannot estimate the actual correlation and complementary correlation by averaging over multiple realizations, we are only able to estimate  $\check{\mathbf{g}}\check{\mathbf{g}}^H$  and  $\check{\mathbf{g}}\check{\mathbf{g}}^T$ , which is sufficient for our application.

First, let us try to estimate it from the eigenvalue decomposition (EVD) of the equivalent channel sample autocorrelation matrix. We can perform a rank 1 approximation of this matrix such as  $\check{\mathbf{R}}_{\check{\mathbf{g}}} \approx \lambda_1 \mathbf{u}_1 \mathbf{u}_1^H$ . Here  $\sqrt{\lambda_1} \mathbf{u}_1$  is an approximation for the channel using the square root of the largest eigenvalue and its eigenvector, respectively. This approach contains insufficient information since there exist infinite vectors that satisfy the above relation, up to a complex phase shift. To eliminate the phase ambiguity, we must resort to a more complete description of the channel using the sample augmented covariance matrix  $\check{\mathbf{R}}_{e,\check{\mathbf{g}}}$ .

We will now perform the augmented eigenvalue decomposition (AEVD), as described in [23], of the sample channel augmented covariance matrix and use it to obtain an approximation for the equivalent channel. The following procedure with the AEVD allows us to find the vector that has the desired covariance and complementary covariance matrices. We will treat  $\check{\mathbf{g}}$  as a *deterministic* (not random) vector. This is justified by the assumption that the channel is constant throughout the whole transmission and only one transmission ever takes place, thus treating the channel as a random quantity is unnecessary. We keep the nomenclature of covariance and complementary covariance matrices for convenience, but it must be clear that the expectation operator is irrelevant in the deterministic case, e.g.  $\check{\mathbf{R}}_{\check{\mathbf{g}}} = \mathbb{E} \{ \check{\mathbf{g}}\check{\mathbf{g}}^H \} = \check{\mathbf{g}}\check{\mathbf{g}}^H$ .

Let  $\check{\mathbf{g}}$  be an arbitrary complex vector in  $\mathbb{C}^n$ , and let  $\check{\mathbf{g}} = \mathbf{a} + j\mathbf{b}$  and  $\mathbf{z} = [\mathbf{a}^T \mathbf{b}^T]^T$ . Also define

$$\mathbf{T} = \begin{bmatrix} \mathbf{I} & j\mathbf{I} \\ \mathbf{I} & -j\mathbf{I} \end{bmatrix} \quad (4.11)$$

We write the EVD of  $\mathbf{R}_{\mathbf{z}} = \mathbf{z}\mathbf{z}^T$  as

$$\mathbf{R}_{\mathbf{z}} = \mathbf{U} \begin{bmatrix} \frac{1}{2}\mathbf{\Xi}_1 & \mathbf{0} \\ \mathbf{0} & \frac{1}{2}\mathbf{\Xi}_2 \end{bmatrix} \mathbf{U}^H, \quad (4.12)$$

where the eigenvalues are organized in an descending order and  $\mathbf{\Xi}_1$  and  $\mathbf{\Xi}_2$  are the diagonal matrices with the odd and even eigenvalues

$$\mathbf{\Xi}_1 = \mathbf{Diag}(\lambda_1, \lambda_3, \dots, \lambda_{2n-1}) \quad (4.13)$$

$$\mathbf{\Xi}_2 = \mathbf{Diag}(\lambda_2, \lambda_4, \dots, \lambda_{2n}). \quad (4.14)$$

From (4.12) and the relation  $\check{\mathbf{R}}_{e,\check{\mathbf{g}}} = \mathbf{T}\mathbf{R}_{\mathbf{z}}\mathbf{T}^H$ , where

$$\check{\mathbf{R}}_{e,\check{\mathbf{g}}} = \begin{bmatrix} \check{\mathbf{g}} \\ \check{\mathbf{g}}^* \end{bmatrix} \begin{bmatrix} \check{\mathbf{g}}^H & \check{\mathbf{g}}^T \end{bmatrix} \quad (4.15)$$

we get

$$\mathbf{R}_{e,\check{\mathbf{g}}} = \begin{bmatrix} \mathbf{R}_{\check{\mathbf{g}}} & \mathbf{Q}_{\check{\mathbf{g}}} \\ \mathbf{Q}_{\check{\mathbf{g}}}^* & \mathbf{R}_{\check{\mathbf{g}}}^* \end{bmatrix} = \mathbf{V}\Lambda_e\mathbf{V}^H \quad (4.16)$$

$$\mathbf{V} = \left( \frac{1}{2} \mathbf{T} \mathbf{U} \mathbf{T}^H \right) = \begin{bmatrix} \mathbf{V}_1 & \mathbf{V}_2 \\ \mathbf{V}_2^* & \mathbf{V}_1^* \end{bmatrix} \quad (4.17)$$

$$\Lambda_e = \frac{1}{2} \begin{bmatrix} \bar{\boldsymbol{\Xi}}_1 + \bar{\boldsymbol{\Xi}}_2 & \bar{\boldsymbol{\Xi}}_1 - \bar{\boldsymbol{\Xi}}_2 \\ \bar{\boldsymbol{\Xi}}_1 - \bar{\boldsymbol{\Xi}}_2 & \bar{\boldsymbol{\Xi}}_1 + \bar{\boldsymbol{\Xi}}_2 \end{bmatrix} = \begin{bmatrix} \Lambda_1 & \Lambda_2 \\ \Lambda_2 & \Lambda_1 \end{bmatrix}, \quad (4.18)$$

where  $\mathbf{R}_{\check{\mathbf{g}}} = \mathbb{E} \{ \check{\mathbf{g}} \check{\mathbf{g}}^H \}$  and  $\mathbf{Q}_{\check{\mathbf{g}}} = \mathbb{E} \{ \check{\mathbf{g}} \check{\mathbf{g}}^T \}$

Let us take the AEVD of  $\mathbf{R}_{e,\check{\mathbf{g}}} = \mathbf{V}\Lambda_e\mathbf{V}^H$  and explicitly carry out the block matrix products. For our purposes, we only care about the top left block  $\mathbf{R}_{\check{\mathbf{g}}}$ . Because  $\check{\mathbf{g}}$  is not a random variable,  $\mathbf{R}_{\check{\mathbf{g}}}$  is a rank 1 matrix and all the eigenvalues besides  $\lambda_1$  are zero. In that case,  $\Lambda_1 = \Lambda_2 = \text{Diag}(\lambda_1, 0, \dots, 0)$ , and the top left block, which corresponds to the covariance matrix of  $\mathbf{x}$ , is equal to  $\lambda_1(\mathbf{v}_1\mathbf{v}_1^H + \mathbf{v}_2\mathbf{v}_1^H + \mathbf{v}_1\mathbf{v}_2^H + \mathbf{v}_2\mathbf{v}_2^H)$ , where  $\mathbf{v}_1$  and  $\mathbf{v}_2$  are the eigenvectors associated with  $\lambda_1$  in  $\mathbf{V}_1$  and  $\mathbf{V}_2$ , respectively, i.e., the first column if the eigenvectors are arranged in decreasing order. For estimating the equivalent channel, we first take the AEVD of the sample augmented covariance matrix of the equivalent channel  $\tilde{\mathbf{R}}_{e,\check{\mathbf{g}}} = \tilde{\mathbf{V}}\tilde{\Lambda}_e\tilde{\mathbf{V}}^H$ . Denote the largest eigenvalue by  $\tilde{\lambda}_1$  and denote its associated eigenvectors in  $\tilde{\mathbf{V}}_1$  and  $\tilde{\mathbf{V}}_2$  as  $\tilde{\mathbf{v}}_1$  and  $\tilde{\mathbf{v}}_2$ , respectively. We want a vector  $\check{\check{\mathbf{g}}}$  such that  $\check{\check{\mathbf{g}}}\check{\check{\mathbf{g}}}^H = \tilde{\lambda}_1(\tilde{\mathbf{v}}_1\tilde{\mathbf{v}}_1^H + \tilde{\mathbf{v}}_2\tilde{\mathbf{v}}_1^H + \tilde{\mathbf{v}}_1\tilde{\mathbf{v}}_2^H + \tilde{\mathbf{v}}_2\tilde{\mathbf{v}}_2^H)$ . It is easy to see that  $\check{\check{\mathbf{g}}} = \pm\sqrt{\tilde{\lambda}_1}(\tilde{\mathbf{v}}_1 + \tilde{\mathbf{v}}_2)$  satisfies this requirement and is unique up to the sign. In this framework,  $\check{\check{\mathbf{g}}}$  is already constrained to satisfy  $\check{\check{\mathbf{g}}}\check{\check{\mathbf{g}}}^T = \tilde{\mathbf{Q}}_{\check{\mathbf{g}}}$ . We only need now to estimate if the sign is positive or negative. Since we are using a pilot sequence, one possible method is to compare the squared error of the received signal and the predicted received signal using the channel as in

$$\sum_{i=1}^{N_s} \|\tilde{\mathbf{G}}\mathbf{s}_e(i) - \mathbf{y}(i + \hat{k}_s)\|^2 \underset{\check{\check{\mathbf{g}}}}{\underset{\mathbf{g}}{\geq}} \sum_{i=1}^{N_s} \|\check{\check{\mathbf{G}}}\mathbf{s}_e(i) - \mathbf{y}(i + \hat{k}_s)\|^2, \quad (4.19)$$

where  $\tilde{\mathbf{G}}$  is the channel in matrix form obtained from  $\check{\check{\mathbf{g}}}$  and  $\hat{k}_s$  is a propagation delay estimate in samples. In other words, always opt for the sign that produces predictions with smaller sum of square errors.

#### 4.4 IQI parameter and signal estimation

In this section, we derive the estimator of the IQI coefficients and system parameters. The derivations below are valid when RF chains share the same IQI coefficients. If the IQI characteristics of the chains are different, then the following procedure is equivalent to restricting the computations to the subsystem where the coefficients are the same.

Considering (4.1), (4.2), and (4.3), we can show that the covariance and complementary covariance of  $\mathbf{y}$  are given by

$$\mathbf{R}_y = \boldsymbol{\Theta}\mathbf{H}_e\mathbb{E} \{ \mathbf{s}_e\mathbf{s}_e^H \} \mathbf{H}_e^H\boldsymbol{\Theta}^H + \mathbf{R}_n \quad (4.20)$$

$$\mathbf{Q}_y = \boldsymbol{\Theta}\mathbf{H}_e\mathbb{E} \{ \mathbf{s}_e\mathbf{s}_e^T \} \mathbf{H}_e^T\boldsymbol{\Theta}^T + \mathbf{Q}_n, \quad (4.21)$$

where  $\mathbf{R}_n$  and  $\mathbf{Q}_n$  are the covariance and complementary covariance matrices of  $\mathbf{n}$ , respectively. The expectations are known, because  $\mathbf{s}$  is a deterministic pilot sequence

From  $\check{\mathbf{y}}$ , we can estimate  $\check{\mathbf{R}}_{\check{\mathbf{g}}}$  and  $\check{\mathbf{Q}}_{\check{\mathbf{g}}}$  by applying (4.9) and (4.10) with  $\mathbb{E}\{\check{\mathbf{y}}\check{\mathbf{y}}^H\} \approx \check{\mathbf{y}}\check{\mathbf{y}}^H$  and  $\mathbb{E}\{\check{\mathbf{y}}\check{\mathbf{y}}^T\} \approx \check{\mathbf{y}}\check{\mathbf{y}}^T$ . Then we use the channel estimation procedure of Section 4.3 to get an estimate of the equivalent channel  $\check{\mathbf{G}} \approx \mathbf{O}\mathbf{H}_e$ . We can get an estimate of  $\mathbf{H}$ , *conditioned* on candidate values for the IQI parameters  $(\hat{\epsilon}_r, \hat{\psi}_r)$ , by computing the least squares solution on  $\hat{\mathbf{H}}$  of

$$\check{\mathbf{G}} = \hat{\mathbf{\Theta}}(\hat{\epsilon}_r, \hat{\psi}_r) \begin{bmatrix} \hat{\mathbf{H}} & \mathbf{0} \\ \mathbf{0} & \hat{\mathbf{H}}^* \end{bmatrix}. \quad (4.22)$$

This can be done by breaking the equivalent channel estimate into its real and imaginary components and writing it as a set of matrix equations

$$\begin{bmatrix} \check{\mathbf{G}}_1^r \\ \check{\mathbf{G}}_1^i \\ \check{\mathbf{G}}_2^r \\ \check{\mathbf{G}}_2^i \end{bmatrix} = \begin{bmatrix} \hat{\mathbf{\Theta}}_A^r & -\hat{\mathbf{\Theta}}_A^i \\ \hat{\mathbf{\Theta}}_A^i & \hat{\mathbf{\Theta}}_A^r \\ \hat{\mathbf{\Theta}}_B^r & -\hat{\mathbf{\Theta}}_B^i \\ \hat{\mathbf{\Theta}}_B^i & \hat{\mathbf{\Theta}}_B^r \end{bmatrix} \begin{bmatrix} \hat{\mathbf{H}}^r \\ \hat{\mathbf{H}}^i \end{bmatrix} = \check{\mathbf{G}}_s = \mathbf{T}(\hat{\epsilon}_r, \hat{\psi}_r)\hat{\mathbf{H}}_s \quad (4.23)$$

where the  $\check{\mathbf{G}}_1$  and  $\check{\mathbf{G}}_2$  are the first and second  $N_r \times N_t$  sized blocks of  $\check{\mathbf{G}}$ , respectively, and the superscripts indicate real or imaginary parts, i.e.,  $\check{\mathbf{G}}_1^r = \Re\{\check{\mathbf{G}}_1\}$ ,  $\hat{\mathbf{\Theta}}_A^i = \Im\{\hat{\mathbf{\Theta}}_A\}$ , and so on. This can be solved directly with the pseudoinverse of  $\mathbf{T}$ , which has a simple expression if  $\hat{\mathbf{\Theta}}_A = \hat{\alpha}_r \mathbf{I}$  and  $\hat{\mathbf{\Theta}}_B = \hat{\beta}_r \mathbf{I}$

$$\mathbf{T}^\dagger = \frac{1}{|\hat{\alpha}_r|^2 + |\hat{\beta}_r|^2} \mathbf{T}^T. \quad (4.24)$$

This yields the candidate channel estimates

$$\hat{\mathbf{H}}(\hat{\epsilon}_r, \hat{\psi}_r) = \hat{\mathbf{H}}^r + j\hat{\mathbf{H}}^i = \frac{\hat{\alpha}_r^* \check{\mathbf{G}}_1 + \hat{\beta}_r \check{\mathbf{G}}_2^*}{|\hat{\alpha}_r|^2 + |\hat{\beta}_r|^2} \quad (4.25)$$

$$\hat{\mathbf{H}}_e(\hat{\epsilon}_r, \hat{\psi}_r) = \begin{bmatrix} \hat{\mathbf{H}}(\hat{\epsilon}_r, \hat{\psi}_r) & \mathbf{0} \\ \mathbf{0} & \hat{\mathbf{H}}^*(\hat{\epsilon}_r, \hat{\psi}_r) \end{bmatrix}. \quad (4.26)$$

Another option which, somewhat surprisingly, yields similar results is to compute the block diagonal structure preserving least squares solution of

$$\check{\mathbf{h}}_e^{\text{LS}}(\hat{\epsilon}_r, \hat{\psi}_r) = \underset{\check{\mathbf{h}}_e}{\text{argmin}} \|\check{\mathbf{g}} - \check{\mathbf{\Theta}}(\hat{\epsilon}_r, \hat{\psi}_r)\check{\mathbf{h}}_e\|_2^2, \quad (4.27)$$

s.t.  $\check{\mathbf{h}}_e' = 0$  if it is a secondary diagonal block element,

where  $\check{\mathbf{g}}$ , in this context, denotes the estimated equivalent channel. This can be computed by translating the usual minimum norm solution along the null-space of  $\check{\mathbf{\Theta}}(\hat{\epsilon}_r, \hat{\psi}_r)$  to zero-out the desired  $2N_r N_t$  elements. This solution does not exist when the null space of  $\check{\mathbf{\Theta}}$  does not span the secondary diagonal blocks. In that case the solution with nonzero left upper block and at most  $2N_r N_t$  zeros in total must be used (such as the output of Matlab's *mldivide*). Then, omitting the dependence on  $\hat{\epsilon}_r$  and  $\hat{\psi}_r$  to avoid heavy notation,  $\hat{\mathbf{H}}$  is the upper left  $N_r \times N_t$  block of  $\text{vec}^{-1}(\check{\mathbf{h}}_e^{\text{LS}})$ , and  $\hat{\mathbf{H}}_e = \text{Diag}(\hat{\mathbf{H}}, \hat{\mathbf{H}}^*)$ . The outputs of both methods are numerically very close and present no noticeable difference in the simulations.

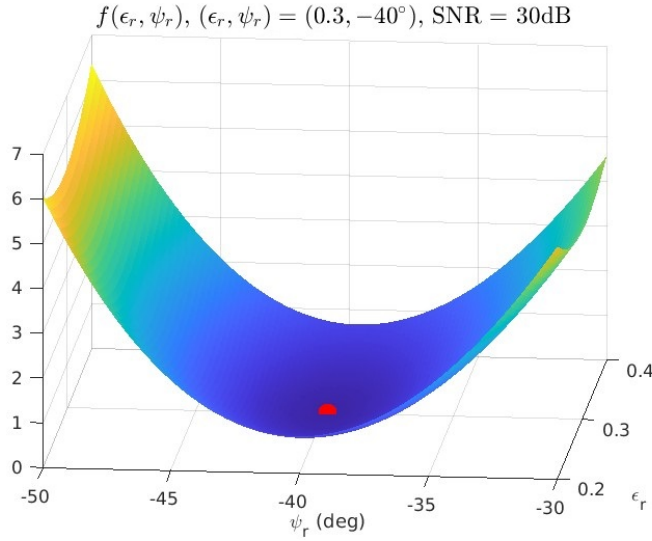


Figure 4.2. Surface plot of  $f(\epsilon_r, \psi_r)$  for an  $8 \times 2$  Rayleigh channel at 30 dB SNR and a 1000 sample white Gaussian noise pilot sequence. The red dot shows the position of the optimal value.

Suppose we also know  $\mathbf{R}_n$  and  $\mathbf{Q}_n$  with sufficient precision. We thereby have candidate covariance and complementary covariance matrices of  $\mathbf{y}$  as functions of  $\epsilon_r$  and  $\psi_r$

$$\hat{\mathbf{R}}_y(\epsilon_r, \psi_r) = \hat{\mathbf{G}}\mathbb{E}\{\mathbf{s}_e\mathbf{s}_e^H\}\hat{\mathbf{G}}^H + \mathbf{R}_n \quad (4.28)$$

$$\hat{\mathbf{Q}}_y(\epsilon_r, \psi_r) = \hat{\mathbf{G}}\mathbb{E}\{\mathbf{s}_e\mathbf{s}_e^T\}\hat{\mathbf{G}}^T + \mathbf{Q}_n \quad (4.29)$$

$$\hat{\mathbf{G}}(\hat{\epsilon}_r, \hat{\psi}_r) = \hat{\mathbf{\Theta}}(\hat{\epsilon}_r, \hat{\psi}_r)\hat{\mathbf{H}}_e(\hat{\epsilon}_r, \hat{\psi}_r). \quad (4.30)$$

If the pilot sequence is sufficiently long, the true covariance and complementary covariance matrices can be estimated with an arbitrary precision. Suppose we have sufficiently accurate estimates of  $\mathbf{R}_y$  and  $\mathbf{Q}_y$ , then choose the candidate matrices that minimize the objective function

$$f(\hat{\epsilon}_r, \hat{\psi}_r) = \|\mathbf{E}_R(\hat{\epsilon}_r, \hat{\psi}_r)\|_F^2 + \|\mathbf{E}_Q(\hat{\epsilon}_r, \hat{\psi}_r)\|_F^2 \quad (4.31)$$

$$= \text{tr}\{\mathbf{E}_R^H\mathbf{E}_R\} + \text{tr}\{\mathbf{E}_Q^H\mathbf{E}_Q\}, \quad (4.32)$$

in which  $\mathbf{E}_R = \mathbf{R}_y - \hat{\mathbf{R}}_y$  and  $\mathbf{E}_Q = \mathbf{Q}_y - \hat{\mathbf{Q}}_y$ . And finally  $(\epsilon_r^{\text{opt}}, \psi_r^{\text{opt}}) = \text{argmin} f(\hat{\epsilon}_r, \hat{\psi}_r)$ . The optimization problem is usually well-behaved and the optima are easy to find assuming the starting point is within typical values for the IQI parameters. An example of the objective function shape around the optimal point is shown in Fig. 4.2.

We then use the estimated IQI parameters to get  $\mathbf{x}$  from  $\mathbf{y}$  using

$$\begin{bmatrix} \tilde{\mathbf{x}} \\ \tilde{\mathbf{x}}^* \end{bmatrix} = \begin{bmatrix} \hat{\mathbf{\Theta}}_A(\epsilon_r^{\text{opt}}, \psi_r^{\text{opt}}) & \hat{\mathbf{\Theta}}_B(\epsilon_r^{\text{opt}}, \psi_r^{\text{opt}}) \\ \hat{\mathbf{\Theta}}_B^*(\epsilon_r^{\text{opt}}, \psi_r^{\text{opt}}) & \hat{\mathbf{\Theta}}_A^*(\epsilon_r^{\text{opt}}, \psi_r^{\text{opt}}) \end{bmatrix}^{-1} \begin{bmatrix} \mathbf{y} \\ \mathbf{y}^* \end{bmatrix} \quad (4.33)$$

#### 4.5 Analysis of the objective function

In this section, we will explore the characteristics of the objective function to verify if it is suitable to be optimized with gradient based descent methods. Specifically, we will try to find

a region in which the function is convex or quasi-convex, and provide an expression for its gradient.

The initial tries in finding conditions for convexity of  $f$  were by exploring the eigenvalues of the Hessian of  $f$ . Notice that the hessian is a  $2 \times 2$  matrix, and thus has an closed form expression for its eigenvalues. These expressions are, however, very long and complicated functions of  $\hat{\epsilon}_r$  and  $\hat{\psi}_r$ , and extracting information from them proved to be an ineffective approach. Another approach, which proved to be more insightful, was to assume that the WL channel estimate  $\tilde{\mathbf{G}}$  is ideal and then studying this function. This is what we will do in the following derivations.

Assume that we have a perfect WL channel estimate  $\tilde{\mathbf{G}}$ . Then

$$\tilde{\mathbf{G}} = \mathbf{G} = [\mathbf{G}_1 \quad \mathbf{G}_2] = [\alpha_r \mathbf{H} \quad \beta_r \mathbf{H}^*]. \quad (4.34)$$

From (4.20) and (4.21), by denoting  $\mathbf{R}_s = \mathbb{E} \{\mathbf{s}\mathbf{s}^H\}$  and assuming  $\mathbf{Q}_s = \mathbb{E} \{\mathbf{s}\mathbf{s}^T\} = 0$ , we can say that

$$\mathbf{R}_y = \mathbf{G}_1 \mathbf{R}_s \mathbf{G}_1^H + \mathbf{G}_2 \mathbf{R}_s \mathbf{G}_2^H + \mathbf{R}_n = |\alpha_r|^2 \mathbf{H} \mathbf{R}_s \mathbf{H}^H + |\beta_r|^2 \mathbf{H}^* \mathbf{R}_s^* \mathbf{H}^T + \mathbf{R}_n \quad (4.35)$$

$$\mathbf{Q}_y = \mathbf{G}_1 \mathbf{R}_s \mathbf{G}_2^T + \mathbf{G}_2 \mathbf{R}_s^* \mathbf{G}_1^T + \mathbf{R}_n = \alpha_r \beta_r (\mathbf{H} \mathbf{R}_s \mathbf{H}^H + \mathbf{H}^* \mathbf{R}_s^* \mathbf{H}^T) + \mathbf{Q}_n. \quad (4.36)$$

If we define

$$a = \frac{\alpha_r |\hat{\alpha}_r|^2 + \beta_r^* \hat{\alpha}_r \hat{\beta}_r}{|\hat{\alpha}_r|^2 + |\hat{\beta}_r|^2} \quad (4.37)$$

$$b = \frac{\alpha_r^* \hat{\alpha}_r \hat{\beta}_r + \beta_r |\hat{\beta}_r|^2}{|\hat{\alpha}_r|^2 + |\hat{\beta}_r|^2}, \quad (4.38)$$

from (4.25) we get

$$\hat{\mathbf{R}}_y = |a|^2 \mathbf{H} \mathbf{R}_s \mathbf{H}^H + |b|^2 \mathbf{H}^* \mathbf{R}_s^* \mathbf{H}^T + \mathbf{R}_n \quad (4.39)$$

$$\hat{\mathbf{Q}}_y = ab (\mathbf{H} \mathbf{R}_s \mathbf{H}^H + \mathbf{H}^* \mathbf{R}_s^* \mathbf{H}^T) + \mathbf{Q}_n. \quad (4.40)$$

The matrix errors are

$$\mathbf{E}_R = (|\alpha_r|^2 - |a|^2) \mathbf{H} \mathbf{R}_s \mathbf{H}^H + (|\beta_r|^2 - |b|^2) \mathbf{H}^* \mathbf{R}_s^* \mathbf{H}^T \quad (4.41)$$

$$\mathbf{E}_Q = (\alpha_r \beta_r - ab) \mathbf{H} \mathbf{R}_s \mathbf{H}^H + (\alpha_r \beta_r - ab) \mathbf{H}^* \mathbf{R}_s^* \mathbf{H}^T \quad (4.42)$$

Expressing the Frobenius norm of the matrix errors we get

$$\begin{aligned} \|\mathbf{E}_R\|_F^2(\hat{\epsilon}_r, \hat{\psi}_r) &= \left( |\alpha_r|^2 - |a|^2 \right)^2 \|\mathbf{H} \mathbf{R}_s \mathbf{H}^H\|_F + \left( |\beta_r|^2 - |b|^2 \right)^2 \|\mathbf{H}^* \mathbf{R}_s^* \mathbf{H}^T\|_F \\ &\quad + 2\Re \left\{ \left( |\alpha_r|^2 - |a|^2 \right) \left( |\beta_r|^2 - |b|^2 \right) \langle \mathbf{H} \mathbf{R}_s \mathbf{H}^H, \mathbf{H}^* \mathbf{R}_s^* \mathbf{H}^T \rangle_F \right\}, \end{aligned} \quad (4.43)$$

where  $\langle \mathbf{A}, \mathbf{B} \rangle_F \equiv \text{Tr}\{\mathbf{A}^H \mathbf{B}\}$  is the Frobenius inner product. The above equation comes from the property that  $\|\mathbf{A} + \mathbf{B}\|_F^2 = \|\mathbf{A}\|_F^2 + \|\mathbf{B}\|_F^2 + 2\Re \{ \langle \mathbf{A}, \mathbf{B} \rangle_F \}$ . Similarly, for  $\mathbf{E}_Q$

$$\|\mathbf{E}_Q\|_F^2(\hat{\epsilon}_r, \hat{\psi}_r) = |\alpha_r \beta_r - ab|^2 \|\mathbf{H} \mathbf{R}_s \mathbf{H}^H\|_F + |\alpha_r \beta_r - ab|^2 \|\mathbf{H}^* \mathbf{R}_s^* \mathbf{H}^T\|_F \quad (4.44)$$

$$+ 2\Re \left\{ (\alpha_r \beta_r - ab)^2 \langle \mathbf{H} \mathbf{R}_s \mathbf{H}^H, \mathbf{H}^* \mathbf{R}_s^* \mathbf{H}^T \rangle_F \right\}. \quad (4.45)$$

Respectively, (4.43) and (4.44) can be simplified to

$$\|\mathbf{E}_R\|_F^2(\hat{\epsilon}_r, \hat{\psi}_r) = \left[ |\alpha_r|^2 + |\beta_r|^2 - |a|^2 - |b|^2 \right]^2 \|\mathbf{H}_R \mathbf{S} \mathbf{H}^H\|_F^2 \quad (4.46)$$

$$\|\mathbf{E}_Q\|_F^2(\hat{\epsilon}_r, \hat{\psi}_r) = |2\Re\{\alpha_r \beta_r - ab\}|^2 \|\mathbf{H}_R \mathbf{S} \mathbf{H}^H\|_F^2 \quad (4.47)$$

Expanding and simplifying (4.46) yields

$$\|\mathbf{E}_R\|_F^2(\hat{\epsilon}_r, \hat{\psi}_r) = |\gamma(\hat{\epsilon}_r, \hat{\psi}_r)|^2 \|\mathbf{H}_R \mathbf{S} \mathbf{H}^H\|_F^2 \quad (4.48)$$

$$\gamma(\hat{\epsilon}_r, \hat{\psi}_r) = \frac{1}{2} + \frac{\epsilon_r^2 + 2\epsilon_r - 2(\epsilon_r + 1)(\hat{\epsilon}_r + 1)}{2(\hat{\epsilon}_r^2 + 2\hat{\epsilon}_r + 2)} \cos(\hat{\psi}_r - \psi_r). \quad (4.49)$$

Let us further study the  $\gamma$  function so that we can get some insight on the properties of our objective function. In Appendix 2 it is shown that  $\gamma$  is quasiconvex on the domain

$$\Omega = \left\{ (\hat{\epsilon}_r, \hat{\psi}_r) : \gamma(\hat{\epsilon}_r, \hat{\psi}_r) \leq \frac{(\epsilon_r + 1)^2}{2}, -1 < \hat{\epsilon}_r < 1, -\frac{\pi}{2} < \hat{\psi}_r < \frac{\pi}{2} \right\}. \quad (4.50)$$

and has a unique minimum at  $(\epsilon_r, \psi_r)$ . Besides, if we take its second order Taylor expansion around the  $(\epsilon_r, \psi_r)$  point we get

$$\gamma_T(\hat{\epsilon}_r, \hat{\psi}_r) = \frac{(\hat{\epsilon}_r - \epsilon_r)^2 + (\epsilon_r + 1)^2(\hat{\psi}_r - \psi_r)^2}{2(\epsilon_r^2 + 2\epsilon_r + 2)}, \quad (4.51)$$

which is obviously convex on  $(\hat{\epsilon}_r, \hat{\psi}_r)$ , with minimum on  $(\epsilon_r, \psi_r)$ . This indicates that, in the neighborhood around the optimal point,  $\gamma$  is quadratic and convex. Taking higher order Taylor expansions does not produce any particular insightful expression, only adding increasingly complicated terms.

The results obtained so far show that using only  $\|\mathbf{E}_R\|_F^2(\hat{\epsilon}_r, \hat{\psi}_r)$  should already be enough to achieve convergence to the true values of the IQI coefficients. However, experience from the simulations shows that incorporating the  $\|\mathbf{E}_Q\|_F^2(\hat{\epsilon}_r, \hat{\psi}_r)$  massively improves convergence, requiring shorter sequence lengths and not being as sensitive to the SNR. We will only present the expression for  $2\Re\{\alpha_r \beta_r - ab\}$ , from that we'll assume intuitively (thus, without proof) that it has a minimum at the true value of the IQI coefficients and is also quasiconvex (and it is very likely also convex) on the neighborhood of its optimum. The expression  $2\Re\{\alpha_r \beta_r - ab\}$  can be written as

$$\begin{aligned} & 2\Re\{\alpha_r \beta_r - ab\} = \\ & \frac{-\epsilon_r(\epsilon_r + 2)(3\hat{\epsilon}_r^2 + 6\hat{\epsilon}_r + 4) + 2(\epsilon_r + 1)(\hat{\epsilon}_r^2 + \hat{\epsilon}_r)(\hat{\epsilon}_r + 2) \cos(\hat{\psi}_r - \psi_r) + \hat{\epsilon}_r(\hat{\epsilon}_r + 2)(\hat{\epsilon}_r^2 + 2\hat{\epsilon}_r + 2)}{2(\hat{\epsilon}_r^2 + 2\hat{\epsilon}_r + 2)^2}, \end{aligned} \quad (4.52)$$

which is considerably more complicated to analyse in the same fashion that we did with  $\gamma$ , because it is a higher order polynomial. However, to confirm that there exists an optimum at the desired point, it can be shown that  $2\Re\{\alpha_r \beta_r - ab\} = 0$  if  $\hat{\epsilon}_r = \epsilon_r$  and  $\hat{\psi}_r = \psi_r$ .

## 4.6 Numerical results

The simulation setup used to evaluate the effectiveness of the proposed method is a single anchor position estimation problem using the first samples of a 5G NR random OFDM waveform as a

Table 4.1. Fundamental simulation parameters.

Channel Model	Single LOS path
Path gain	0 dB
Subcarrier Spacing	60 kHz
Resource Blocks	52
Cyclic Prefix	Extended
Modulation	QPSK
Carrier Frequency	4 GHz
Tx Antennas	1
Rx Antennas	8
Channel Sample Density	$inf$
DoA Algorithm	MUSIC
Ranging Algorithm	Matched filter detector

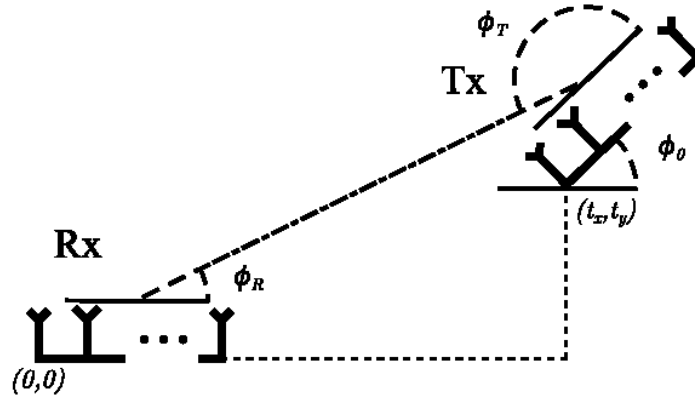


Figure 4.3. Transmitter and receiver geometry.

pilot sequence. The used waveform is just one example to demonstrate the performance. Many other reasonable pilot sequences could be used in a straightforward manner. The simulations use the resources offered by the Matlab 5G NR package, and the fundamental simulation parameters are described in Table 4.1. A 5G NR waveform with 52 resource blocks and 60 kHz subcarrier spacing has a 37.44 MHz bandwidth. The transmitter (Tx) and receiver (Rx) are coplanar with geometry and angles as defined in Fig. 4.3. In all results the receiver is located at (0 m, 0 m) and the transmitter at (40 m, 10 m) with an angle of  $\phi_0 = \pi/2$  rad. The  $\phi_0$  angle matters even in single antenna scenario, because the antenna elements are modeled according to Section 7.3 of [41] and are not isotropic elements. The objective function is optimized using the Nelder-Mead simplex search algorithm as defined by Lagarias *et al.* [42].

Signal detection and synchronization is conducted by finding the maximum value of the output of a matched filter. This procedure ensures coarse timing and symbol synchronization if the waveform is properly oversampled. Oversampling ensures that adjacent samples are highly correlated, thus making the channel estimation and IQI computations more robust to minor synchronization errors. We assume known transmission time and perfectly synchronized clocks between Tx and Rx as a way of isolating the impacts of IQI on ranging accuracy.

The equivalent channel estimation and the IQI parameter estimation procedures as described consider that the received signal samples  $\mathbf{y}(i)$  are detected at the correct instant, i.e., at the true first signal sample. If this is satisfied, then the correct relation between the received sample  $\mathbf{y}(i)$

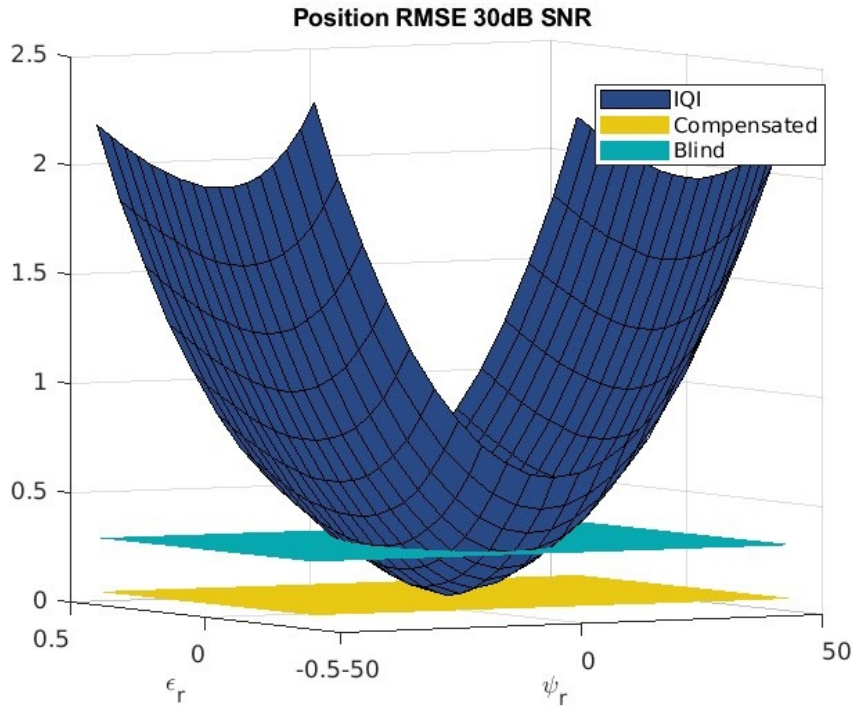


Figure 4.4. Position RMSE grid sweep for the IQI affected signal, signal compensated signal with our method, and signal compensated with the blind estimator at 30 dB SNR.

and the transmitted sample of the pilot sequence  $\mathbf{s}(i)$  can be established.

In general, the signal may not be detected at the perfect time instant, because in a practical situation it is difficult to determine the optimum sampling time and avoiding such a strict synchronization requirement simplifies the procedure. The equations for the maximum likelihood covariance and complementary covariance matrices of  $\mathbf{y}$ , will now incorporate this error in their calculation. The effects of this error are not noticeable at all in the root mean square error (RMSE) of the position estimates, to the point where results of the simulations with imperfect synchronization are indistinguishable from the perfectly synchronized case by simply visualizing the plots.

We consider that all RF chains share the same IQI coefficients in the simulations, this allows us to visualize the impact of the phase and amplitude IQI parameters in the MSE of the position estimates. We first present an IQI parameter grid sweep over  $(\epsilon_r, \psi_r)$  in Figs. 4.4 and 4.5 for SNR values of 30 dB and 10 dB, respectively. The number of iterations per grid point is 50, the pilot sequence has 50 samples before interpolation with rate 16. The signal sampling rate is originally set by the OFDM modulator as a function of the bandwidth. We linearly interpolate the samples to increase the time resolution of the detector up to values that are acceptable in a ranging context, this is analogous to an oversampling operation. The method is very successful at eliminating the impact of IQI on positioning accuracy. By analysing Figs. 4.4 and 4.5 we can see that the compensated and the original signals without IQI produce positioning estimates of almost identical RMSE, i.e., the compensated RMSE is close to the plane tangent to the IQI RMSE surface at the  $(\epsilon_r, \psi_r) = (0, 0)$  point and parallel to the  $\epsilon_r, \psi_r$ -plane. This represents a major improvement in comparison to the RMSE of the positioning estimates extracted from the IQI corrupted signal. We also observe that the performance is almost the same at both SNR values, which is an interesting phenomenon and will be addressed below.

As a reference point, to verify the relative performance of the method presented in this section,

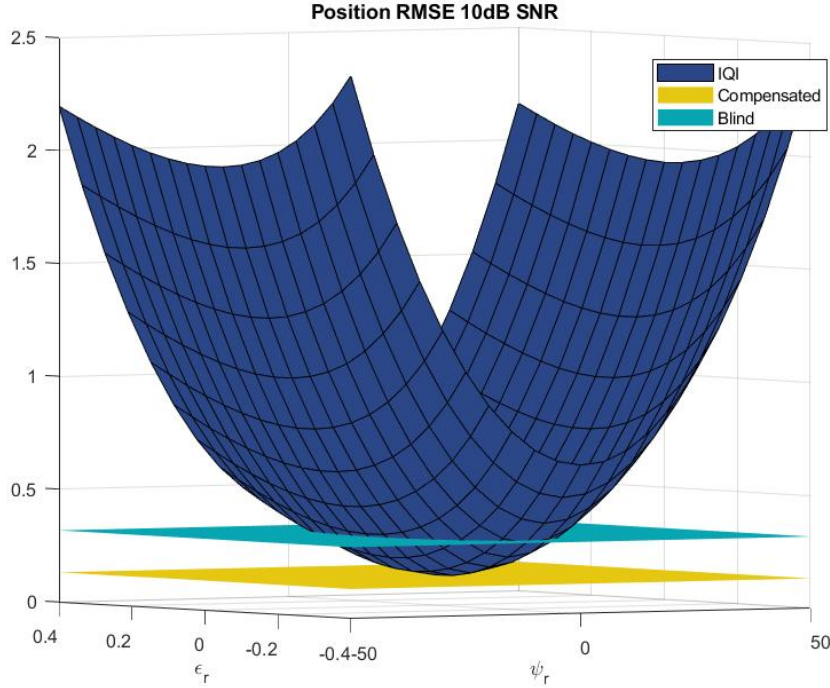


Figure 4.5. Position RMSE grid sweep for the IQI affected signal, signal compensated signal with our method, and signal compensated with the blind estimator at 10 dB SNR.

we compare it to a blind maximum likelihood estimator for the IQI parameters assuming Gaussian received signal, equivalent to the estimator described in [15], restated in (3.10) and (3.11). This blind estimator is essentially the one in [15] adapted to conform with the IQI model used here. The details of this process are contained in Appendix 3.

In the described simulation scenario at 30 dB SNR, our method outperformed the blind estimator by an average 24.56 cm reduction in position RMSE. For the same scenario at 10 dB SNR, our method outperforms the blind estimator by an average reduction of 18.23 cm.

If all RF chains share IQI coefficients, one may substitute  $\sum_{n=0}^{N-1} y_k(n)y_k^*(n)$  by

$$\text{mean} \left( \text{diag} \left( \sum_{n=0}^{N-1} \mathbf{y}_k(n)\mathbf{y}_k^H(n) \right) \right),$$

and similarly for  $\sum_{n=0}^{N-1} y_k(n)y_k(n)$  by using a transpose instead of a hermitian conjugate. This concludes the derivation of the blind estimator, we will now resume the analysis of the numerical results.

In Fig. 4.6 we assess the impacts of the SNR and the transmitted pilot sequence length on the estimated position MSE. We present the results as the MSE ratio in dB, i.e., the difference of the MSE logarithms of a particular case and the clean case. This keeps the values within a convenient range. Notice that once the pilot sequence is long enough (around 600 samples in this particular example) our method is capable of perfectly compensating the IQI impacts on the position estimate at all tested SNR points. For negative (in dB) SNR, the position estimate without IQI is already very inaccurate and IQI does not significantly worsen the estimates in this case, thus the values to the left approach 0. Another interesting effect is that the uncompensated position estimates somewhat improve for larger sequence length, this is largely because more samples allow a better pseudospectrum estimate in the MUSIC algorithm, used for DoA estimation. A

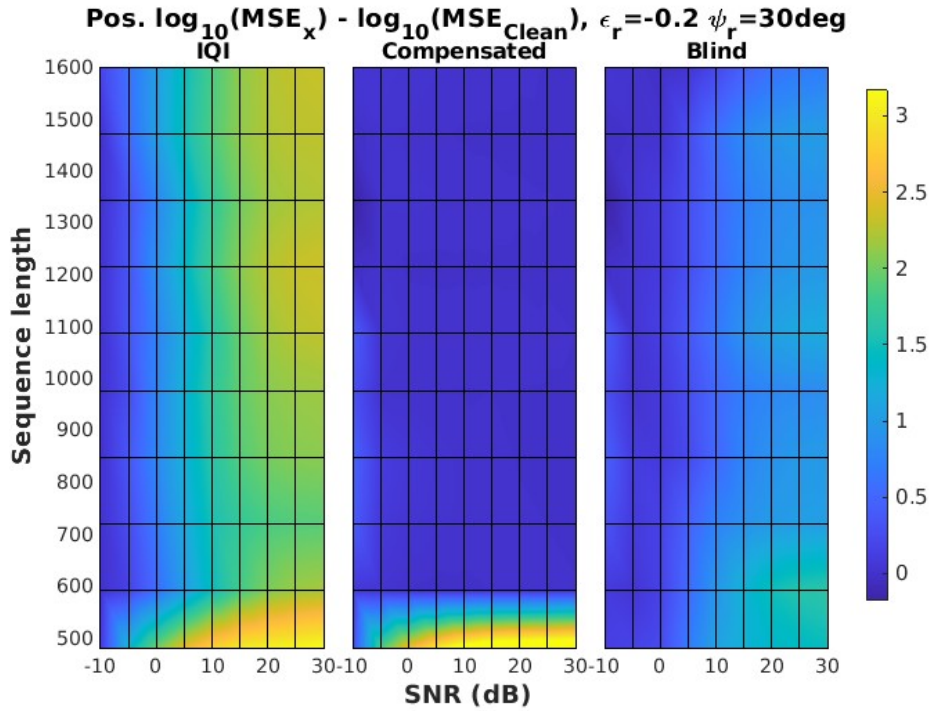


Figure 4.6. Difference between the base 10 logarithms of the position estimate MSE of a particular case and the case without IQI (Clean) as a function of the transmitted sequence length and SNR. IQI parameters set to  $\epsilon_r = -0.2$  and  $\psi_r = 30^\circ$ . The plots show from left to right: the uncompensated case (IQI), the case with the compensated signal using our method (Compensated), and the case where compensation is done with a blind estimator (Blind).

longer pilot sequence also makes the matched filter include more samples, reducing the chance of spurious detections.

In Fig. 4.7 we present a comparison between the estimated position RMSE values achieved by our method (Compensated), the blind estimator (Blind), the uncompensated signal (IQI), and the case where no IQI exists (Clean). In this figure, the IQI coefficients are kept constant at  $\epsilon_r = -0.4$  and  $\psi_r = 30^\circ$  and the results are averaged over 50 iterations. The pilot sequence length is also kept constant at 800 samples (50 samples interpolated at a rate of 16). We observe that our method almost completely eliminates the IQI for all SNR values, i.e., the Compensated and Clean curves basically overlap. Additionally, the proposed method clearly presents a major performance improvement when compared to the blind estimator or the uncompensated case.

It is also noticeable in Fig. 4.7 that the RMSE saturates at high SNR instead of improving arbitrarily. This can be attributed to finite time resolution due to sampling rate, finite DoA angle resolution in the MUSIC algorithm, suboptimal pilot sequence choice, because the used waveform is not optimized for the application, and possibly short pilot sequence length. Exploring this SNR performance saturation in more detail is left for future work.

Comparing computational complexity and execution time between both methods, we have timed them on a simulation of the transmission of  $N_s = 800$  samples,  $N_r = 8$  receiver antennas,  $N_t = 1$  transmit antennas, over a complex Rayleigh channel with  $\text{Var}\{h_{ij}\} = 1$ , averaged over 500 trials. The proposed method takes on average (excluding channel estimation) 22.363 ms of simulation time in a Linux server in an Intel Xeon Gold 6126 CPU, while the blind estimation takes 0.808 ms on the same hardware. Our method comes at the disadvantage of requiring channel estimation of a channel in widely-linear form. The proposed method, including channel

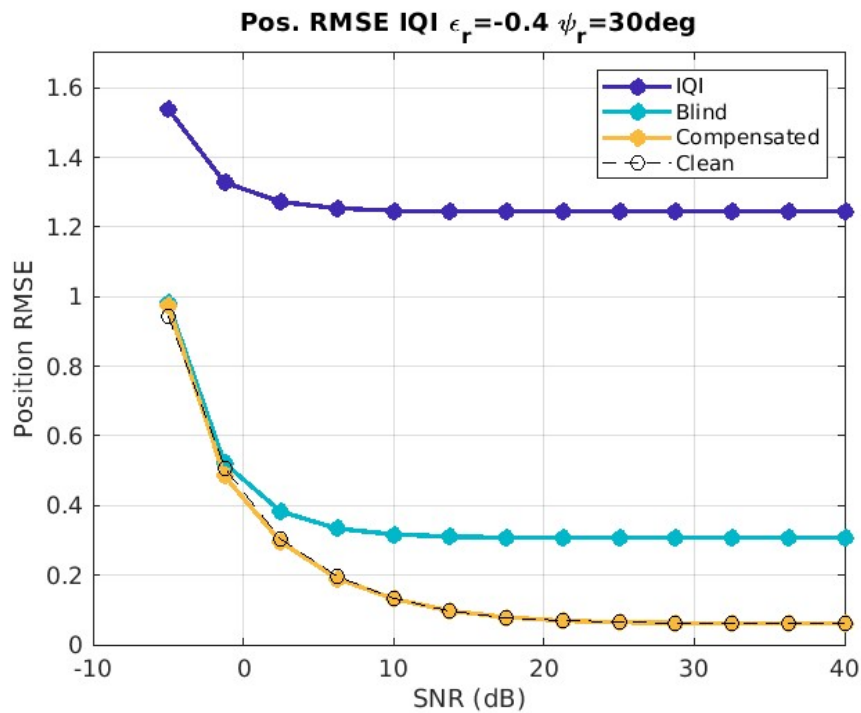


Figure 4.7. Position estimate RMSE as a function of the SNR with fixed pilot sequence length.

estimation, took on average 1.170 seconds to compute. Naturally, the channel estimate can be used for other procedures that would also require a channel estimate. We want to emphasize that the presented times are computer simulation times used just for relative comparisons, and the actual computing time on dedicated hardware would be much faster. Furthermore, the IQI coefficients only need to be estimated once (or periodically at relatively long periods), so even if the IQI estimation takes long enough to render the latest positioning data obsolete, the obtained IQI estimates can now be reused for future transmissions.

## 5 5G NEW RADIO COMPLIANT IQI COMPENSATION

This chapter we will address some approaches to perform IQI parameter estimation and compensation within OFDM and 5G NR environments. First we will contemplate the transmission of entire pilot frames or subframes, i.e., when the entire transmitted frame is known. This is in general not the most resource economic approach since it requires spending entire subframes almost exclusively for IQI compensation. Nevertheless it has some justification, mainly because IQI parameters do not vary significantly over time and the estimates may be reliably used for a long time. Therefore, it also does not impact the throughput of the data, due to the relative sparsity of the pilot subframes.

As a second possible approach, we may use some of the reference signals specified by the 5G standard [43], such as the demodulation reference signal (DM-RS) and the phase tracking reference signal (PT-RS), to continuously estimate the IQI coefficients. The advantage of using standard defined reference signals is that they are frequently and reliably transmitted during normal operation of a 5G data link, thus no extra implementation-specific pilot frames for IQI compensation need to be scheduled

### 5.1 Estimating over pilot slots

Consider the transmission of an OFDM signal adhering to the 5G NR standard. Consider the case of a single transmission layer, then a time-invariant channel can be modeled as

$$\mathbf{h}(\omega) = \mathbf{H}_{\text{phy}}(\omega)\mathbf{p} = \begin{bmatrix} h_0(\omega) \\ h_1(\omega) \\ \vdots \\ h_{N_R-1}(\omega) \end{bmatrix}, \quad (5.1)$$

where  $\mathbf{p}$  is the  $N_t \times 1$  analog precoding vector that maps transmission layers to physical antenna elements,  $\mathbf{H}_{\text{phy}}(\omega)$  is the frequency dependent physical  $N_r \times N_t$  channel matrix, where  $N_r$  and  $N_t$  are the number of receive and transmit antennas respectively. Consider also that all antennas share IQI coefficients, this is justified by noticing that any antennas that do not share IQI may simply be excluded from the computations. Following the reasoning on [12], we assume that the cyclic prefix length is at least as long as the channel impulse response, to avoid inter-symbol interference (ISI). Under perfect timing and frequency synchronization, disregarding RF front-end imperfections, and under no inter-carrier interference (ICI), the  $m$ th OFDM received symbol at the  $k$ th subcarrier can be expressed as

$$\mathbf{x}_k(m) = \mathbf{h}_k s_k(m) + \mathbf{n}_k(m), \quad k \in \{-K, \dots, K\}, \quad (5.2)$$

where  $s_k(m)$  is the  $m$ th transmitted symbol at the  $k$ th subcarrier, and  $k = 0$  indicates the DC subcarrier, with  $k$  increasing in frequency from  $-K$  to  $K$ . The received symbol  $\mathbf{x}_k(m)$  has  $N_r$  elements, each one associated with one of the receive antennas. We can treat each of the subcarriers as orthogonal, static subchannels.

Let us now incorporate the effects of receiver IQI. Since the Fourier transform of the conjugate  $\mathcal{F}\{x^*(t)\}(\omega)$  is equal to  $\mathcal{F}\{x(t)\}^*(-\omega)$ , the effects of IQI can be expressed in the OFDM

subcarriers following the expression

$$\mathbf{y}_k(m) = [\Theta_A \quad \Theta_B] \begin{bmatrix} \mathbf{x}_k(m) \\ \mathbf{x}_{-k}^*(m) \end{bmatrix} \quad (5.3)$$

$$= [\Theta_A \quad \Theta_B] \begin{bmatrix} \mathbf{h}_k & \mathbf{0} \\ \mathbf{0} & \mathbf{h}_{-k}^* \end{bmatrix} \begin{bmatrix} s_k(m) \\ s_{-k}^*(m) \end{bmatrix} + [\Theta_A \quad \Theta_B] \begin{bmatrix} \mathbf{n}_k(m) \\ \mathbf{n}_{-k}^*(m) \end{bmatrix} \quad (5.4)$$

$$= \begin{bmatrix} y_{k,0}(m) \\ y_{k,1}(m) \\ \vdots \\ y_{k,N_r-1}(m) \end{bmatrix} = \begin{bmatrix} g_{k,0}^1 & g_{k,0}^2 \\ g_{k,1}^1 & g_{k,1}^2 \\ \vdots & \vdots \\ g_{k,N_r-1}^1 & g_{k,N_r-1}^2 \end{bmatrix} \begin{bmatrix} s_k(m) \\ s_{-k}^*(m) \end{bmatrix} + \mathbf{w}_k(m), \quad (5.5)$$

where  $\mathbf{w}_k(m) = \Theta_A \mathbf{n}_k(m) + \Theta_B \mathbf{n}_{-k}^*(m)$  is the IQI affected noise at the  $k$ th subcarrier and  $m$ th OFDM symbol. Suppose that we receive  $N_s$  OFDM pilot symbols. Then we can compute a WL-LS estimate of the subchannel of the  $k$ th subcarrier and  $l$ th antenna

$$\begin{bmatrix} \tilde{g}_{k,l}^1 \\ \tilde{g}_{k,l}^2 \end{bmatrix} = \begin{bmatrix} s_{k,l}(0) & s_{-k,l}^*(0) \\ s_{k,l}(1) & s_{-k,l}^*(1) \\ \vdots & \vdots \\ s_{k,l}(N_s-1) & s_{-k,l}^*(N_s-1) \end{bmatrix}^\dagger \begin{bmatrix} y_{k,l}(0) \\ y_{k,l}(1) \\ \vdots \\ y_{k,l}(N_s-1) \end{bmatrix}, \quad (5.6)$$

where  $\dagger$  denotes the Moore-Penrose pseudoinverse. We compute WL channel estimates over all subcarriers which contain known transmitted symbols, we will refer to those estimates as WL channel estimates or as equivalent channel estimates, interchangeably.

Let  $N_c = 2K + 1$  denote the number of OFDM subcarriers, which is a direct consequence of the defined numerology. We now select only a fraction  $N'_c = \lceil \nu N_c \rceil$  of the subcarriers, with  $\nu \in (0, 1)$ , which we will use to estimate the IQI parameters. Different criteria may be used to specify the subset of used subcarriers, for example: one may compute a linear subchannel LS estimate  $\hat{\mathbf{H}}_k$  for each subcarrier, the  $N'_c$  subcarriers with higher sum of squared magnitudes  $\hat{\mathbf{H}}_k^H \hat{\mathbf{H}}_k$  are then selected. Other possibility would be to select the subchannels with highest  $\sum_{l=0}^{N_r-1} |g_{k,l}^1|^2 + |g_{k,l}^2|^2$ , or subchannel-antenna pairs  $(k, l)$  with highest  $|g_{k,l}^1|^2 + |g_{k,l}^2|^2$ , this is justified in the sense that, if one wants to avoid computing another set of channel estimates (as would happen when computing linear channel estimates),  $\hat{\mathbf{H}}_k^H \hat{\mathbf{H}}_k$  can be very roughly approximated by this method. One might state, however, that linear channel estimates are going to be computed anyway for the purposes of equalization. This would be a valid argument, except that any linear channel estimate computed before compensating for IQI would include errors provoked by it, leading to inaccurate channel estimates in the worst cases. Therefore, it is important to first address the IQI issue before attempting to equalize the channel. Hence, in case we are not using all available pilot subcarriers, the idea is to select the subcarriers which experience the best SNR due to channel gains. On section 5.6, we study the case with subchannel-antenna pairs based on the highest  $|g_{k,l}^1|^2 + |g_{k,l}^2|^2$  criterion, in which case the channel matrices reduce to scalar channel coefficients.

With the set of selected subcarriers  $\mathcal{S}^*$  computed, we now proceed directly to the estimation of IQI parameters. We vectorize the WL estimated channel matrix

$$\check{\mathbf{g}}_k = \text{vec}(\tilde{\mathbf{G}}_k) = \text{vec} \left( \begin{bmatrix} \tilde{g}_{k,0}^1 & \tilde{g}_{k,0}^2 \\ \tilde{g}_{k,1}^1 & \tilde{g}_{k,1}^2 \\ \vdots & \vdots \\ \tilde{g}_{k,N_r-1}^1 & \tilde{g}_{k,N_r-1}^2 \end{bmatrix} \right), \quad (5.7)$$

and compute the channel estimates from the equivalent WL channel *conditioned* on a given value for the IQI coefficients. This can be done by computing from  $\tilde{\mathbf{G}}_k$  and  $\tilde{\mathbf{G}}_{-k}$  the least squares solution for  $\hat{\mathbf{h}}_k$  and  $\hat{\mathbf{h}}_{-k}$  of

$$\begin{bmatrix} \tilde{\mathbf{G}}_k \\ \tilde{\mathbf{G}}_{-k} \end{bmatrix} = \begin{bmatrix} \tilde{\mathbf{g}}_{1,k} & \tilde{\mathbf{g}}_{2,k} \\ \tilde{\mathbf{g}}_{1,-k} & \tilde{\mathbf{g}}_{2,-k} \end{bmatrix} = \begin{bmatrix} \hat{\Theta}_A \hat{\mathbf{h}}_k & \hat{\Theta}_B \hat{\mathbf{h}}_{-k}^* \\ \hat{\Theta}_A \hat{\mathbf{h}}_{-k} & \hat{\Theta}_B \hat{\mathbf{h}}_k^* \end{bmatrix}, \quad (5.8)$$

then breaking (5.8) into its real and imaginary components and writing it as a set of matrix equations

$$\begin{bmatrix} \tilde{\mathbf{g}}_{1,k}^r \\ \tilde{\mathbf{g}}_{1,k}^i \\ \tilde{\mathbf{g}}_{2,k}^r \\ \tilde{\mathbf{g}}_{2,k}^i \\ \tilde{\mathbf{g}}_{1,-k}^r \\ \tilde{\mathbf{g}}_{1,-k}^i \\ \tilde{\mathbf{g}}_{2,-k}^r \\ \tilde{\mathbf{g}}_{2,-k}^i \end{bmatrix} = \begin{bmatrix} \hat{\Theta}_A^r & -\hat{\Theta}_A^i & 0 & 0 \\ \hat{\Theta}_A^i & \hat{\Theta}_A^r & 0 & 0 \\ 0 & 0 & \hat{\Theta}_B^r & \hat{\Theta}_B^i \\ 0 & 0 & \hat{\Theta}_B^i & -\hat{\Theta}_B^r \\ 0 & 0 & \hat{\Theta}_A^r & -\hat{\Theta}_A^i \\ 0 & 0 & \hat{\Theta}_A^i & \hat{\Theta}_A^r \\ \hat{\Theta}_B^r & \hat{\Theta}_B^i & 0 & 0 \\ \hat{\Theta}_B^i & -\hat{\Theta}_B^r & 0 & 0 \end{bmatrix} \begin{bmatrix} \hat{\mathbf{h}}_k^r \\ \hat{\mathbf{h}}_k^i \\ \hat{\mathbf{h}}_{-k}^r \\ \hat{\mathbf{h}}_{-k}^i \end{bmatrix} \Rightarrow \mathbf{g}_k^s = \mathbf{T} \mathbf{h}_k^s, \quad (5.9)$$

where the superscripts indicate the real or imaginary parts, i.e.,  $\tilde{\mathbf{g}}_{1,k}^r = \Re\{\tilde{\mathbf{g}}_{1,k}\}$ ,  $\hat{\Theta}_A^i = \Im\{\hat{\Theta}_A\}$ , and so on. This can be solved directly with the pseudoinverse of  $\mathbf{T}$ , which has a simple expression if  $\hat{\Theta}_A = \hat{\alpha}_r \mathbf{I}$  and  $\hat{\Theta}_B = \hat{\beta}_r \mathbf{I}$

$$\mathbf{T}^\dagger = \frac{1}{|\hat{\alpha}_r|^2 + |\hat{\beta}_r|^2} \mathbf{T}^T. \quad (5.10)$$

Which leads to the channel estimates

$$\hat{\mathbf{h}}_k(\hat{\epsilon}_r, \hat{\psi}_r) = \hat{\mathbf{h}}_k^r + j\hat{\mathbf{h}}_k^i = \frac{\hat{\alpha}_r^* \tilde{\mathbf{g}}_{1,k} + \hat{\beta}_r \tilde{\mathbf{g}}_{2,-k}^*}{|\hat{\alpha}_r|^2 + |\hat{\beta}_r|^2} \quad (5.11)$$

$$\hat{\mathbf{h}}_{-k}(\hat{\epsilon}_r, \hat{\psi}_r) = \hat{\mathbf{h}}_{-k}^r + j\hat{\mathbf{h}}_{-k}^i = \frac{\hat{\alpha}_r^* \tilde{\mathbf{g}}_{1,-k} + \hat{\beta}_r \tilde{\mathbf{g}}_{2,k}^*}{|\hat{\alpha}_r|^2 + |\hat{\beta}_r|^2} \quad (5.12)$$

$$\hat{\mathbf{H}}_{e,k}(\hat{\epsilon}_r, \hat{\psi}_r) = \begin{bmatrix} \hat{\mathbf{h}}_k(\hat{\epsilon}_r, \hat{\psi}_r) & \mathbf{0} \\ \mathbf{0} & \hat{\mathbf{h}}_{-k}^*(\hat{\epsilon}_r, \hat{\psi}_r) \end{bmatrix}. \quad (5.13)$$

Now we define

$$\mathbf{G}'_k(\hat{\epsilon}_r, \hat{\psi}_r) = \hat{\Theta}(\hat{\epsilon}_r, \hat{\psi}_r) \hat{\mathbf{H}}_{e,k}(\hat{\epsilon}_r, \hat{\psi}_r), \quad (5.14)$$

and choose an objective function to optimize over the candidate IQI coefficients  $(\hat{\epsilon}_r, \hat{\psi}_r)$ . Minimizing the sum of the Frobenius norms of the covariance and complementary covariance matrices of  $\mathbf{y}_k$  is not a reliable approach when dealing with just a few time domain symbols, because the covariance matrices cannot be accurately estimated unless we have many samples. However, if we have sufficient time domain samples, using the covariance matrices is an option. Another approach, which is more computationally costly but capitalizes on the available more precise symbol synchronization (compared to the previous positioning scenario which only had

a matched filter detector for detecting the beginning of signal reception) and pilot symbols, is to minimize the sum of the square errors between received samples and expected samples:

$$(\hat{\epsilon}_r^{\text{opt}}, \hat{\psi}_r^{\text{opt}}) = \underset{\hat{\epsilon}_r, \hat{\psi}_r}{\text{argmin}} f(\hat{\epsilon}_r, \hat{\psi}_r) \quad (5.15)$$

$$f(\hat{\epsilon}_r, \hat{\psi}_r) = \sum_{k \in \mathcal{S}^*} \sum_{m=0}^{N_s-1} \|\mathbf{e}_{k,m}(\hat{\epsilon}_r, \hat{\psi}_r)\|^2 \quad (5.16)$$

$$\mathbf{e}_{k,m}(\hat{\epsilon}_r, \hat{\psi}_r) = \mathbf{y}_k(m) - \mathbf{G}'_k(\hat{\epsilon}_r, \hat{\psi}_r) \mathbf{s}_{e,k}(m) \quad (5.17)$$

The drawbacks of the described objective function are related with the computational load associated with it and its vulnerability to low SNR. Naturally, as more subcarriers and symbols are included, the better the estimates become, at the cost of more computations needed per iteration of the optimization algorithm due to the cost of computing the objective function itself. Numerical experimentation shows that the Nelder-Mead simplex search optimization methods can reliably solve this optimization problem when the equivalent channel estimates are accurate.

There is also the option of selecting subsets of antennas within each subcarrier, so we exclude the antennas that experience the worse channel gains. We may then select only subchannels and antennas with higher channel gain to strike a balance between quality of the IQI estimates and computational cost if computing resources are scarce. As previously mentioned, this is the option considered on Section 5.6, where subchannel-antenna pairs with highest  $|g_{k,l}^1|^2 + |g_{k,l}^2|^2$  are selected. For this, the objective function is modified such that (5.17) is no longer a vector, but a scalar corresponding to the  $l$ th entry of  $\mathbf{e}_{k,m}$ , and the summation over  $k$  in (5.16) is now performed over the selected  $(k, l)$  pairs.

## 5.2 Analysis of the objective function

In this section, we will explore the characteristics of the objective function to verify if it is suitable to be optimized with gradient based descent methods, similar to what was done in Section 4.5. Again, we will try to find a region in which the function is convex or quasi-convex, and provide an expression for its gradient. This is done similarly to what was developed in Section 4.5, by showing quasiconvexity assuming perfect WL channel estimates, and by computing the gradient without any ideality assumptions.

Assume  $\tilde{\mathbf{G}}_k$  and  $\tilde{\mathbf{G}}_{-k}$  are perfect WL channel estimates. Then

$$\tilde{\mathbf{G}}_k = [\alpha_r \mathbf{h}_k \quad \beta_r \mathbf{h}_{-k}^*] \quad (5.18)$$

The linear channel estimates from (5.11) and (5.12) then become

$$\hat{\mathbf{h}}_k(\hat{\epsilon}_r, \hat{\psi}_r) = \frac{\hat{\alpha}_r^* \alpha_r + \hat{\beta}_r \beta_r^*}{|\hat{\alpha}_r|^2 + |\hat{\beta}_r|^2} \mathbf{h}_k \quad (5.19)$$

$$\hat{\mathbf{h}}_{-k}(\hat{\epsilon}_r, \hat{\psi}_r) = \frac{\hat{\alpha}_r^* \alpha_r + \hat{\beta}_r \beta_r^*}{|\hat{\alpha}_r|^2 + |\hat{\beta}_r|^2} \mathbf{h}_{-k} \quad (5.20)$$

The “hat” variables, i.e.,  $\hat{\epsilon}_r$  and  $\hat{\psi}_r$ , are the candidate IQI coefficients, while the same variables

without a hat indicate the ground truth values. The error  $\mathbf{e}_{k,m}(\hat{\epsilon}_r, \hat{\psi}_r)$  becomes

$$\mathbf{e}_{k,m} = \begin{bmatrix} \alpha_r \mathbf{h}_k - \hat{\alpha}_r \hat{\mathbf{h}}_k & \beta_r \mathbf{h}_{-k}^* - \hat{\beta}_r \hat{\mathbf{h}}_{-k}^* \end{bmatrix} \begin{bmatrix} s_k(m) \\ s_{-k}^*(m) \end{bmatrix} + \mathbf{n}_k(m) \quad (5.21)$$

$$= \begin{bmatrix} \left( \alpha_r - \hat{\alpha}_r \frac{\hat{\alpha}_r^* \alpha_r + \hat{\beta}_r \beta_r^*}{|\hat{\alpha}_r|^2 + |\hat{\beta}_r|^2} \right) \mathbf{h}_k & \left( \beta_r - \hat{\beta}_r \frac{\hat{\alpha}_r \alpha_r^* + \hat{\beta}_r^* \beta_r}{|\hat{\alpha}_r|^2 + |\hat{\beta}_r|^2} \right) \mathbf{h}_{-k}^* \end{bmatrix} \begin{bmatrix} s_k(m) \\ s_{-k}^*(m) \end{bmatrix} + \mathbf{n}_k(m) \quad (5.22)$$

where  $\mathbf{n}_k(m)$  is IQI affected noise, the dependencies on  $\hat{\epsilon}_r$  and  $\hat{\psi}_r$  have been omitted for notation cleanliness. We then have

$$\|\mathbf{e}_{k,m}(\hat{\epsilon}_r, \hat{\psi}_r)\|^2 = \left| \alpha_r - \hat{\alpha}_r \frac{\hat{\alpha}_r^* \alpha_r + \hat{\beta}_r \beta_r^*}{|\hat{\alpha}_r|^2 + |\hat{\beta}_r|^2} \right|^2 \|\mathbf{h}_k s_k(m)\|^2 + \left| \beta_r - \hat{\beta}_r \frac{\hat{\alpha}_r \alpha_r^* + \hat{\beta}_r^* \beta_r}{|\hat{\alpha}_r|^2 + |\hat{\beta}_r|^2} \right|^2 \|\mathbf{h}_{-k}^* s_{-k}^*(m)\|^2 + \|\mathbf{n}_k(m)\|^2 + \text{cross terms} \quad (5.23)$$

Assume that  $s_k(m)$ ,  $s_{-k}(m)$ , and  $\mathbf{n}_k(m)$  are all zero mean, statistically independent, ergodic random processes. Assume also that  $N_s$  is large enough such that  $\sum_{m=0}^{N_s-1} \|\mathbf{e}_{k,m}(\hat{\epsilon}_r, \hat{\psi}_r)\|^2 = N_s \mathbb{E}_m \{ \|\mathbf{e}_{k,m}(\hat{\epsilon}_r, \hat{\psi}_r)\|^2 \}$ , in this case the cross terms in (5.23) are averaged out by ergodicity in  $f$ . If we further assume that the summation in  $k$  always includes both  $k$  and  $-k$ , then  $f$  can be further simplified to

$$f(\hat{\epsilon}_r, \hat{\psi}_r) = \gamma(\hat{\epsilon}_r, \hat{\psi}_r) \cdot N_s \sum_{k=0}^K \mathbb{E}_m \{ \|\mathbf{h}_k s_k(m)\|^2 + \|\mathbf{h}_{-k}^* s_{-k}^*(m)\|^2 \} \quad (5.24)$$

$$\gamma_k(\hat{\epsilon}_r, \hat{\psi}_r) = \left| \alpha_r - \hat{\alpha}_r \frac{\hat{\alpha}_r^* \alpha_r + \hat{\beta}_r \beta_r^*}{|\hat{\alpha}_r|^2 + |\hat{\beta}_r|^2} \right|^2 + \left| \beta_r - \hat{\beta}_r \frac{\hat{\alpha}_r \alpha_r^* + \hat{\beta}_r^* \beta_r}{|\hat{\alpha}_r|^2 + |\hat{\beta}_r|^2} \right|^2. \quad (5.25)$$

Yielding the important result that  $f(\hat{\epsilon}_r, \hat{\psi}_r) \propto \gamma(\hat{\epsilon}_r, \hat{\psi}_r)$ , under the given assumptions. In Appendix 2 we show that  $\gamma$  is a quasiconvex function and in Appendix 4 we derive the gradient for  $f(\hat{\epsilon}_r, \hat{\psi}_r)$  as defined in (5.16), without any assumptions on the ideality of the WL channel estimates.

### 5.3 Low SNR or signal-less IQI estimation

Additionally, in situations with no signal transmitted or a transmission under very low SNR, if the noise statistics are known and stationary (or approximately stationary during transmission time), one may try to estimate the IQI coefficients directly from them by assuming the noise is proper. This is more easily done and more robust by taking the waveform statistics directly, instead of performing OFDM demodulation. Say that the IQI affected noise variance  $r_{n,l}$  and complementary variance  $q_{n,l}$  are known to a sufficient precision in antenna  $l$ , then by assuming that  $\mathbb{E} \{ w_l w_l \} = 0$  we can state that

$$\mathbf{n}(m) = \mathbf{\Theta}_A \mathbf{w}(m) + \mathbf{\Theta}_B \mathbf{w}^*(m) \Rightarrow n_l(m) = \alpha_r w_l(m) + \beta_r w_l^*(m) \quad (5.26)$$

$$r_{n,l} = \mathbb{E} \{ n_l n_l^* \} = \sigma_{w,l}^2 \frac{1 + m_r^2}{2} \quad (5.27)$$

$$q_{n,l} = \mathbb{E} \{ n_l n_l \} = \sigma_{w,l}^2 \left( \frac{1 - m_r^2}{2} - j m_r \sin \psi_r \right), \quad (5.28)$$

we may search for the tuple  $(\hat{\sigma}_{w,l}^2, \hat{m}_r, \hat{\psi}_r)$  that minimizes the sum of the square norms of the differences between the sample variance and sample complementary covariance and their expected values given  $(\hat{\sigma}_{w,l}^2, \hat{m}_r, \hat{\psi}_r)$ , in a non-linear least squares problem:

$$E_n(\hat{\sigma}_{w,l}^2, \hat{m}_r, \hat{\psi}_r) = \sum_{l=0}^{N_r-1} \left| r_{n,l} - \hat{\sigma}_{w,l}^2 \frac{1 + \hat{m}_r^2}{2} \right|^2 + \left| q_{n,l} - \hat{\sigma}_{w,l}^2 \left( \frac{1 - \hat{m}_r^2}{2} - j\hat{m}_r \sin \hat{\psi}_r \right) \right|^2. \quad (5.29)$$

The above problem is a nonlinear optimization problem which is not as straightforward to solve compared to linear least squares. However, we have all the methods for solving non-linear least squares problems at our disposal. One possible heuristic method is to break it in  $N_r$  subproblems, each associated with one of the terms in the summation, and average the solutions. In that case, dimensionality issues are greatly alleviated and solving the subproblems can be done by many methods such as: multiple start gradient methods, direct search such as Nelder-Mead simplex methods, or by discretizing the search space and applying exhaustive search heuristics such as tabu-search, simulated annealing, or even naive grid-search. Of course we may also use these methods to tackle the main problem directly. Also, in the case that all receive antennas are expected to have the same noise variance,  $\hat{\sigma}_{n,l}^2$  can be substituted for  $\hat{\sigma}_n^2$ , which greatly simplifies the optimization procedure.

A weighted combination of both the noise-based and the signal-based objective functions may even be considered, with the signal-based objective being more heavily weighted than the noise-based when the estimated SNR is high, and vice-versa. This would lead to a more general procedure which works well under all kinds of SNR conditions.

#### 5.4 Using the demodulation and phase tracking reference signals to estimate IQI

The following parameters are used for defining the physical resource allocation for the DM-RS [43]:

- $k$  indicates the subcarrier index.
- $l_0$  is the index of the first DM-RS OFDM symbol ( $l_0$  is always 0 in mapping type B).
- $l_d$  is, for mapping type A, the number of OFDM symbols between the first OFDM symbol of the slot and the last OFDM symbol of the allocated PUSCH resources. For mapping type B it is equal to the duration of scheduled PUSCH resources. If intra-slot frequency hopping is used, then  $l_d$  is the duration per hop, regardless of mapping type.
- the higher-layer parameter *maxLength* in *DMRS-UplinkConfig* specifies whether double-symbol DM-RS may be used.
- the higher-layer parameter *dmrs-AdditionalPosition* defines the maximum number of additional DM-RS symbols to be transmitted within the slot.

The precise definitions, particular details, and contexts of each parameter are described in [43]. The used set of used subcarriers  $\mathcal{K}^{\text{DMRS}}$  then follows the rule

$$k \in \mathcal{K}^{\text{DMRS}} \text{ if } k = \begin{cases} 4n + 2k' + \Delta, & \text{Configuration type 1} \\ 6n + k' + \Delta, & \text{Configuration type 2} \end{cases} ; k' = 0, 1; n = 0, 1, \dots \quad (5.30)$$

For  $\Delta$ , we refer the reader to Tables 6.4.1.1.3-1 and 6.4.1.1.3-2 in [43]. For our purposes it suffices to state that  $\Delta \in \{0, 1\}$  in configuration type 1.

As we have derived in the previous section, knowledge of transmitted signal in both the  $k$ th subcarrier and its frequency domain mirror image, the  $-k$ th subcarrier, is needed to perform LS WL channel estimation in the standard fashion. We then rely on the DM-RS occupied subcarriers having some symmetry with respect to frequency domain mirroring. The OFDM baseband waveform for all channels except the physical random access channel (PRACH) and except for the remote interference management reference signal (RIM-RS) is given by

$$s_l^{(p,\mu)}(t) = \begin{cases} \bar{s}_l^{(p,\mu)}(t) & t_{\text{start},l}^\mu \leq t < t_{\text{start},l}^\mu + T_{\text{sym},l}^\mu \\ 0 & \text{otherwise} \end{cases} \quad (5.31)$$

$$\bar{s}_l^{(p,\mu)}(t) = \sum_{k=0}^{N_{\text{grid},x}^{\text{size},\mu} N_{\text{sc}}^{\text{RB}} - 1} a_{k,l}^{(p,\mu)} e^{j2\pi(k+k_0^\mu - N_{\text{grid},x}^{\text{size},\mu} N_{\text{sc}}^{\text{RB}}/2)\Delta f(t - N_{\text{cp},l}^\mu T_c - t_{\text{start},l}^\mu)}, \quad (5.32)$$

where  $p$  denotes the antenna port,  $\mu$  the subcarrier spacing configuration,  $k_0^\mu$  is a frequency domain offset that depends on the values within the higher-layer parameter list *scs-SpecificCarrierList* (this list is specifically used in the context of carrier aggregation and contains subcarrier spacing parameters),  $\Delta f$  is the subcarrier spacing,  $N_{\text{sc}}^{\text{RB}}$  is the number of subcarriers per resource blocks (always 12),  $N_{\text{grid},x}^{\text{size},\mu}$  is the size of the resource grid (i.e., the number of resource blocks). For the DM-RS,  $a_{k,l}^{(p,\mu)}$  is computed from the intermediary DM-RS symbols  $\tilde{a}_{k,l}^{(\tilde{p},\mu)}$ , these in turn are mapped to  $a_{k,l}^{(p,\mu)}$  with a precoding matrix and an amplitude scaling factor  $\beta^{\text{DMRS}}$ .

We need to select the DM-RS symbols which have a known signal transmitted at its frequency domain mirrored subcarrier, i.e., we use the set of DM-RS subcarriers  $\mathcal{K}^\mu$  that satisfy

$$\mathcal{K}^\mu = \left\{ k : -\left(k + k_0^\mu - N_{\text{grid},x}^{\text{size},\mu} N_{\text{sc}}^{\text{RB}}/2\right) \cap \left(k + k_0^\mu - N_{\text{grid},x}^{\text{size},\mu} N_{\text{sc}}^{\text{RB}}/2\right) \neq \emptyset, k \in \mathcal{K}^{\text{DMRS}} \right\}. \quad (5.33)$$

To make this clearer, we present an example. Consider the case of transmission over the PUSCH with a single resource block (RB), no carrier aggregation, DM-RS configuration type 1, over the first antenna port. In this case we have  $N_{\text{grid},x}^{\text{size},\mu} N_{\text{sc}}^{\text{RB}} = 12$  subcarriers,  $k_0^\mu = 0$ , and  $\Delta = 0$ , therefore the set of subcarriers occupied by DM-RS is  $\mathcal{K}^{\text{DMRS}} = \{0, 2, 4, 6, 8, 10, 12\}$ , which are related to the frequency bands:  $-6\Delta f, -5\Delta f, \dots, 5\Delta f$ , respectively. When the received OFDM waveform is complex conjugated, the DM-RS original carriers get mapped to their frequency mirror images in the fashion described by Table 5.1. This means that if we want to perform a procedure similar as the one defined in the previous section using the DM-RS, it would require us to include only subcarriers in  $\mathcal{K}^\mu$ , and using only the OFDM symbols which are allocated to DM-RS. Because of these restrictions, including additional DM-RS symbols per slot with the *dmrs-AdditionalPosition* parameter is beneficial to estimation performance.

The PT-RS may also be used to estimate the IQI coefficients. Using exclusively the PT-RS elements may not be a viable approach due to its low density in the frequency resources. According to [43] Section 6.4.1.2.2, PT-RS frequency density in the uplink is governed by the parameter  $K_{\text{PT-RS}} \in \{2, 4\}$ , which indicates whether PT-RS is present every 2 or 4 RBs, respectively. In the time domain however, it is possibly much denser than DM-RS, occupying either every available symbol, 1 every 2 symbols, or 1 every 4 symbols not already allocated to DM-RS. The time density of the PT-RS signal is governed mainly by the  $L_{\text{PT-RS}} \in \{1, 2, 4\}$  parameter. The specifics concerning the definition and application of the parameters  $K_{\text{PT-RS}}$  and  $L_{\text{PT-RS}}$  is detailed in TS 38.214 [44]. In conclusion, it is reasonable to expect the inclusion

Table 5.1. Mapping of original DM-RS occupied subcarriers to the frequency mirrored subcarriers for PUSCH transmission with a single resource block, no carrier aggregation, DM-RS configuration type 1, over the first antenna port

$k$	Freq.	Symbol	Conjugate
0	$-6\Delta f$	$a_{0,l}^{(p,\mu)}$	0
2	$-4\Delta f$	$a_{2,l}^{(p,\mu)}$	$(a_{10,l}^{(p,\mu)})^*$
4	$-2\Delta f$	$a_{4,l}^{(p,\mu)}$	$(a_{8,l}^{(p,\mu)})^*$
6	0	$a_{6,l}^{(p,\mu)}$	$(a_{6,l}^{(p,\mu)})^*$
8	$2\Delta f$	$a_{8,l}^{(p,\mu)}$	$(a_{4,l}^{(p,\mu)})^*$
10	$4\Delta f$	$a_{10,l}^{(p,\mu)}$	$(a_{2,l}^{(p,\mu)})^*$

of the PT-RS for IQI coefficients estimation to be effectively used exclusively to augment the performance of the DM-RS based estimator.

### 5.5 Analysis on subcarrier spacing and channel coherence time

It is intuitive that using more pilot slots to estimate IQI should produce lower MSE estimates. However, more training slots requires a longer transmission window in the time domain, which may become problematic if the channel has a short coherence time. A fast varying channel requires repeated channel estimation even within a single frame, this is expected to deteriorate IQI coefficient estimation performance. According to the 5G standard [43], a frame has 10 ms duration, which is divided into 10 subframes of 1 ms, which are in turn split into  $2^\mu$  slots according to Table 4.3.2-1 of [43] (for normal cyclic prefix), where  $\mu$  is the selected subcarrier spacing numerology. For example, at  $\mu = 4$  (240 kHz subcarrier spacing), 160 slots can be fit into a 10 ms frame.

Wang *et al.* [45] report a typical suburban LOS 5G vehicular channel scenario at 3.5 GHz with a receiver moving at 70 km/h relative to the transmitter to have a mean coherence time of about 24.9 ms. He *et al.* [46] present an approximate expression and simulated coherence times in a high speed rail radio channel for a 500 MHz bandwidth mmWave signal centered at 25.25 GHz. It is reported in their work that the average coherence time in the simulations approximately obeys the expression  $\bar{T} = 5 \cdot 10^{-3} v$ , where  $v$  is the transmitter relative speed in m/s and  $\bar{T}$  is the average coherence time in milliseconds. For a train moving in straight line through an urban environment at speeds of 500 km/h and 120 km/h, they report coherence times of 1.4 ms and 5.9 ms respectively. For a curved trajectory with radius of curvature between 400 m and 10 km and a train moving at 100 km/h, the reported coherence time is 7.2 ms.

We may also use the well established theoretical expressions to approximate a reasonable range of 5G-related coherence times. The coherence time is approximately the inverse of the Doppler spread [47]

$$T_c \approx \frac{1}{B_D} = \frac{c}{v f_c}, \quad (5.34)$$

where  $c$  is the speed of light,  $v$  is the relative velocity between transmitter and receiver, and  $f_c$  is the center frequency of the emitter. As explained by [48], mmWave applications are not only

focused on local area network (LAN) and personal area network (PAN) contexts, but extend even to urban microcellular and picocellular deployments. In a typical scenario at 60 GHz carrier frequency and 60 km/h mobile velocity, the coherence time is approximately 0.3 ms, yielding around a third of a 5G subframe. With a third of a subframe, not even a single slot can be transmitted at subcarrier spacing index  $\mu = 0$ . If we increase the subcarrier spacing to  $\mu = 6$ , then 21 slots can be transmitted in the same timeframe. This leads us to the logical conclusion that higher subcarrier spacing configurations allow IQI coefficient estimation that is more robust to channel time variation by exploiting the increased OFDM symbol rate, transmitting more slots in approximately the same channel conditions.

If the IQI estimation relies on a static channel assumption, then the channel coherence time is a limiting factor for maximum pilot sequence length. Adapting the estimation method to consider time-varying channels should lead to performance improvement. A possible technique could be roughly described as using a sliding window in the time domain and using the pilot symbols within this window to compute a channel estimate. The sliding window can be shifted with a non-unit stride length, i.e. sliding by moving it by more than one symbol. The channel estimate at a particular instant can be some combination of the channel estimates obtained from windows that included the symbol transmitted at that instant. Many variations of this problem can be formulated and tackling channel time variation within IQI estimation is a worthwhile research direction. The impact of using multiple channel estimates to account for time-varying channels in IQI coefficient estimation is left for future work.

## 5.6 Numerical Results

In this section we will present the results of some Monte Carlo simulations designed to assess the efficacy of the methods introduced in this chapter. The first set of simulations considers the case of fully known pilot slots and computes the MSE of the estimated IQI coefficients. They also present normalized mean squared error (NMSE) values defined as

$$\text{NMSE} = \frac{\sum_{n=0}^{N-1} |x_n - \hat{x}_n|^2}{\sum_{n=0}^{N-1} |x_n|^2}, \quad (5.35)$$

where  $x_n$  and  $\hat{x}_n$  are the true and estimated values of observation  $n$ , respectively. In the simulations, the true value is kept constant throughout the Monte Carlo trials, the Normalized MSE then can be expressed as

$$\text{NMSE} = \frac{\frac{1}{N} \sum_{n=0}^{N-1} |x - \hat{x}_n|^2}{|x|^2}, \quad (5.36)$$

with the MSE being now normalized by the magnitude of  $x$ .

We will first observe the effects of training sequence length in the accuracy of the IQI coefficient estimates. We will study transmission in an uplink context, using the PUSCH. We use 5G-like pilot slots of random quadriphase phase shift keying (QPSK) modulated cyclic prefix (CP)-OFDM subcarriers, normal cyclic prefix, 4 RBs, 15 kHz subcarrier spacing, 4 receive antennas, and 2 transmit antennas. However, because the transmission scheme is set to non-codebook with no precoding (i.e., identity precoding), and only one PUSCH layer is active, only one of the transmit antennas is effectively transmitting. By 5G-like slots it is meant that, while the slots observe general frame structure parameters of the 5G standard such as the specified subcarrier spacing, number of symbols per slot, number of subcarriers per

resource block, etc., they do not include hybrid automatic repeat request (HARQ) features or the reference signals, i.e. they are purely QPSK random data with 5G-compliant number of time-domain OFDM symbols and number of subcarriers. This approach was chosen for simplicity of implementation, specially because, when evaluating IQI coefficient estimation performance, all the data integrity related features of 5G HARQ such as cyclic redundancy check (CRC), forward error correction, and retransmission, as well as all the reference signal's sequence generation and resource allocation details are not relevant to the estimation process. Standard 5G transmission will be included in the throughput simulations which will be presented right after the IQI estimation MSE figures. All the curves in the figures are averaged over 1000 Monte Carlo trials unless stated otherwise. Transmission happens through a CDL-A channel as defined in Table 7.7.1-1 of TR 38.901 [41], the channel is set at to a delay spread of 30 ns and is constant throughout the whole transmission, i.e., the maximum Doppler shift is 0 Hz.

In the presented figures, the MSE and Normalized MSE are presented as a function of the fraction of the total available subcarriers used for IQI estimation. As suggested by the theory in the previous section, we select the subcarrier and antenna pairs that experience the highest  $|g_{k,l}^1|^2 + |g_{k,l}^2|^2$  computed from the WL LS channel estimates and then minimize the objective stated in (5.16). We start with Fig. 5.1, which considers 0 dB SNR with all receive antennas sharing IQI parameters fixed at  $\epsilon_r = 0.3$  and  $\psi_r = 20^\circ$  and varies the slot quantity and fraction of used subcarriers. We first see that using more subcarriers for IQI estimation produces better estimation performance until roughly about half of the “best” subcarriers. It is also clear that the MSE decreases drastically when the quantity of training slots is increased. The benefits of using more slots are intuitive, it improves the quality of channel estimates and helps average out the objective function, thus making the optimization procedure more likely to converge close to the actual IQI coefficient values. By analysing Fig. 5.2 it is also evident that using only one slot, i.e., 14 OFDM symbols, produces relatively bad estimates with square errors of almost the same order of magnitude as the estimated coefficients themselves.

In Figs. 5.3 and 5.4 similar results are presented, but for -10 dB SNR instead. The observed results are as expected: the overall idea of the simulations at 0 dB is roughly the same but now with slightly higher MSE values. We see once again that using only one slot for estimation is not viable, specially at this SNR value. The MSE values for 1 training slot are now higher than the parameter's square values, as can be seen in Fig. 5.4. It is also noticeable that using 10 slots and roughly half of the best subcarriers already produces reasonably valued estimates with Normalized MSE around  $10^{-2}$ .

We will now observe the effects of SNR on the IQI coefficient estimates. These simulations consider the same conditions as the previous ones, but always use 100 pilot slots for estimation, varying the SNR instead. Figures 5.5 and 5.6 show the MSE and Normalized MSE, respectively, for IQI estimation with 100 slots and different SNR values. One notable fact that can be observed from both of the aforementioned figures is that MSE can be almost arbitrarily improved at 100 pilot slots by improving the SNR. This means that, if the training sequence is long enough and if the SNR is high enough, the IQI coefficients can be estimated almost perfectly with the described method. Estimation performance is notably very poor in low SNR conditions such as -30 dB, particularly because the objective function is signal-based. In this particular situation, the data indicates that abandoning the signal based objective function and using an objective function based on the statistics of the noise and interference, such as the one proposed in (5.29), might be more effective.

In the next simulation, we will assess the impacts of the number of slots and SNR on the MSE of the IQI parameters using the 5G compliant DM-RS based IQI estimation proposed in Section 5.4. The transmitted signal has 4 RBs with 15 kHz subcarrier spacing, QPSK symbols, CP-OFDM modulation with normal cyclic prefix. The signal is transmitted through a static TDL-A

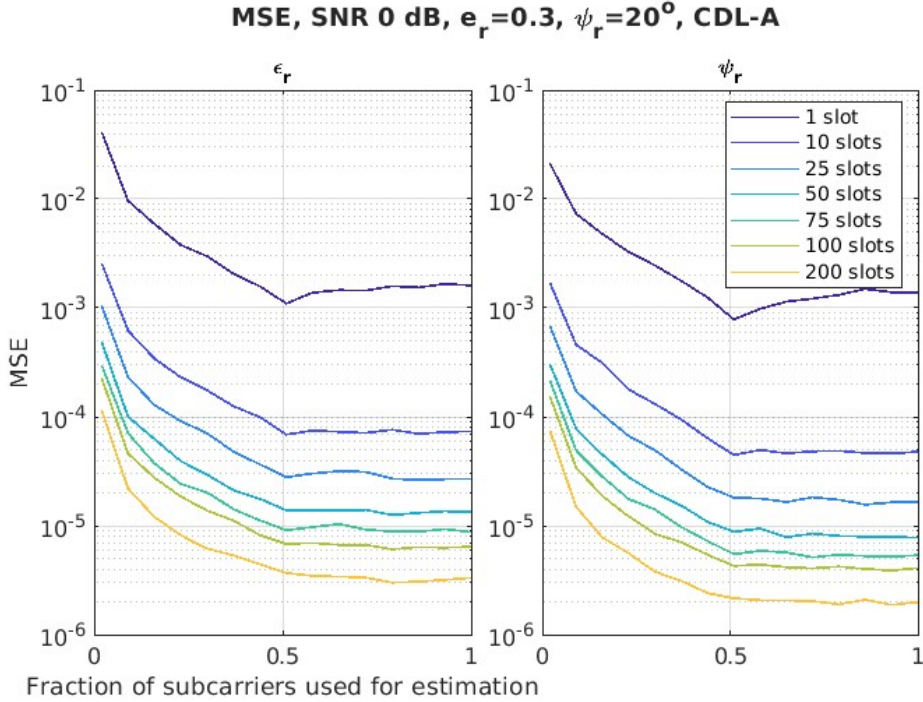


Figure 5.1. MSE of the amplitude (left) and phase (right) IQI coefficients as a function of the fraction of subcarriers used for estimation, CDL-A channel at 0 dB SNR. Curves varying in quantity of training slots are presented according to the legend.

[41] channel with 30 ns delay spread, 4 receive antennas and 2 transmit antennas (but only one PUSCH layer and no precoding, so again only one antenna is effectively transmitting). Timing estimation is assumed perfect. Each data point is averaged over 48 runs. The IQI parameters are set to  $e_r = 0.3$  and  $\psi_r = 20^\circ$ . In Fig. [5.7] we present the MSE of the  $e_r$  and  $\psi_r$  estimates using the method proposed herein, and we also present the MSE of the blind estimator from [15] that was used in Section [4.6]. Analysing the results, it is clear that the blind estimator produces consistent estimates with MSE of around  $10^{-4}$ , not showing much variation regarding the SNR or number of slots. This is expected behaviour, because as long as the received signal has a *proper complex Gaussian* distribution, i.e., it is complex Gaussian with null complementary covariance  $\mathbf{Q}_y = \mathbb{E}\{\mathbf{y}\mathbf{y}^T\} = \mathbf{0}$ , the blind estimator is going to produce acceptable estimates. Since the noise is assumed to be proper, white, and Gaussian, decreasing the SNR should not deteriorate the quality of the blind estimates in any way. One clear drawback of the blind estimator is that, in the case that any IQI exists in the transmitter, the received signal is no longer proper, i.e.  $\mathbf{Q}_y \neq \mathbf{0}$ , and the blind estimator is no longer effective. This shows a clear advantage in terms of the versatility and flexibility of our method in comparison to other existing techniques.

Observing the upper row of Fig. [5.7], we draw the intuitive conclusion: the IQI estimates become increasingly better as the SNR and the number of training slots increase. With 40 training slots, the blind estimator is outperformed in the whole observed SNR range. If we consider  $\text{SNR} > 0$  dB, then more than 30 training slots seems to be sufficient to achieve better results than the blind estimator. One of the main ideas that can be extracted from this figure is that, the proposed method is capable of getting almost perfect estimates if the conditions allow it, but if the SNR and available number of slots (due to channel coherence time, for example) are not high enough, then a simpler blind estimator can outperform it.

For the last simulation of this section, with results in Fig. [5.8], we consider the impacts of IQI

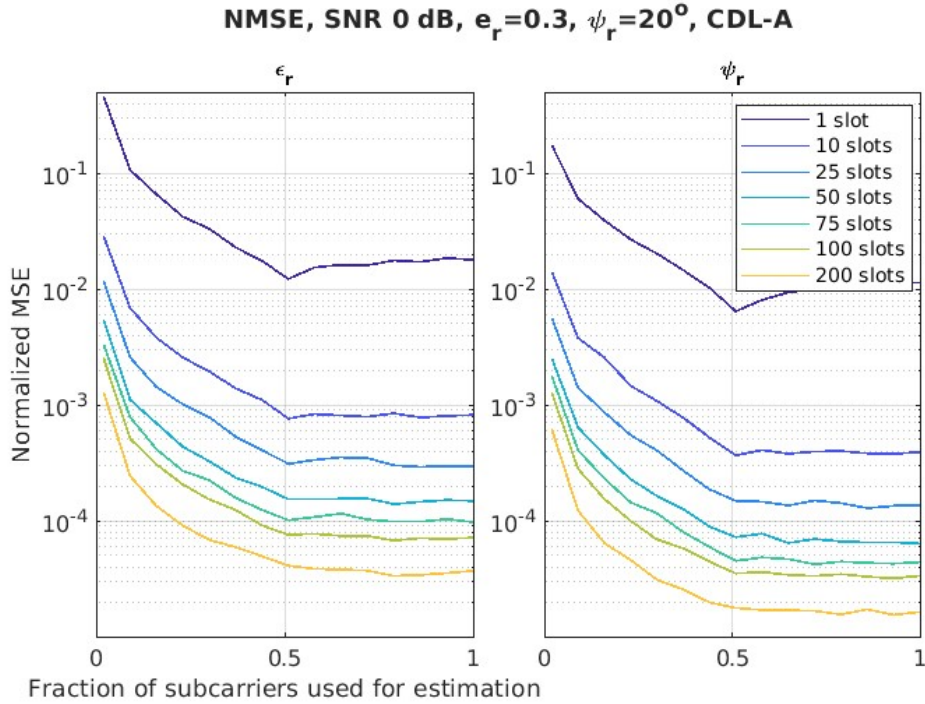


Figure 5.2. Normalized MSE of the amplitude (left) and phase (right) IQI coefficients as a function of the fraction of subcarriers used for estimation, CDL-A channel at 0 dB SNR.

on the throughput of 5G NR PUSCH transmission. The transmitted signal configuration and channel are the same as the last simulation and the throughput is computed as the percentage of data correctly decoded from a total of 500 transmitted frames. Incorrectly received blocks are detected in standard fashion through CRC checksums. HARQ retransmissions are disabled. The radio channel (not including the IQI effects) is assumed perfectly known for the purposes of equalization only, and it is equalized with a MMSE equalizer. Equalization is performed after IQI compensation, thus the equalizer computes the noise variance estimate from IQI compensated noise samples. After equalization, the soft symbols are computed and decoded with the uplink shared channel (UL-SCH) transport block processing chain defined in Section 6.2 of TS 38.212 [49]. The target code rate is set to 193/1024, maximum low density parity check (LDPC) Belief Propagation iterations is set to 12. The used IQI coefficients are  $\epsilon_r = -0.25$  and  $\psi_r = 35^\circ$ .

The results of Fig. 5.8 are not averaged over many iterations, instead they are computed from a single transmission of many frames and the averaging is done over time. A subset of the first transmitted slots is used to compute estimates of the IQI coefficients from the DM-RS symbols as described in Sections 5.1 and 5.4. The number of slots used for estimation in each particular curve is indicated by the figure's legend, where *Clean* and *IQI* indicate the cases with no IQI and with fully uncompensated IQI, respectively. First one must pay attention to the impact on the throughput caused by IQI, effectively shifting the throughput curve by more than 1 dB to the right. We can conclude from this that uncompensated heavy IQI has a noticeable effect on the throughput. One can see that the curves related to 5 and 10 training slots already produce a significant improvement in the throughput when compared to the uncompensated IQI curve. IQI compensation using 50 training slots was able to almost completely eliminate all of IQI's impact on the throughput at all SNR values. Yet, one of the more interesting curves is the one related to 2 training slots. It is clear that 2 slots are not enough to accurately estimate the IQI coefficients at around -10 dB SNR. In fact, the "compensation" actually deteriorates the

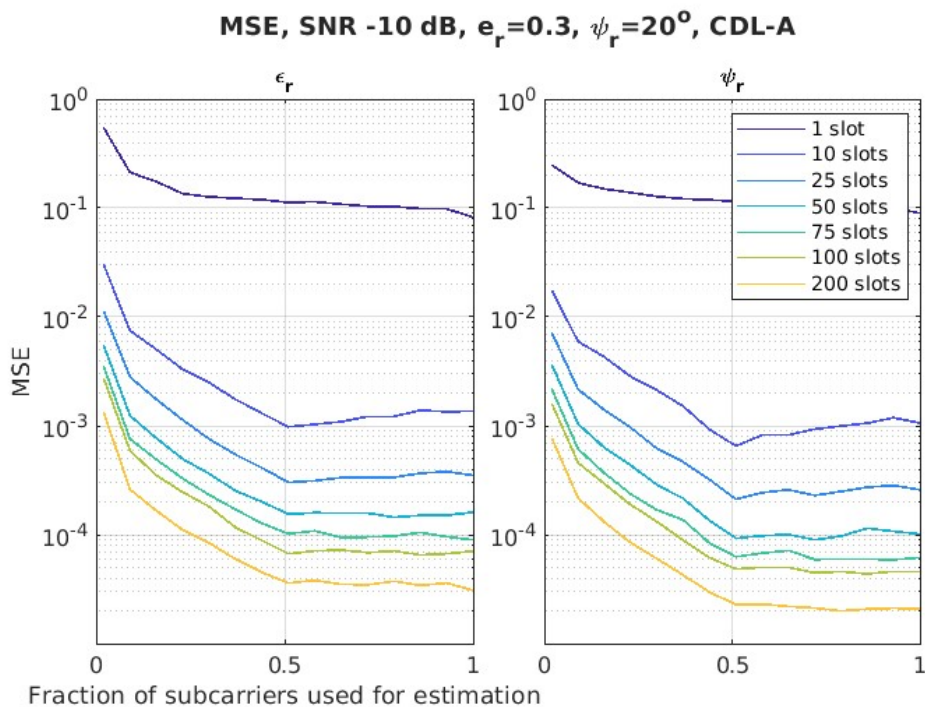


Figure 5.3. MSE of the amplitude (left) and phase (right) IQI coefficients as a function of the fraction of subcarriers used for estimation, CDL-A channel at -10 dB SNR.

throughput performance at those conditions. Nonetheless, once the SNR reaches values around -9.5 dB, estimating with 2 slots starts to produce improvement. This is an evident direct consequence of the lower noise allowing for better estimates of the IQI coefficients and, thus, throughput improvement by means of IQI compensation.

From the presented results in this section we can state that we have achieved an effective pilot-based method for IQI coefficient estimation and compensation that conforms with the 5G standard by effectively exploiting its reference signals. In Chapter 7 we will also compare the performance of the method here introduced with other OFDM based IQI estimation procedures. From these comparisons we will be able to extract the advantages and disadvantages of each procedure and also judge their overall effectiveness.

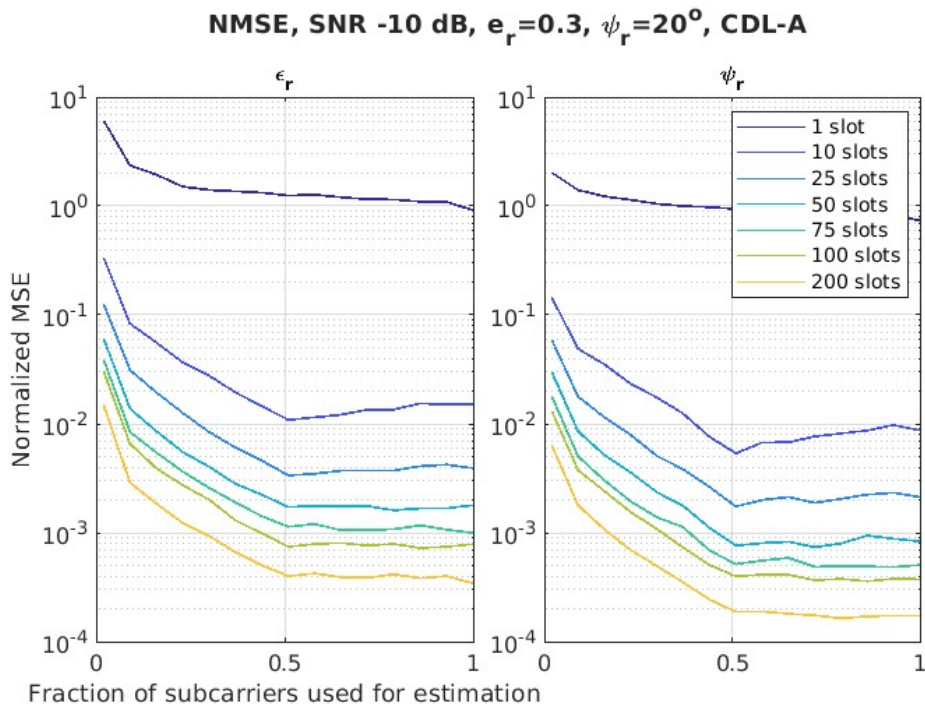


Figure 5.4. Normalized MSE of the amplitude (left) and phase (right) IQI coefficients as a function of the fraction of subcarriers used for estimation, CDL-A channel at -10 dB SNR.

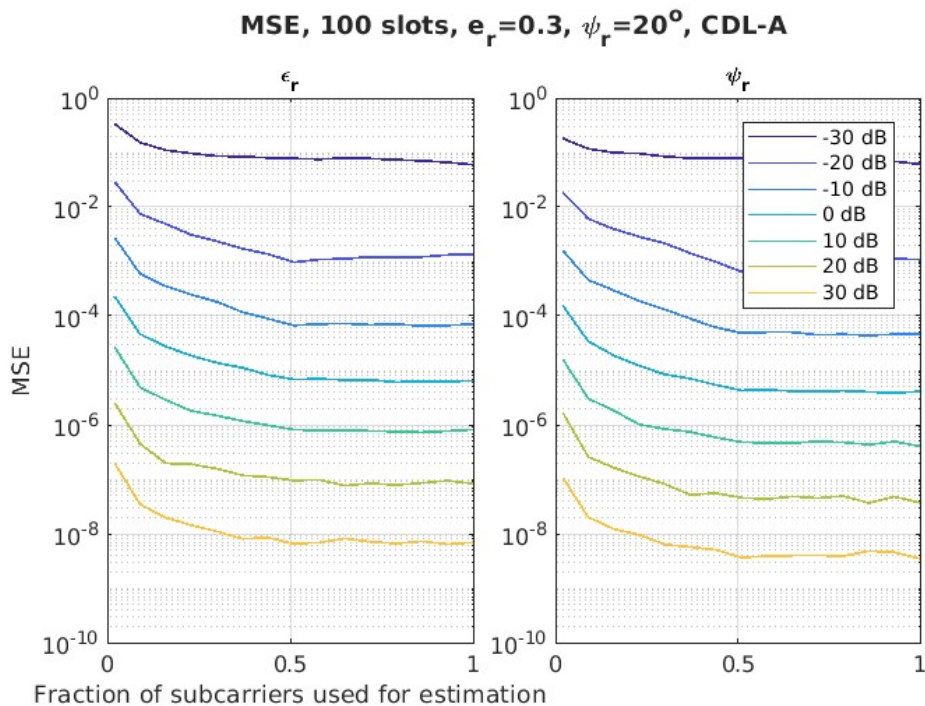


Figure 5.5. MSE of the amplitude (left) and phase (right) IQI coefficients as a function of the fraction of subcarriers used for estimation, CDL-A channel with 100 pilot slots for estimation.

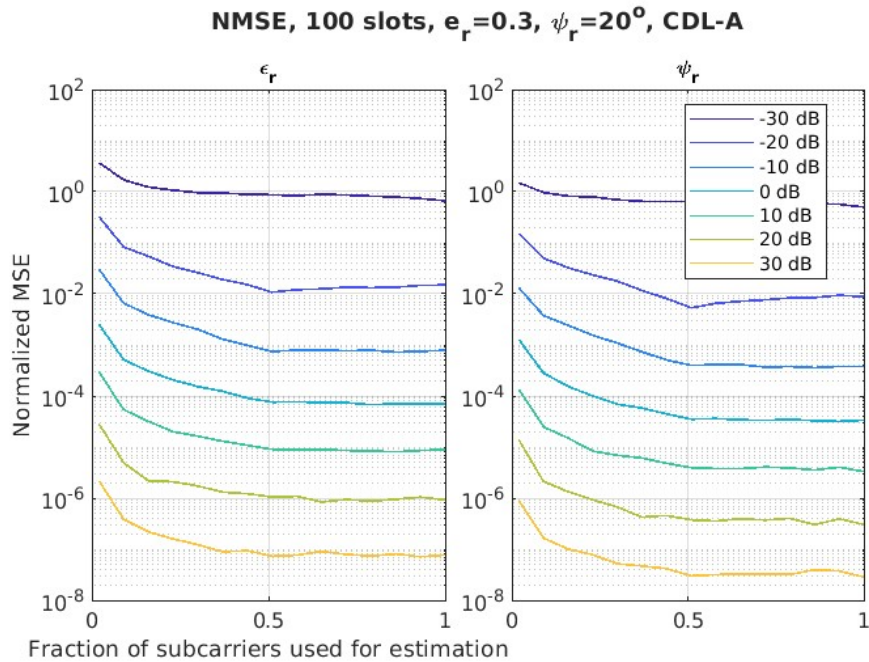


Figure 5.6. Normalized MSE of the amplitude (left) and phase (right) IQI coefficients as a function of the fraction of subcarriers used for estimation, CDL-A channel with 100 pilot slots for estimation.

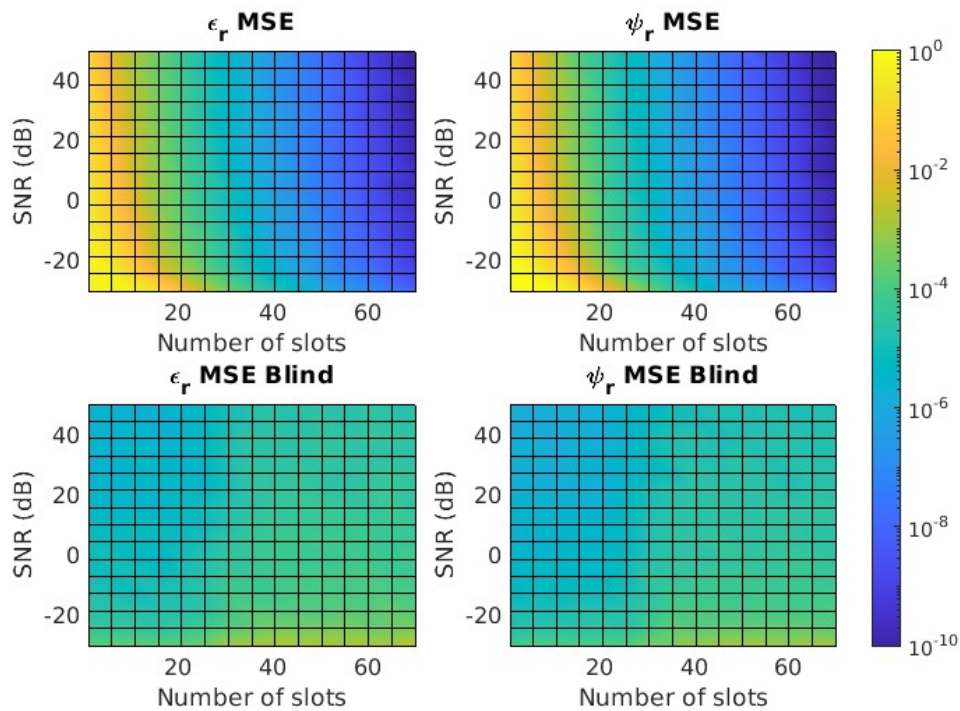


Figure 5.7. IQI parameter estimates' MSE as a function of the SNR and the number of training slots. The top row presents the results achieved by the proposed 5G compliant IQI estimation procedure, and the bottom row presents the results from a blind estimator.

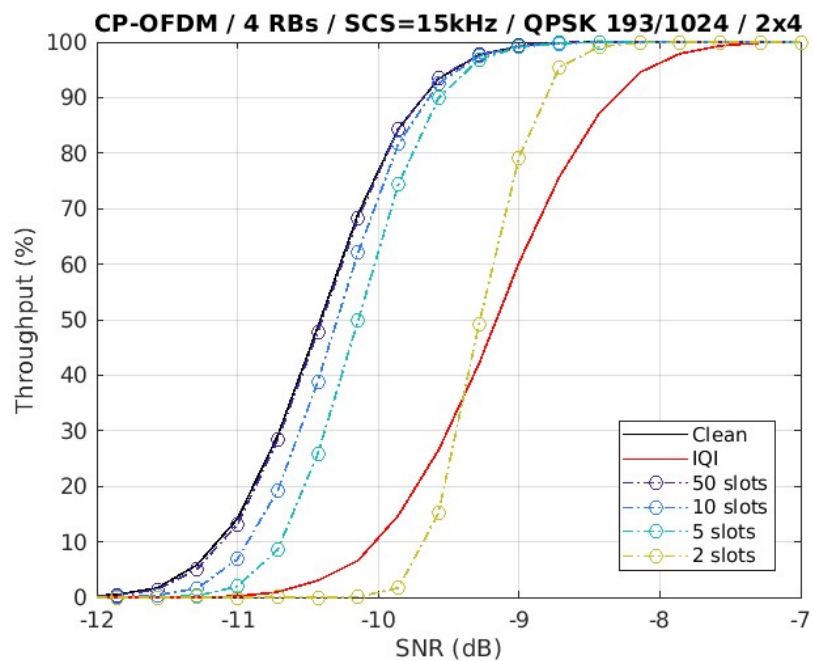


Figure 5.8. 5G NR PUSCH simulation assessing the effects of IQI on throughput. A total of 500 10 ms frames are transmitted over a TDL-A channel with 30 ns delay spread, 4 receive and 2 transmit antennas. The resource grid has 4 resource blocks, QPSK symbols, and is CP-OFDM modulated with 15 kHz subcarrier spacing, normal cyclic prefix. The IQI coefficients are fixed to  $\epsilon_r = -0.25$  and  $\psi_r = 35^\circ$ . The different curves indicate different number of slots used for IQI coefficient estimation, as well as the uncompensated and no IQI cases (*IQI* and *Clean*, respectively).

## 6 JOINT TRANSMITTER AND RECEIVER IQI ESTIMATION

In this chapter, we will extend the proposed method to perform joint estimation of the IQI parameters in the transmitter and receiver. This is a considerably more complicated problem with significantly less bibliography compared to the problem of estimating Rx imbalance only. For example, from the many IQI compensation schemes mentioned in Chapter 3, only three of them considered Tx and Rx IQ imbalance simultaneously [16] [26] [27]. From those methods, Zhang *et al.* [26] considers the knowledge of some hard to know parameters and [16] proposes a solution with hardware loopback. As mentioned in Chapter 3, both of these approaches have some complications associated with them in the sense that they either require information that is hard to obtain, or they require specific hardware modifications or design choices to tackle IQI compensation. The method that is more similar to the one proposed here is the one in [27], that relies exclusively on the transmitted and received information to extract the IQI coefficients. Let us now detail the proposed joint Tx/Rx IQI estimation and compensation procedure.

### 6.1 System model

The model that will be used in this chapter is similar to the model in Chapter 5 and is based on the analysis done in [12]. Consider the theoretical case of  $N_c$  transmitter RF chains with  $N_c \times 1$  baseband equivalent output  $\mathbf{s}_T(t)$ . Because this is the output of an IQ imbalanced RF chain, we can express it as

$$\mathbf{s}_T(t) = \Theta_{AT}\mathbf{s}(t) + \Theta_{BT}\mathbf{s}^*(t), \quad (6.1)$$

where  $\mathbf{s}(t)$  is the ideal baseband equivalent output of the RF chains, and  $\Theta_{AT}$  and  $\Theta_{BT}$  are the Tx IQI matrices, diagonal matrices of coefficients defined in (2.30) and (2.31), respectively. This signal is analog precoded with the  $N_t \times N_c$  precoding matrix  $\mathbf{P}$  and transmitted, where  $N_t$  is the number of transmit antennas. From [12], assume the cyclic prefix length is at least as long as the channel impulse response length to avoid ISI, assume also that timing and frequency synchronization at the receiver are ideal, then the  $m$ th OFDM symbol at the  $k$ th subcarrier can be written as

$$\mathbf{y}_k(m) = \begin{bmatrix} \Theta_{AR} & \Theta_{BR} \end{bmatrix} \begin{bmatrix} \mathbf{x}_k(m) \\ \mathbf{x}_k^*(m) \end{bmatrix} \quad (6.2)$$

$$= \begin{bmatrix} \Theta_{AR} & \Theta_{BR} \end{bmatrix} \begin{bmatrix} \mathbf{H}_k(\Theta_{AT}\mathbf{s}_k(m) + \Theta_{BT}\mathbf{s}_{-k}^*(m)) \\ \mathbf{H}_{-k}^*(\Theta_{AT}^*\mathbf{s}_{-k}^*(m) + \Theta_{BT}^*\mathbf{s}_k(m)) \end{bmatrix} + (\Theta_{AR}\mathbf{n}_k(m) + \Theta_{BR}\mathbf{n}_{-k}^*(m)) \quad (6.3)$$

$$= \begin{bmatrix} \Theta_{AR} & \Theta_{BR} \end{bmatrix} \begin{bmatrix} \mathbf{H}_k & \mathbf{0} \\ \mathbf{0} & \mathbf{H}_{-k}^* \end{bmatrix} \begin{bmatrix} \Theta_{AT} & \Theta_{BT} \\ \Theta_{BT}^* & \Theta_{AT}^* \end{bmatrix} \begin{bmatrix} \mathbf{s}_k(m) \\ \mathbf{s}_{-k}^*(m) \end{bmatrix} + \mathbf{w}_k(m), \quad (6.4)$$

where the  $N_r \times 1$  vector  $\mathbf{x}_k(m)$  denotes the ideal received signal for the  $m$ th OFDM symbol and  $k$ th subcarrier at the  $N_r$  receive antennas,  $\Theta_{AR}$  and  $\Theta_{AB}$  denote the receiver IQI matrices,  $\mathbf{H}_k$  denotes the channel matrix at the  $k$ th subcarrier (including all analog precoding and beamforming processing), and  $\mathbf{n}_k(m)$  is the noise at the  $m$ th OFDM symbol and  $k$ th subcarrier. We use  $\mathbf{n}(m)$  to model any noise and interference experienced by the system, it is reasonable to assume that  $n_k(m)$  may be modeled as AWGN and that it is added before IQI at the LNA, since the input stages are the ones that most deteriorate the receiver noise figure. The combination of receiver

IQI, channel, and transmitter IQI can be modeled as WL channel

$$\begin{bmatrix} y_{k,0}(m) \\ y_{k,1}(m) \\ \vdots \\ y_{k,N_r-1}(m) \end{bmatrix} = \begin{bmatrix} \mathbf{g}_{k,0}^1 & \mathbf{g}_{k,0}^2 \\ \mathbf{g}_{k,1}^1 & \mathbf{g}_{k,1}^2 \\ \vdots & \vdots \\ \mathbf{g}_{k,N_r-1}^1 & \mathbf{g}_{k,N_r-1}^2 \end{bmatrix} \begin{bmatrix} \mathbf{s}_k(m) \\ \mathbf{s}_{-k}^*(m) \end{bmatrix} + \mathbf{w}_k(m) \quad (6.5)$$

$$= [\mathbf{G}_k^1 \quad \mathbf{G}_k^2] \mathbf{s}_{e,k}(m) + \mathbf{w}_k(m) \quad (6.6)$$

$$= \mathbf{G}_k \mathbf{s}_{e,k}(m) + \mathbf{w}_k(m), \quad (6.7)$$

where  $\mathbf{g}_{k,l}^i$  is a  $1 \times N_c$  vector. We call  $\mathbf{G}_k$  the effective channel at the  $k$ th subcarrier, or the  $k$ th effective subchannel.

Consider now a LS WL channel estimate computed in the standard way. Suppose we receive  $N_s$  symbols and that the channel remains static during the whole transmission, i.e., the channel coherence time is much larger than the transmission time, then the subchannel of the  $k$ th subcarrier at the  $l$ th antenna is estimated as a widely linear operator in the same manner as in the previous chapter, applying (5.6). From (6.4) we know that

$$\mathbf{G}_k^1 = \Theta_{AR} \mathbf{H}_k \Theta_{AT} + \Theta_{BR} \mathbf{H}_{-k}^* \Theta_{BT}^* \quad (6.8)$$

$$\mathbf{G}_k^2 = \Theta_{BR} \mathbf{H}_{-k}^* \Theta_{AT}^* + \Theta_{AR} \mathbf{H}_k \Theta_{BT}. \quad (6.9)$$

Assume that the transmitter RF chains all have the same IQI, assume the same thing for the receiver, i.e.,  $\Theta_{AT} = \alpha_t \mathbf{I}$ ,  $\Theta_{BT} = \beta_t \mathbf{I}$ ,  $\Theta_{AR} = \alpha_r \mathbf{I}$ ,  $\Theta_{BR} = \beta_r \mathbf{I}$ , then we can write (6.8) and (6.9) as

$$\mathbf{G}_k^1 = \alpha_r \alpha_t \mathbf{H}_k + \beta_r \beta_t^* \mathbf{H}_{-k}^* \quad (6.10)$$

$$\mathbf{G}_k^2 = \beta_r \alpha_t^* \mathbf{H}_{-k}^* + \alpha_r \beta_t \mathbf{H}_k. \quad (6.11)$$

The equivalent channel  $\mathbf{G}_{-k}$  also depends on the values of  $\mathbf{H}_k$  and  $\mathbf{H}_{-k}$ , so we may set up a system of matrix equations using these expressions

$$\begin{cases} \mathbf{G}_k^1 = \alpha_r \alpha_t \mathbf{H}_k + \beta_r \beta_t^* \mathbf{H}_{-k}^* \\ \mathbf{G}_k^2 = \beta_r \alpha_t^* \mathbf{H}_{-k}^* + \alpha_r \beta_t \mathbf{H}_k \\ \mathbf{G}_{-k}^1 = \alpha_r \alpha_t \mathbf{H}_{-k} + \beta_r \beta_t^* \mathbf{H}_k^* \\ \mathbf{G}_{-k}^2 = \beta_r \alpha_t^* \mathbf{H}_k^* + \alpha_r \beta_t \mathbf{H}_{-k} \end{cases}. \quad (6.12)$$

Renaming  $a = \alpha_r \alpha_t$ ,  $b = \beta_r \beta_t^*$ ,  $c = \beta_r \alpha_t^*$ , and  $d = \alpha_r \beta_t$ , and breaking down into real and imaginary parts we may write

$$\begin{bmatrix} \mathbf{G}_{1,k}^r \\ \mathbf{G}_{1,k}^i \\ \mathbf{G}_{2,k}^r \\ \mathbf{G}_{2,k}^i \\ \mathbf{G}_{1,-k}^r \\ \mathbf{G}_{1,-k}^i \\ \mathbf{G}_{2,-k}^r \\ \mathbf{G}_{2,-k}^i \end{bmatrix} = \left( \begin{bmatrix} a^r & -a^i & b^r & b^i \\ a^i & a^r & b^i & -b^r \\ d^r & -d^i & c^r & c^i \\ d^i & d^r & c^i & -c^r \\ b^r & b^i & a^r & -a^i \\ b^i & -b^r & a^i & a^r \\ c^r & c^i & d^r & -d^i \\ c^i & -c^r & d^i & d^r \end{bmatrix} \otimes \mathbf{I} \right) \begin{bmatrix} \mathbf{H}_k^r \\ \mathbf{H}_k^i \\ \mathbf{H}_{-k}^r \\ \mathbf{H}_{-k}^i \end{bmatrix} \Rightarrow \mathbf{G}_k^s = \mathbf{T} \mathbf{H}_k^s, \quad (6.13)$$

where  $\otimes$  is the Kronecker product, and the  $r$  and  $i$  superscripts respectively denote real and imaginary parts, e.g.,  $a^r = \Re\{a\}$ ,  $\mathbf{H}_k^i = \Im\{\mathbf{H}_k\}$ , etc. The general expression equivalent to (6.13) for any Tx and Rx IQI coefficients may be obtained by removing the Kronecker product and substituting the IQI coefficients for the corresponding IQI matrices in the definitions of  $a$ ,  $b$ ,  $c$ , and  $d$ .

## 6.2 IQI estimation

Suppose that we have WL channel estimates  $\tilde{\mathbf{G}}_k$  and  $\tilde{\mathbf{G}}_{-k}$ , then we may compute channel estimates  $\hat{\mathbf{H}}_k$  and  $\hat{\mathbf{H}}_{-k}$  conditioned on candidate values of Tx and Rx IQI parameters  $\hat{\epsilon}_t$ ,  $\hat{\psi}_t$ ,  $\hat{\epsilon}_r$ , and  $\hat{\psi}_r$ , by substituting the true channels for the estimates in (6.13), using the conditioned values of IQI parameters to set up  $\hat{\mathbf{T}}$ , and applying the pseudoinverse

$$\hat{\mathbf{H}}_k^s = \hat{\mathbf{T}}^\dagger(\hat{\epsilon}_t, \hat{\psi}_t, \hat{\epsilon}_r, \hat{\psi}_r) \tilde{\mathbf{G}}_k^s. \quad (6.14)$$

This pseudoinverse has an closed-form expression, but it is generally too complicated to be more useful than computing it numerically. We can now define the estimated channels conditioned on the IQI parameters as

$$\hat{\mathbf{H}}_k = \hat{\mathbf{H}}_k^r + j\hat{\mathbf{H}}_k^i \quad (6.15)$$

$$\hat{\mathbf{H}}_{-k} = \hat{\mathbf{H}}_{-k}^r + j\hat{\mathbf{H}}_{-k}^i. \quad (6.16)$$

Define the objective function over the candidate IQI parameters

$$f(\hat{\epsilon}_t, \hat{\psi}_t, \hat{\epsilon}_r, \hat{\psi}_r) = \sum_{k \in \mathcal{K}^*} \sum_{m=0}^{N_s-1} \left\| \mathbf{y}_k(m) - \begin{bmatrix} \hat{\mathbf{G}}_{AR} & \hat{\mathbf{G}}_{BR} \end{bmatrix} \begin{bmatrix} \hat{\mathbf{H}}_k & \mathbf{0} \\ \mathbf{0} & \hat{\mathbf{H}}_{-k}^* \end{bmatrix} \begin{bmatrix} \hat{\mathbf{G}}_{AT} & \hat{\mathbf{G}}_{BT} \\ \hat{\mathbf{G}}_{BT}^* & \hat{\mathbf{G}}_{AT}^* \end{bmatrix} \begin{bmatrix} \mathbf{s}_k(m) \\ \mathbf{s}_{-k}^*(m) \end{bmatrix} \right\|^2, \quad (6.17)$$

where  $\mathcal{K}^* \subseteq \mathcal{K}$  is a subset of the subcarriers selected according to some criterion. We state that the Tx and Rx IQI coefficients can be reliably estimated by minimizing  $f$ .

In the case that the receiver has many RF chains with different IQI coefficients, the estimates of the transmitter IQI coefficients become coupled by the objective functions associated with each set of receiver RF chains. Let  $N_c^r$  denote the number of receiver RF chains with distinct IQI coefficients, denote their IQI parameters by  $\epsilon_r^p$  and  $\psi_r^p$ , with  $p = 0, 1, \dots, N_c^r - 1$ , then they have objective functions such as (6.17). We can define a ‘‘total’’ objective function by coupling all the  $N_c^r$  objectives

$$f_{Total}(\hat{\epsilon}_t, \hat{\psi}_t, \hat{\epsilon}_r^0, \hat{\psi}_r^0, \dots, \hat{\epsilon}_r^{N_c^r-1}, \hat{\psi}_r^{N_c^r-1}) = \sum_{p=0}^{N_c^r-1} f_p(\hat{\epsilon}_t, \hat{\psi}_t, \hat{\epsilon}_r^p, \hat{\psi}_r^p). \quad (6.18)$$

## 6.3 Discussion on optimization issues

The objective function in (6.17) is not well behaved like the ones in Chapter 5. Simulations indicate that there exist many local optima, some of them are even far from the ground truth parameter values. One of the more complicated aspects is that, even for high SNR and long sequence lengths, the final solution is very sensitive to the starting point of the optimizer. If the optimizer is initialized at the true parameter values, provided that the SNR is high and that

the pilot sequence is long, then the optimization algorithm converges almost exactly to the true values (not necessarily at the true values themselves, because the objective function relies on the gathered data and estimated equivalent channel). If the optimizer is initialized to a random valid point in the search space, or even a default starting point such as  $(0, 0)$ , then it is very likely that the optimizer will converge to a local optima that is reasonably far from the true parameter values.

For the case with multiple Rx IQI coefficients in (6.18), with the additional sets of coefficients come all the issues associated with increasing the dimension of the search space. However, it is reasonable to expect this coupled objective function to actually improve convergence and reduce the MSE of the estimates. This can happen because even if two specific combinations of Tx parameters and Rx parameters produce similar  $f_p$  values, it is unlikely that they also produce similar  $f_q$  values (for  $p \neq q$ ), assuming of course that the IQI coefficients between RF chains are sufficiently different. A simpler, but less optimal, option is to optimize all  $f_p$  independently and then take the average of the Tx IQI parameter values from the  $N_c^r$  solutions. There is a trade-off involving the quality of the solution and the time spent in finding a solution, for example, for 2 Rx IQI values and 1 Tx IQI value, the computational cost for solving the fully coupled problem may be almost the same as solving 2 independent subproblems and taking the average of the Tx IQI parameters, because the complexity of a pair of 2-dimensional optimization problems is more or less *comparable* to the complexity of a single 4-dimensional optimization problem. However if we have many more Rx IQI values, i.e.,  $N_c^r \gg 1$  (values larger than 4 may already qualitatively satisfy this property), then the dimension of the joint optimization problem is  $2N_c^r + 1$ , experiencing exponential growth of the search space, while solving the subproblems requires solving  $N_c^r$  4-dimensional problems. In this case it may be much more efficient to solve the subproblems and average out the Tx IQI solution, because the joint problem may even be infeasible under some time and computational constraints.

We will not perform a more detailed analysis of the proposed objective functions in this work. The main reason for this is that this objective function is much more complicated than the ones in previous chapters, specially due to the pseudoinverse of  $\hat{\mathbf{T}}$ . Numerical experimentation can show that it is clearly not *well behaved*, i.e., it is not convex or quasi-convex.

## 6.4 Optimizing the objective function

The performance of the proposed method for joint estimation of Tx and Rx IQI coefficients is a matter of both the conditions (pilot sequence length and SNR) as well as of non-convex optimization itself. In this section, we will present some methods and heuristics that have been shown to be useful in finding the minimum of the objective function, focusing mainly on the function defined in (6.17). The first issue one encounters in the optimization process is the choice of algorithms that will be used. Because of the difficulty in deriving a gradient for this objective function, gradient-less methods like the Nelder-Mead (NM) seem like an attractive option. However, due to the non-convexity of the objective, the NM algorithm will not necessarily converge to the neighborhood of the true parameter values. This leads to the second issue in the optimization process: setting the starting point. Practical observation shows that performing NM search when initializing to  $\mathbf{0}$  leads to massively incorrect estimates, thus we need to find a procedure to better initialize the algorithm. One technique that has led to effective results is running a few iterations of simulated annealing (SA) with short reannealing periods to get a very rough estimate of the optimal point and initialize the NM search with it. Depending on the pilot sequence length and SNR, the NM algorithm will converge to points in the neighborhood of the ground truth parameter values (the NM algorithm does not necessarily

converge to local optima or stationary points [50]).

Using SA+NM leads to approximate estimates which, in many situations, can still be improved by a large margin. We can then explore some techniques to *refine* the SA+NM results so that the quality of the IQI estimates is not limited by the efficacy of the optimization process, but by practical factors such as the SNR and pilot sequence length. To improve the optimization results, we can perform particle swarm (PS) optimization [51] [52] [53] constrained to a neighborhood of the SA+NM output, and from the PS output we can perform NM search again. This Constrained PS+NM can be iterated many times to refine the quality of the IQI estimates, where the constraints restrain the neighborhood to be smaller each time. After many attempts, we arrived at the following procedure, which will be used in the numerical simulations:

- Simulated annealing initialized at  $\mathbf{0}$  with initial temperature of 50, maximum stall iterations of 30, and reannealing after every 3 new points are accepted;
- Applying Nelder-Mead to the output of the SA;
- Applying constrained Particle Swarm to the output of NM, with bounds set to  $\epsilon_{r,t}^{NM1} \pm 0.01$  and  $\psi_{r,t}^{NM1} \pm 1^\circ$ , where the NM1 superscript indicates the output of the first NM optimization process;
- Another round of NM initialized at the output of the PS optimization;
- Another round of constrained PS but with tighter constraints around the output of the last NM optimization, bound set to  $\epsilon_{r,t}^{NM2} \pm 0.002$  and  $\psi_{r,t}^{NM2} \pm 0.2^\circ$ , where the NM2 superscript indicates the output of the second NM optimization process;
- A final round of NM to clean up the results of the last particle swarm.

Naturally, many methods for problems of this kind exist, these are broadly classified as global optimization algorithms, and one may experiment with the multiple available options. The main focus should always be to let SNR, pilot sequence length, and number of subcarriers be the main bottleneck that limits the quality of IQI parameter estimates, and *never* suboptimality.

## 6.5 IQI compensation

With the IQI parameter estimates in hand, it remains for us to compensate the effects of IQI. For the transmitter IQI, we know that

$$\begin{bmatrix} \mathbf{s}_T(t) \\ \mathbf{s}_T^*(t) \end{bmatrix} = \begin{bmatrix} \mathbf{\Theta}_{AT} & \mathbf{\Theta}_{BT} \\ \mathbf{\Theta}_{BT}^* & \mathbf{\Theta}_{AT}^* \end{bmatrix} \begin{bmatrix} \mathbf{s}(t) \\ \mathbf{s}^*(t) \end{bmatrix} \quad (6.19)$$

We can use the block matrix inversion formula

$$\begin{bmatrix} \mathbf{A} & \mathbf{B} \\ \mathbf{C} & \mathbf{D} \end{bmatrix}^{-1} = \begin{bmatrix} \mathbf{S}^{-1} & -\mathbf{S}^{-1}\mathbf{B}\mathbf{D}^{-1} \\ -\mathbf{D}^{-1}\mathbf{C}\mathbf{S}^{-1} & \mathbf{D}^{-1} + \mathbf{D}^{-1}\mathbf{C}\mathbf{S}^{-1}\mathbf{B}\mathbf{D}^{-1} \end{bmatrix}, \quad (6.20)$$

where  $\mathbf{S} = \mathbf{A} - \mathbf{B}\mathbf{D}^{-1}\mathbf{C}$  is the Schur complement of  $\mathbf{D}$ , to compute the *predistortion* that must be applied to the signal to cancel out the transmitter IQI

$$\mathbf{s}_c(t) = \left( \hat{\mathbf{\Theta}}_{AT} - \hat{\mathbf{\Theta}}_{BT} \hat{\mathbf{\Theta}}_{AT}^{-*} \hat{\mathbf{\Theta}}_{BT}^* \right)^{-1} \left( \mathbf{s}(t) - \hat{\mathbf{\Theta}}_{BT} \hat{\mathbf{\Theta}}_{AT}^{-*} \mathbf{s}^*(t) \right), \quad (6.21)$$

where  $\mathbf{s}_c(t)$  denotes the predistorted signal that will be delivered to the RF chains. Similarly for the receiver, because

$$\begin{bmatrix} \mathbf{y}(t) \\ \mathbf{y}^*(t) \end{bmatrix} = \begin{bmatrix} \Theta_{AR} & \Theta_{BR} \\ \Theta_{BR}^* & \Theta_{AR}^* \end{bmatrix} \begin{bmatrix} \mathbf{x}(t) \\ \mathbf{x}^*(t) \end{bmatrix} \quad (6.22)$$

is an almost identical expression, we may compensate receiver IQI by processing the received signal in the following fashion

$$\mathbf{x}_c(t) = \left( \hat{\Theta}_{AR} - \hat{\Theta}_{BR} \hat{\Theta}_{AR}^{-*} \hat{\Theta}_{BR}^* \right)^{-1} \left( \mathbf{y}(t) - \hat{\Theta}_{BR} \hat{\Theta}_{AR}^{-*} \mathbf{y}^*(t) \right), \quad (6.23)$$

where  $\mathbf{x}_c(t)$  is the estimate of the received signal without IQI. All the matrix inversions are easy to perform because all the matrices are diagonal, and inverting a diagonal matrix is the same as taking the multiplicative inverse of its elements. Also notice that the inverses always exist for reasonable values of IQI coefficients, because  $\Theta_{AT} \approx \Theta_{AR} \approx \mathbf{I}$  and  $\Theta_{BT} \approx \Theta_{BR} \approx \mathbf{0}$ , this means that all matrices that are inverted have elements reasonably far from 0.

## 6.6 Numerical results

In this section, we will verify the efficacy of the proposed method by analysing simulation results of the transmission of OFDM pilot slots under Tx/Rx IQI. The simulation setup is very similar to the first setup of Section 5.6, i.e. 5G like CP-OFDM frame structure of QPSK modulated symbols without the reference signals and HARQ. The channel is once again the CDL-A channel model with 30 ns delay spread and 0 Hz maximum Doppler shift, i.e., constant cluster delay line channel. We use 4 resource blocks with subcarrier spacing of 15 kHz, 1 Tx antenna and 4 Rx antennas, and normal cyclic prefix, so each slot contains 14 OFDM symbols. The simulations present the MSE and NMSE values as a function of the fraction of subchannels used for different number of slots and SNR configurations, where a subchannel is defined as a subcarrier and antenna ordered pair  $(k, l)$ . The used fraction of the subchannels is selected according to the estimated *equivalent channel power criterion*, i.e.,  $|g_{k,l}^1|^2 + |g_{k,l}^2|^2$ . The fraction of subchannels can be said to be roughly equivalent to the fraction of subcarriers and the two approaches should be essentially equivalent.

Up to this point, all simulations in previous chapters considered unrealistically large IQI values, e.g.,  $|\epsilon_r| \approx 0.3$  and  $|\psi_r| \approx 20^\circ$ , this was done to show that the proposed method is capable of estimating the IQI parameters even if they are in extreme ranges, because our method does not rely on the ‘‘IQI is approximately ideal’’ assumption. On the other hand, to avoid any possible suspicion that the method may rely on these extreme values to present proper estimates, we will use more realistic values of IQI parameters in this section, namely  $\epsilon_r = 0.1$ ,  $\psi_r = -4^\circ$ ,  $\epsilon_t = -0.08$ , and  $\psi_t = 5^\circ$ . One consequence of reducing the magnitude of the IQI parameters is that we should expect NMSE values to be increased, because simulations show that the MSE is mostly independent of the parameter values (because the numerator is approximately constant but the denominator is reduced).

First, we will observe the impact of varying the number of training slots at a constant SNR value. Fig. 6.1 presents the MSE for both the Tx and Rx IQI parameters estimated at a 10 dB SNR for varying number of training slots. We can see that using up to half of the 48 subcarriers produces equally bad results, regardless of the number of training slots. This is due to some interesting interaction between the objective function and the subcarrier selection criterion. This happens even if the number of resource blocks is increased, and it stops happening if we select

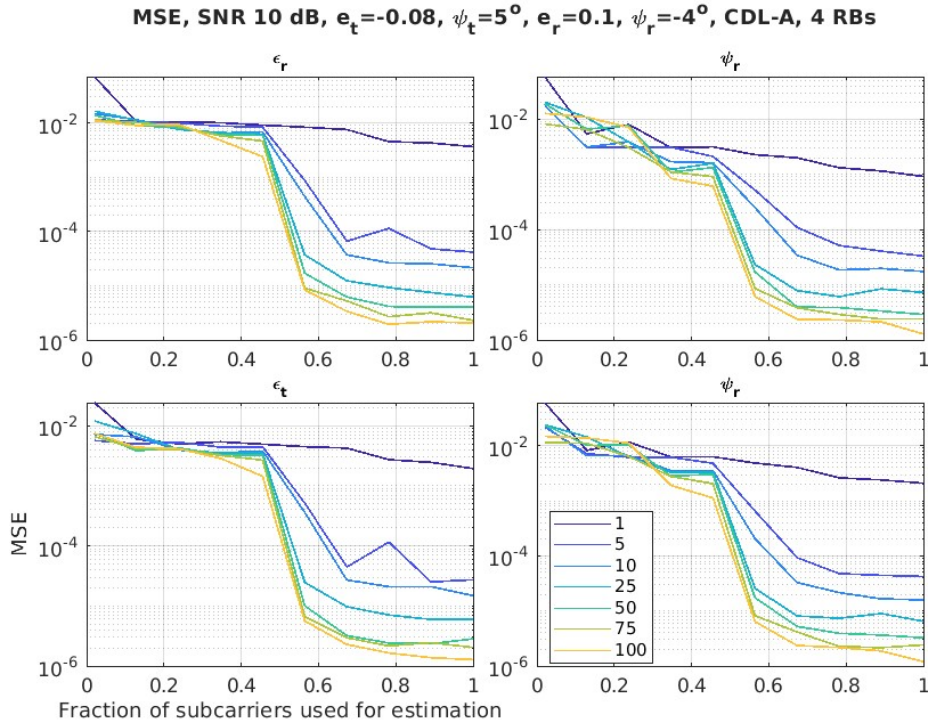


Figure 6.1. MSE of the Tx and Rx IQI coefficients as a function of the fraction of subcarriers used for estimation, CDL-A channel at 10 dB SNR. The legend indicates the number of slots used.

subcarriers randomly or in frequency ascending order, as we will see in another set of figures. One possible justification for this is that, for the CDL-A channel in the current configuration, sorting the channels according to the estimated channel power reduces subchannel diversity, compromising the estimation. Anyway, it can be verified that we can achieve MSEs at the order of  $10^{-4}$  by using only 5 slots with all subcarriers. Increasing the number of training slots yields clearly diminishing returns after roughly 75 slots. By checking Fig. 6.2, we can see that, with the estimated channel power sorting criterion and using less than half of subcarriers, the MSE is roughly at about the same order of magnitude as the IQI parameters themselves, i.e. the NMSE is approximately 1.

In Figs. 6.3 and 6.4 we present the MSE and NMSE, respectively, for 50 training slots IQI coefficient estimation at different SNR values. The same interaction between the subcarrier sorting criterion and the objective function happens here, with less than 50 subcarriers yielding roughly the same results for all SNR values. As expected, higher SNR leads to better estimates generally, and estimates get almost perfect if the SNR and number of slots are high enough. We can see that the proposed method is effective in estimating both the Tx and Rx IQI parameters. However, we have also observed that sorting the subcarriers in the described fashion leads to bad results, basically making any results with less than half of the subcarriers useless. We now present basically the same four figures so far but sorting the subcarriers by increasing frequency. Figures 6.5 and 6.6 show the MSE and NMSE, respectively, for 10 dB SNR and varying number of training slots. The MSE and NMSE curves as a function of the fraction of subcarriers look much smoother than the previous figures. This indicates that, if one wants to use only a fraction of the subcarriers for estimation, it is better to not sort them according to the estimated channel power criterion. It can also be seen that, at 10 dB SNR, using only 1 training slot is not nearly enough for reliable IQI parameter estimation, leading to MSEs of the same order of

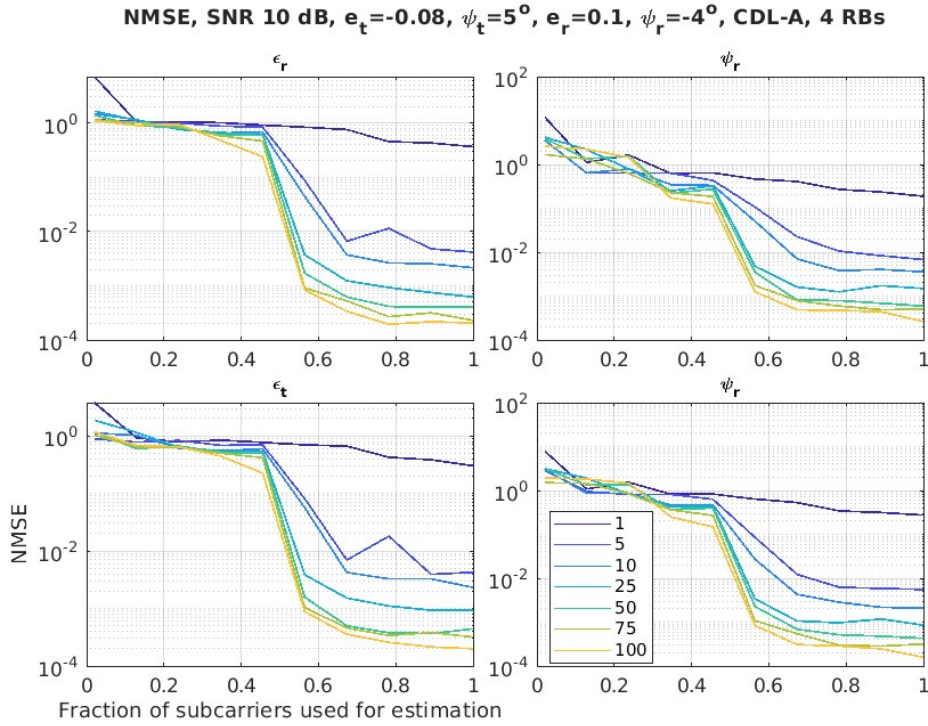


Figure 6.2. NMSE of the Tx and Rx IQI coefficients as a function of the fraction of subcarriers used for estimation, CDL-A channel at 10 dB SNR. The legend indicates the number of slots used.

magnitude as the parameters themselves. Using 200 slots and all the available subcarriers allows us to achieve MSEs with magnitudes of  $10^{-6}$  at 10 dB SNR. As before, Figures 6.7 and 6.8 respectively show the MSE and NMSE for 50 training slots and varying SNR. It can be seen that the  $\log(MSE)$  decreases roughly linearly with the SNR in dB. Also, the MSE can be reduced almost indefinitely by increasing the SNR and tightening the optimizer's stopping tolerance. For example, at 100 dB SNR and 50 slots, MSEs of around  $10^{-15}$  can be reached in the simulations, which is basically perfect IQI estimation. By observing the results herein presented, we can conclude that we have successfully developed a joint Tx and Rx IQI estimation procedure that produces high quality estimates under usual transmission conditions.

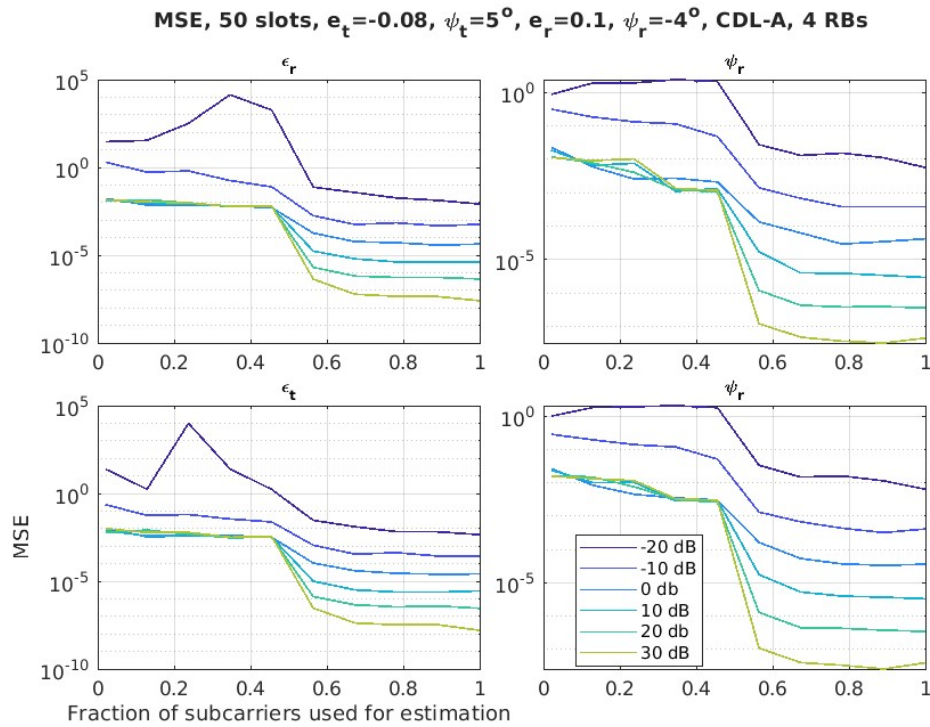


Figure 6.3. MSE of the Tx and Rx IQI coefficients as a function of the fraction of subcarriers used for estimation, CDL-A channel with 50 pilot slots. The legend indicates the SNR of the transmission.

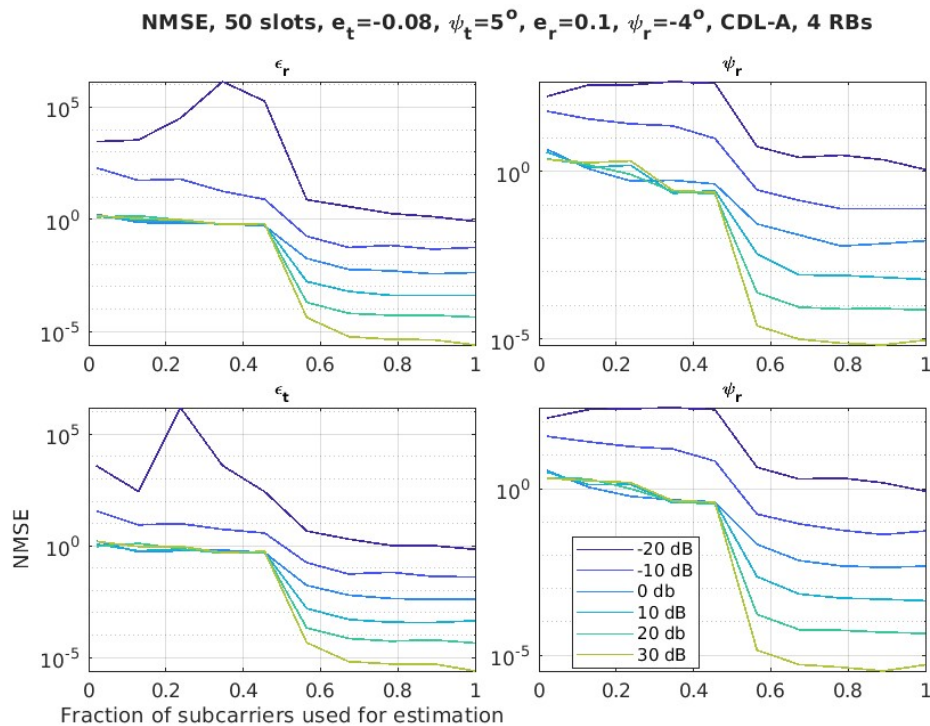


Figure 6.4. NMSE of the Tx and Rx IQI coefficients as a function of the fraction of subcarriers used for estimation, CDL-A channel with 50 pilot slots. The legend indicates the SNR of the transmission.

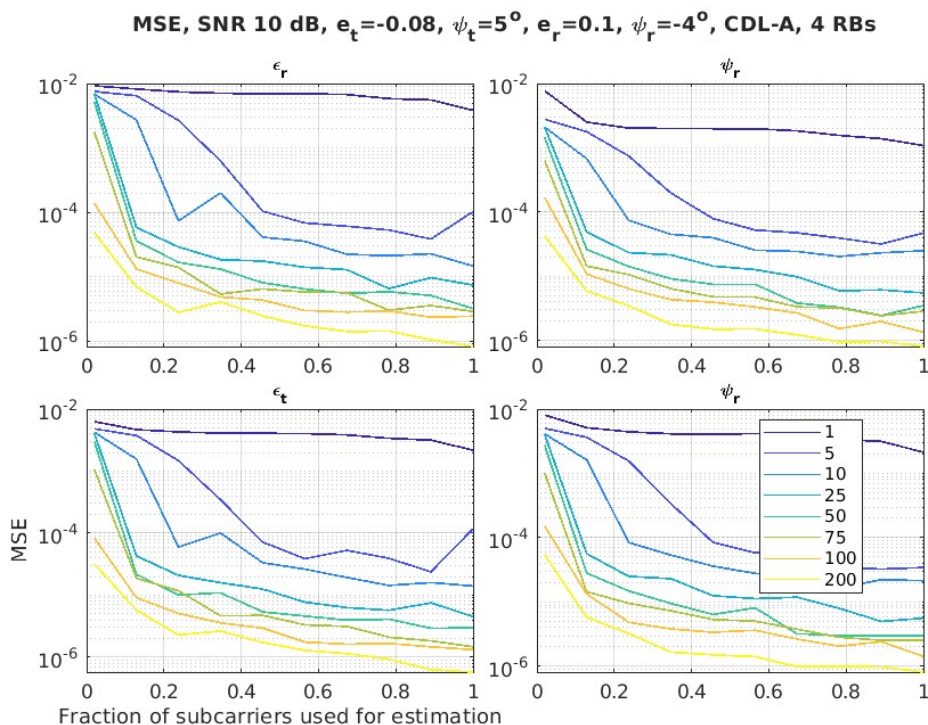


Figure 6.5. MSE of the Tx and Rx IQI coefficients as a function of the fraction of subcarriers used for estimation, CDL-A channel at 10 dB SNR. The legend indicates the number of slots used. Subcarriers sorted in ascending frequency order.

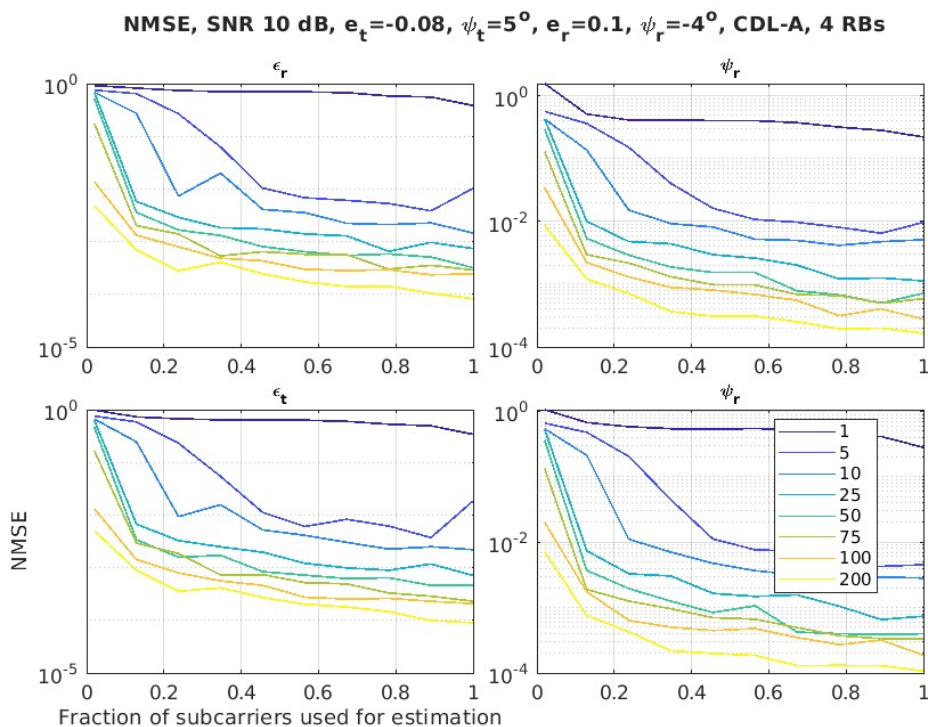


Figure 6.6. NMSE of the Tx and Rx IQI coefficients as a function of the fraction of subcarriers used for estimation, CDL-A channel at 10 dB SNR. The legend indicates the number of slots used. Subcarriers sorted in ascending frequency order.

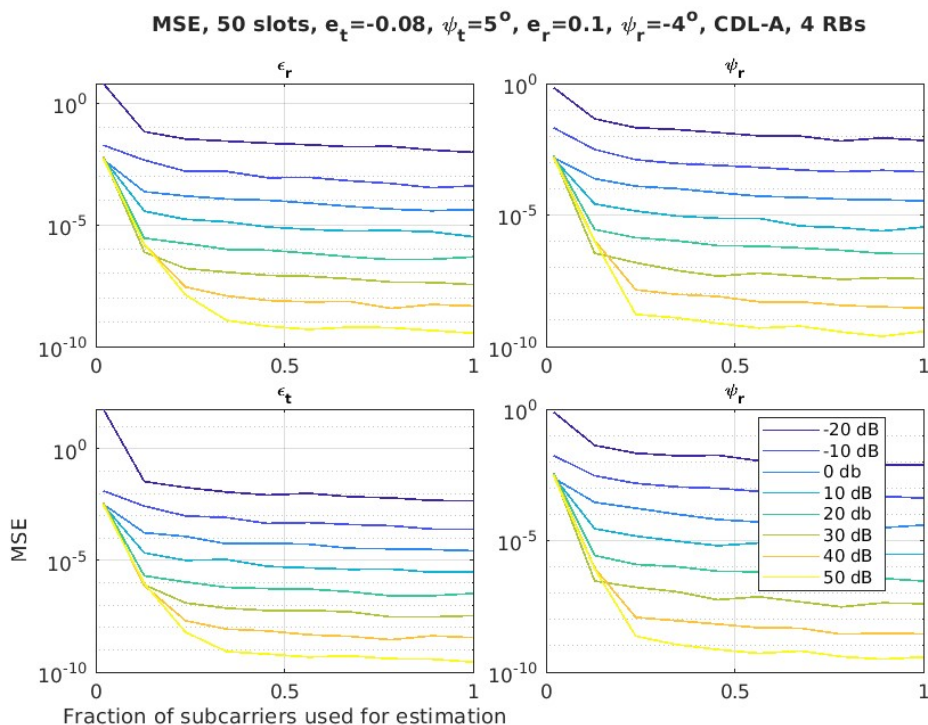


Figure 6.7. MSE of the Tx and Rx IQI coefficients as a function of the fraction of subcarriers used for estimation, CDL-A channel with 50 pilot slots. The legend indicates the SNR of the transmission. Subcarriers sorted in ascending frequency order.

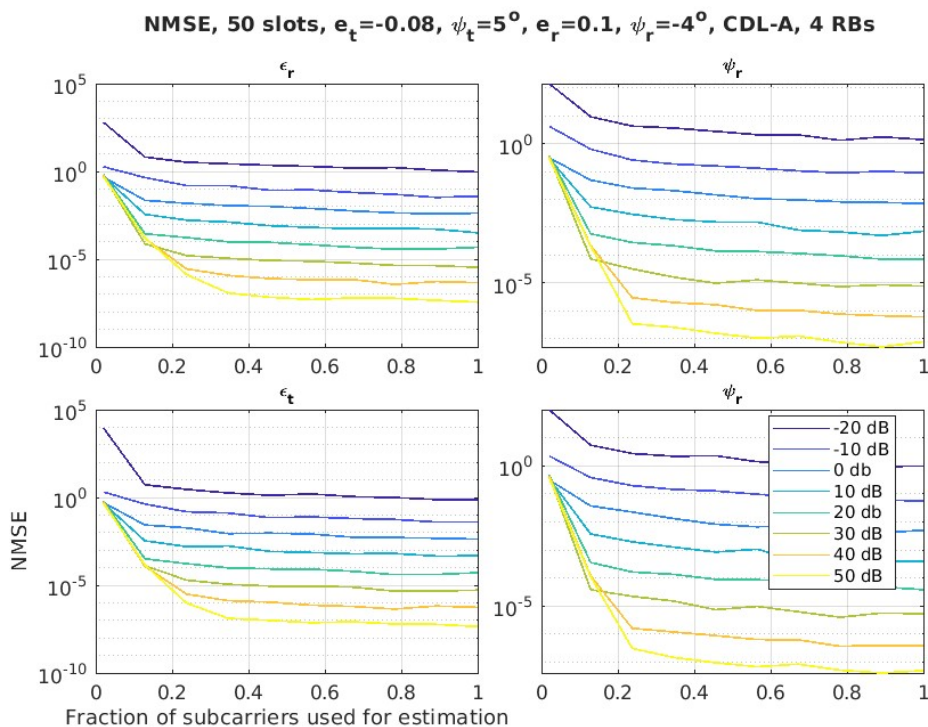


Figure 6.8. NMSE of the Tx and Rx IQI coefficients as a function of the fraction of subcarriers used for estimation, CDL-A channel with 50 pilot slots. The legend indicates the SNR of the transmission. Subcarriers sorted in ascending frequency order.

## 7 COMPARING COMPENSATION METHODS

While the results present up to this point are more than sufficient to draw conclusions regarding the effectiveness and quality of the proposed IQI estimation method, it still should be compared to other existing IQI compensation procedures. In this chapter, we will present numerical results for different IQI compensation methods, commenting on the more interesting characteristics of each method and comparing their advantages and disadvantages relative to each other.

The first important question regarding the comparison between different IQI compensation methods should be the metric used to compare them. The IQI parameter MSE, for example, would be the more direct quantity, but not all IQI compensation methods require IQI parameter estimation as an intermediary step. Other kinds of throughput related quantities can be used, such as the BER or the SER. We have chosen to study the BER in a 5G PUSCH transmission scenario.

As to which methods will be included in the comparison, we have chosen the adapted Matera and Sterle blind estimator [15] (already used in Chapter 4 as a comparison for position estimator MSE), and an adaptive WL filter for each OFDM subcarrier. The adaptive WL filters are trained with the WL-LMS, a straightforward extension of the original LMS algorithm [7]. These methods have been chosen because each one represents a broader class of methods: blind estimators and adaptive WL (or WL-equivalent) filters. Some methods have not been included for one of the three reasons:

- The method requires knowledge of some parameter or quantity that is usually unavailable in a practical scenario, such as the channel covariance matrices or the ratio between  $\alpha_r$  and  $\beta_r$ .
- The method was developed specifically to some particular context that does not translate well to the 5G scenario, thus causing the method to severely underperform. This is the case of [13], for example, which uses the quite rudimentary channel estimation procedures of HiperLAN/2.
- The method is not particularly simple to implement, specifically due to some more complicated optimization methods such as the Rosenbrock search employed in [27]. This is more of a pragmatic consideration, given the scope of this work.

The third item is included strictly for practical reasons, and it should be one of the priorities in any future work in this topic to include these methods in the comparisons.

### 7.1 WL frequency domain equalization

Let us now describe the WL filters used in the simulations. In an FDE procedure, such as included in most practical OFDM and SC-OFDM implementations, each subcarrier is usually treated as experiencing a static subchannel orthogonal to other subcarriers (if no inter-carrier interference exists). Each subchannel can be equalized using the many available equalization methods, such as zero forcing (ZF) or MMSE equalizers, one of which is the WL equalizer which takes the form

$$\hat{x}_k(m) = \eta_{k,1}y_k(m) + \eta_{k,2}y_k^*(m), \quad (7.1)$$

where  $k$  indicates the subcarrier,  $m$  the OFDM symbol,  $\eta_{k,1}$  and  $\eta_{k,2}$  are the WL filter coefficients at subcarrier  $k$ ,  $y_k(m)$  is the received resource grid element, and  $\hat{x}_k(m)$  is the estimated

transmitted resource grid element. The WL filter in each subcarrier is trained independently from the others using the WL-LMS algorithm

$$\hat{x}_k(m) = \eta_{k,1}(m)y_k(m) + \eta_{k,2}(m)y_k^*(m) \quad (7.2)$$

$$e_k(m) = x_k(m) - \hat{x}_k(m) \quad (7.3)$$

$$\begin{bmatrix} \eta_{k,1}(m+1) \\ \eta_{k,2}(m+1) \end{bmatrix} = \begin{bmatrix} \eta_{k,1}(m) \\ \eta_{k,2}(m) \end{bmatrix} + \mu \begin{bmatrix} y_k(m) \\ y_k^*(m) \end{bmatrix} e_k^*(m) \quad (7.4)$$

for  $m = 0, 1, \dots, N_s$ , where  $\mu$  is the step size of the algorithm. The errors  $e_k(m)$  are computed using the known pilot sequence elements  $x_k(m)$ . In a practical scenario, usually only the first elements of the training are from an actual pilot sequence, once the filter is already providing sufficient compensation the system starts to use decision directed training by taking hard decisions on the estimated symbols. In the simulations, for the WL filters, we consider that all transmitted symbols are known, and we compute the BER by checking whether using the estimated transmitted symbols  $\hat{x}_k(m)$  would produce the correct bits. This is done to allow the filter to continuously train throughout the whole transmission. To further improve the WL filter's performance, we reduce the step size  $\mu$  at each frame by applying the update rule  $\mu \leftarrow \kappa\mu$  with  $0 < \kappa < 1$  (usually  $\kappa \approx 1$ ), this allows the filter to output better estimates. In the simulations, we initialize  $\mu = 0.05$  and set  $\kappa = 0.98$ .

## 7.2 Simulation setup

Let us now describe simulation parameters that were used and the reasons behind them. One of the most important transmission parameters in relation to assessing the effectiveness of an IQI compensation procedure is the modulation order. Lower order modulations such as QPSK and BPSK are clearly less susceptible to the effects of IQI, because their decision regions occupy a proportionally larger portion of the symbol space. In these cases, relatively smaller deviations caused by IQI are usually not capable of causing a symbol error unless noise is significant. While compensating the IQI improves the BER performance, these modulations do not distinguish much between how well the IQI is compensated in the first place, this causes all methods, even those that only roughly compensate IQI, to perform similarly BER-wise. Thus, to better identify the differences between the studied IQI compensation procedures, we consider only higher order modulations, such as 256-quadrature amplitude modulation (QAM). As per the 5G standard, forward error correction coding is employed in all PUSCH and physical downlink shared channel (PDSCH) transmissions. The lower the code rate, the lower is the impact of IQI on the decoded bits, because the additional information from the code can be used to guide the decoding process and usually correct any symbol errors caused by IQI. Because we compute the BER after decoding error correcting code, to focus on the effect of IQI, we use the highest available code rate for 256-QAM modulation, which is 948/1024 and is specified in Table 5.1.3.1-2 of [44].

Both our method and the blind estimator can be "trained" separately from the conditions in which the BER is computed, because they estimate the IQI parameters and do not just attempt compensate the IQI effects. For these methods, we estimate the IQI coefficients under a particular SNR and with a predetermined quantity of training slots before computing the BER curves by varying the SNR. This means that we can also assess the impacts of training sequence length and training SNR on the BER curves. The training slots are transmitted at the same transmission parameters as the actual data (except SNR and number of slots obviously), with the entire slots being considered known and employed at the OFDM IQI estimation procedure described in

Chapter 5. The blind estimator does not need any decoding, using the actual received waveform instead. The WL filter, however, needs to be trained at each specific transmission SNR used at each datapoint of the BER curves, this is because it attempts to compute the WL-MMSE estimator of the received signal which depends on the noise power. This is another justification to why we let the WL filters be continuously trained throughout the whole transmission, as mentioned in the previous section.

Similar to the throughput simulation in Section 5.6, the results are not averaged over many realizations of a transmission, instead they are computed from a single transmission of many frames. We consider only severe receiver IQI, with the IQI parameters fixed at  $\epsilon_r = -0.25$  and  $\psi_r = 35^\circ$ . We consider the transmission of 300 frames (unless otherwise stated) over the 5G PUSCH, with 4 resource blocks, 2 transmit antennas and 4 receive antennas, PUSCH mapping type A, DM-RS configuration type 1, first DM-RS symbol at symbol 2, single symbol DM-RS with 3 additional symbols, no group hopping, static (i.e., 0 Hz maximum Doppler shift) TDL-A channel with 30 ns delay spread. HARQ is disabled, i.e., the blocks are only transmitted once at redundancy version (RV) 0, not allowing retransmissions. The signal is modulated with CP-OFDM with normal cyclic prefix. Only a single layer is active and no precoding is employed, thus effectively only 1 transmit antenna is transmitting. Regarding the decoding process, after IQI compensation, the receiver performs practical channel estimation using the DM-RS symbols and then performs MMSE equalization from the estimated noise variance and estimated channel. The soft bits and constellation symbols are computed according to Section 6.3.1 of [43], those are then subjected to the inverse of the encoding process as defined in [49]. This process includes rate recovery, LDPC decoding, desegmentation, and CRC decoding. The LDPC decoding is performed with belief propagation with a maximum of 12 iterations.

### 7.3 Results

We start by estimating the IQI parameters under favorable conditions, with 50 training slots and 20 dB SNR. The results from these estimates are presented in Fig. 7.1. As expected, we can see that the *IQI* curve is basically constant at 0.5, which is equivalent to guessing the bits at random. The *Our Comp.* curve, short for “our compensation method”, almost perfectly overlaps with the *Clean* curve, which is the curve without any IQI. The *Blind Comp.* curve, represents the IQI compensation using the blind estimator, overlaps with the *WL-LMS Comp.* curve, which is the curve related to the WL frequency domain equalization and IQI compensation as described in Section 7.1. In this case, our method clearly outperforms the other procedures and basically perfectly compensates any noticeable effects of IQI on the BER.

If we reduce the SNR under which the IQI parameter estimation is performed to -10 dB, we get the results in Fig. 7.2. The blind estimator now seems to overlap with the curve without IQI, and our compensation scheme gets worse, distancing itself from the *Clean* curve. There are two possible main reasons for this: the first is related to some particular behavior of the blind estimator under this particular received signal and SNR, as it seems that 20 dB SNR produces slightly better IQI parameter estimates; the second is related to the simulation itself not being an average of many estimation runs, but instead using a single IQI estimation trial and evaluating the BER from a long transmission using that estimate. It is intuitive that the true statistic average would probably lie somewhere in between the *WL-LMS* and the *Clean* curves, but computing this is very costly in terms of computational load and simulation time. The mentioned figure once again displays the reliance of our method on the SNR.

If we again consider 20 dB SNR, but now reduce the number of training slots, we get the results presented in Fig. 7.3. Clearly, 10 slots is not sufficient for the blind estimator to equal the

WL filter's performance, as the blind estimator now performs worse than the WL-LMS adaptive filter. The proposed method seems to be mostly unaffected by the sequence length reduction, mostly showing some performance degradation in comparison to the ideal case near the high SNR regime at BER values of approximately  $10^{-6}$ . Reducing the SNR to 0 dB and keeping the training sequence at 10 slots we get the curves in Fig. 7.4. The blind estimator seems to experience some slight improvement due to SNR reduction that happened between Fig. 7.1 and Fig. 7.2, overlapping again with the WL filter curve. The proposed method produces slightly worse estimates in comparison to the 20 dB case, as evidenced by the slight separation between the *Our Comp.* and *Clean* curves in the figure. Still, our method vastly outperforms the others in this scenario.

The figures from this section highlight the already explored characteristics of the method proposed herein, namely the dependence on SNR and pilot sequence length. The dependence on the number of pilot subcarriers was not explored in this section, but it can be approximated by comparing the MSE values presented in Section 5.6. It can be stated with confidence that the IQI compensation procedure developed in this thesis is not only competitive performance-wise in relation to the other explored methods, but it also is superior in many cases, specially if many pilot frames can be allocated and the SNR is favorable.

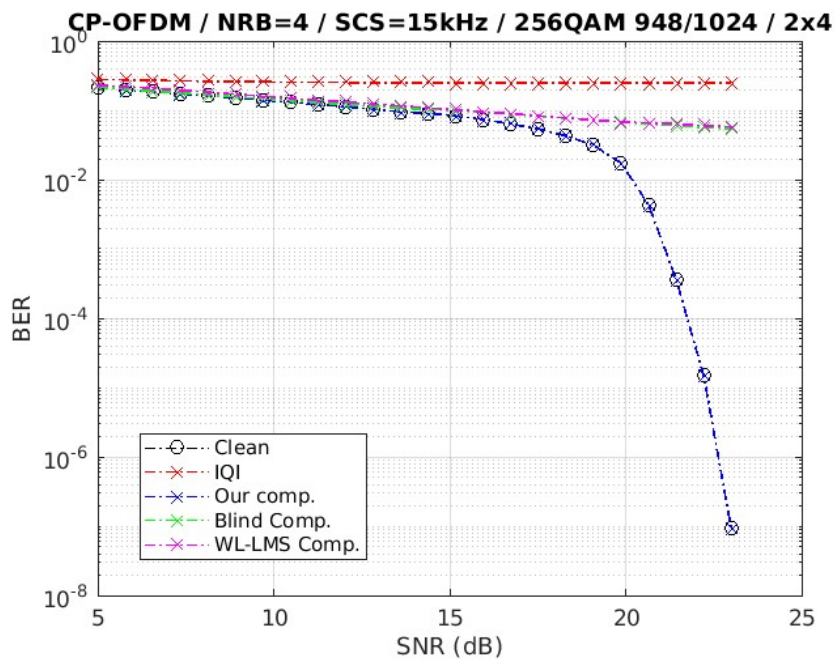


Figure 7.1. BER curves for IQI estimated at 50 training slots at 20 dB SNR.

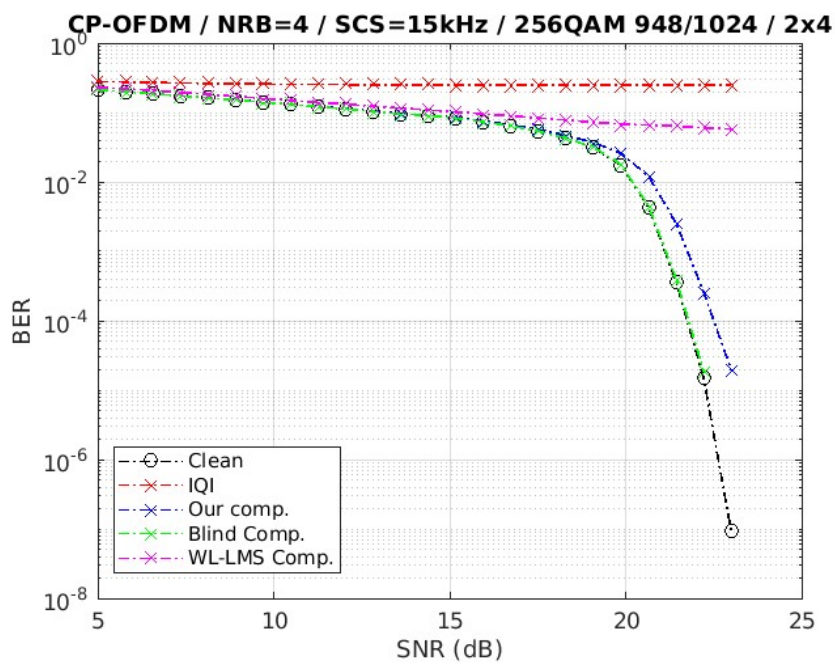


Figure 7.2. BER curves for IQI estimated at 50 training slots at -10 dB SNR.

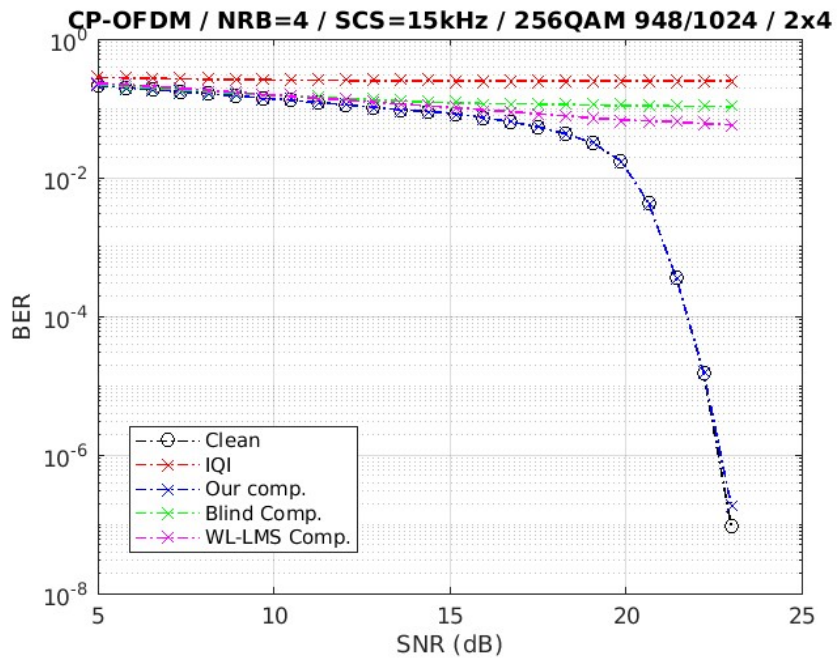


Figure 7.3. BER curves for IQI estimated at 10 training slots at 20 dB SNR.

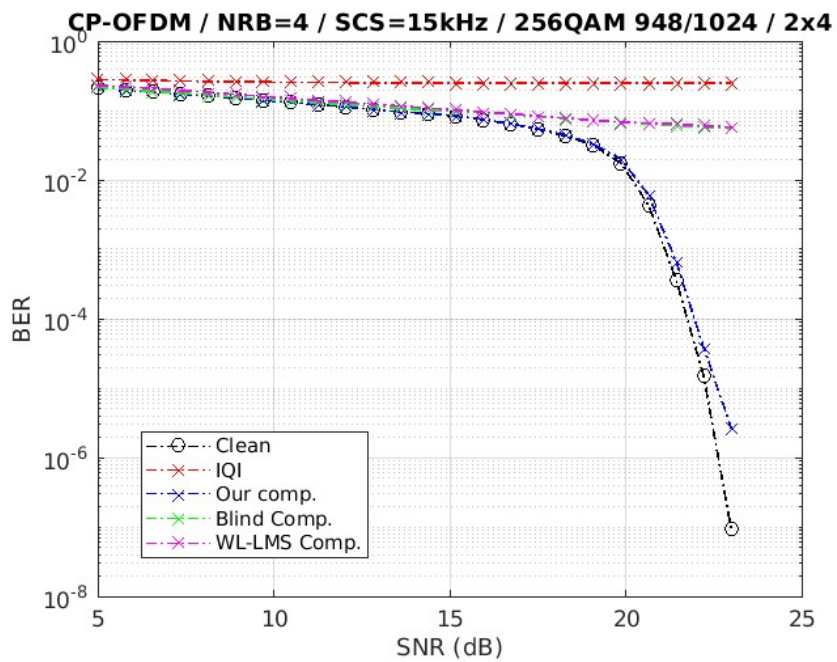


Figure 7.4. BER curves for IQI estimated at 10 training slots at 0 dB SNR.

## 8 CONCLUSION

We have presented a general procedure for IQI modeling, both in the wireless transmitter and receiver. Not only did the derivation lead to two of the most common IQI models, but it also led to a general frequency independent IQI model allowing for arbitrary amplitude and phase imbalances in both the I and Q branches. We have then presented a survey containing some of the more common methods for IQI compensation and estimation. In this survey, we laid out the original expressions for each method and described their assumptions, advantages, and disadvantages.

As a first original contribution of this thesis, an IQI compensation procedure tailored for positioning applications in a flat fading channel conditions was introduced. The effectiveness of the proposed procedure was compared to a blind estimator in a set of numerical results. It was shown that our method produced consistent improvement in relation to the blind estimator, at the expense of increased computational effort. It was shown that the proposed method can noticeably improve positioning estimation performance, basically equaling the case without any IQI.

The proposed method was then adapted and extended to an OFDM context, performing IQI estimation over pilot subcarriers. This led us to use the 5G reference signals to establish a 5G NR compliant IQI estimation technique. The performance of these methods was laid out in a numerical results section, where it was verified that the OFDM and the 5G compliant IQI estimation procedures have the potential to produce accurate IQI estimates under typical conditions. If the scenario is particularly favorable in terms of SNR and pilot sequence length, these methods can vastly outperform the considered blind estimator.

Perhaps the most relevant presented result in this thesis is the derivation of a baseband processing based joint Tx and Rx IQI estimation and compensation method for OFDM systems that does not rely on knowing the signal at adjacent subcarriers. This is a considerably harder problem than estimating or compensating only receiver IQI, as a consequence of this, few satisfactory solutions exist in the bibliography. The resulting optimization problem is non-convex with many local minima, which makes the optimization of the objective function a much bigger issue than in the receiver-only IQI estimation. A combination of Nelder-Mead simplex search and constrained particle swarm optimization was used to very reliably reach the neighborhood of the local optimum. To finish the chapter, the efficacy of our method was verified numerically. It was noticeable that sorting the subcarriers by descending approximate channel magnitude did not provide any improvement in minimizing the needed amount of subcarriers for estimation, instead it deteriorated the estimation performance for when using less than half of the subcarriers. Nonetheless, it was shown that the proposed method can reliably estimate both transmitter and receiver IQI coefficients without relying on small IQI assumptions or needing the knowledge of difficult to estimate values, such as the channel covariance matrices or the ratio between IQI coefficients.

To conclude the thesis, we presented a comparison between our proposed OFDM IQI compensation scheme, the blind estimator, and an adaptive WL equalizer. It was observed that IQI makes the use of higher order constellations impossible, and that IQI compensation is extremely important for those cases. We show that, if the number of pilot slots and the SNR are sufficiently high, our method outperforms both the blind estimator and the adaptive equalizer, demonstrating no perceptible BER performance floor and frequently presenting a BER curve very close to the scenario without IQI.

A general characteristic of the proposed IQI estimation and compensation methods that was repeatedly verified in the numerical results is its reliance on the SNR and pilot sequence length. If the SNR is too low, the method needs very long pilot sequences to equal the performance of a simple blind estimator. Some discussion regarding low SNR IQI estimation was conducted

in Section 5.3, including a possible method for IQI estimation in those scenarios. However, these procedures have not been further developed, neither were they verified numerically in this thesis. Using the ideas from that section to improve the performance of the new method in low SNR conditions may lead to interesting results and is a topic for future work.

Another interesting research direction that should be further explored concerns dealing with time-varying channels. In this thesis, the channels have been treated as static throughout the whole transmission, however this is frequently not the case, specially for mobile links. The static channel assumption is likely to deteriorate the performance of the current version of the proposed IQI estimation method in practical scenarios. Thus, it is relevant to study possible forms of enhancing the method to make it more robust to channel time variation. Moreover, because the estimator relies on the constant channel assumption, we have seen that the coherence time of the channel restricts the maximum length of the pilot sequence. Therefore, extending the algorithm to deal with time varying channels makes it so that the channel coherence time is no longer a limiting factor in the maximum pilot sequence length.

## 9 BIBLIOGRAPHY

- [1] Naskas N., Alexiou N., Gkardiakos S., Agathokleous A., Tsoutsos N., Kontaxis K., Ntounas G. & Kousparis I. (2022) Wideband mmWave Transceiver IC for 5G Radios. In: *2022 17th European Microwave Integrated Circuits Conference (EuMIC)*, pp. 196–199.
- [2] Yang X., Matthaïou M., Yang J., Wen C.K., Gao F. & Jin S. (2019) Hardware-Constrained Millimeter-Wave Systems for 5G: Challenges, Opportunities, and Solutions. *IEEE Communications Magazine* Vol. 57, pp. 44–50.
- [3] Ghaseminajm F., Abu-Shaban Z., Ikki S.S., Wymeersch H. & Benson C.R. (2020) Localization Error Bounds for 5G mmWave Systems Under I/Q Imbalance. *IEEE Transactions on Vehicular Technology* 69, pp. 7971–7975.
- [4] Schenk T.C.W. & Fledderus E.R. (2008) RF Impairments in High-Rate Wireless Systems - Understanding the Impact of TX/RX-asymmetry. In: *2008 3rd Int. Symp. on Commun., Control and Signal Process.*, pp. 117–122.
- [5] Valkama M., Renfors M. & Koivunen V. (2001) Compensation of Frequency-Selective I/Q Imbalances in Wideband Receivers: Models and Algorithms. In: *2001 IEEE Third Workshop on Signal Processing Advances in Wireless Communications (SPAWC'01). Workshop Proceedings (Cat. No.01EX471)*, pp. 42–45.
- [6] Mailand M., Richter R. & Jentschel H.J. (09 2006) IQ-imbalance and Its Compensation for Non-Ideal Analog Receivers Comprising Frequency-Selective Components. *Advances in Radio Science - Kleinheubacher Berichte* 4.
- [7] Widrow B. & Hoff M.E. (1960) Adaptive Switching Circuits. Technical report, Stanford Univ Ca Stanford Electronics Labs.
- [8] Razavi S.M., Gunnarsson F., Rydén H., Busin A., Lin X., Zhang X., Dwivedi S., Siomina I. & Shreevastav R. (2018) Positioning in Cellular Networks: Past, Present, Future. In: *2018 IEEE Wireless Communications and Networking Conference (WCNC)*, pp. 1–6.
- [9] Dwivedi S., Shreevastav R., Munier F., Nygren J., Siomina I., Lyazidi Y., Shrestha D., Lindmark G., Ernström P., Stare E., Razavi S.M., Muruganathan S., Masini G., Busin A. & Gunnarsson F. (2021) Positioning in 5G Networks. *IEEE Communications Magazine* 59, pp. 38–44.
- [10] Koivisto M., Hakkarainen A., Costa M., Kela P., Leppanen K. & Valkama M. (2017) High-Efficiency Device Positioning and Location-Aware Communications in Dense 5G Networks. *IEEE Communications Magazine* 55, pp. 188–195.
- [11] Proakis J.G. (2007) *Digital Communications* 5th Edition. McGraw Hill.
- [12] Schenk T., Fledderus E. & Smulders P. (12 2007) Performance Analysis of Zero-IF MIMO OFDM Transceivers with IQ imbalance. *Journal of Communications* 2.
- [13] Tubbax J., Come B., Van der Perre L., Deneire L., Donnay S. & Engels M. (2003) Compensation of IQ imbalance in OFDM Systems. In: *IEEE International Conference on Communications, 2003. ICC '03*, volume 5, pp. 3403–3407 vol.5.
- [14] Tarighat A. & Sayed A.H. (2007) Joint Compensation of Transmitter and Receiver Impairments in OFDM Systems. *IEEE Transactions on Wireless Communications* 6, pp. 240–247.

- [15] Maltera D. & Sterle F. (2007) ML Estimation of Receiver IQ Imbalance Parameters. In: *2007 Int. Waveform Diversity and Des. Conf.*, pp. 160–164.
- [16] Aoki Y., Dao M.T., Min K., Hwang Y., Kim Y. & Yang S.G. (2019) 1.4-GHz Bandwidth Frequency-Dependent I/Q Imbalance Calibration for 5G mmWave Communications. In: *2019 IEEE MTT-S International Microwave Symposium (IMS)*, pp. 626–629.
- [17] Aziz M., Ghannouchi F.M. & Helaoui M. (2017) Blind Compensation of I/Q Impairments in Wireless Transceivers. *Sensors* 17.
- [18] Hafez M., Khattab T. & Shalaby H.M.H. (2015) Blind SNR Estimation of Gaussian-Distributed Signals in Nakagami Fading Channels. *IEEE Transactions on Wireless Communications* 14, pp. 3509–3518.
- [19] Schuchert A., Hasholzner R. & Antoine P. (2001) A Novel IQ Imbalance Compensation Scheme for the Reception of OFDM Signals. *IEEE Transactions on Consumer Electronics* 47, pp. 313–318.
- [20] Tsui E. & Lin J. (2004) Adaptive IQ Imbalance Correction for OFDM Systems with Frequency and Timing Offsets. In: *IEEE Global Telecommun. Conf., 2004. GLOBECOM '04.*, volume 6, pp. 4004–4010 Vol.6.
- [21] Chen Y., You L., Lu A.A. & Gao X. (2021) Widely-Linear Processing for the Uplink of the Massive MIMO with IQ Imbalance: Channel Estimation and Data Detection. *IEEE Transactions on Signal Processing* 69, pp. 4685–4698.
- [22] Picinbono B. & Chevalier P. (1995) Widely linear estimation with complex data. *IEEE Transactions on Signal Processing* 43, pp. 2030–2033.
- [23] Schreier P.J. & Scharf L.L. (2010) *Statistical Signal Processing of Complex-Valued Data: The Theory of Improper and Noncircular Signals*. Cambridge Univ. Press.
- [24] Zhang X., Li H., Liu W. & Qiao J. (2017) Iterative IQ Imbalance Compensation Receiver for Single Carrier Transmission. *IEEE Transactions on Vehicular Technology* 66, pp. 8238–8248.
- [25] Benvenuto N. & Tomasin S. (2005) Iterative Design and Detection of a DFE in the Frequency Domain. *IEEE Transactions on Communications* 53, pp. 1867–1875.
- [26] Zhang W., de Lamare R.C., Pan C. & Chen M. (2015) Joint TX/RX IQ Imbalance Parameter Estimation Using a Generalized System Model. In: *2015 IEEE International Conference on Communications (ICC)*, pp. 4704–4709.
- [27] Cheng X., Luo Z. & Liu J. (2015) Joint Estimation and Compensation of Transmitter and Receiver IQ Imbalances in Millimeter-Wave SC-FDE Systems. In: *2015 IEEE International Conference on Communications (ICC)*, pp. 1274–1279.
- [28] Rosenbrock H.H. (01 1960) An Automatic Method for Finding the Greatest or Least Value of a Function. *The Computer Journal* 3, pp. 175–184.
- [29] Mensing C. & Plass S. (2006) Positioning Algorithms for Cellular Networks Using TDOA. In: *2006 IEEE International Conference on Acoustics Speech and Signal Processing Proceedings*, volume 4, pp. IV–IV.

- [30] Fokin G. (2018) TDOA Measurement Processing for Positioning in Non-Line-of-Sight Conditions. In: *2018 IEEE International Black Sea Conference on Communications and Networking (BlackSeaCom)*, pp. 1–5.
- [31] Oumar O.A., Siyau M.F. & Sattar T.P. (2012) Comparison Between MUSIC and ESPRIT Direction of Arrival Estimation Algorithms for Wireless Communication Systems. In: *The First International Conference on Future Generation Communication Technologies*, pp. 99–103.
- [32] Win M.Z., Conti A., Mazuelas S., Shen Y., Gifford W.M., Dardari D. & Chiani M. (2011) Network Localization and Navigation Via Cooperation. *IEEE Communications Magazine* 49, pp. 56–62.
- [33] Shen Y., Mazuelas S. & Win M.Z. (2011) A Theoretical Foundation of Network Navigation. In: *2011 IEEE Global Telecommunications Conference - GLOBECOM 2011*, pp. 1–6.
- [34] Çelik G., Çelebi H. & Tuna G. (2017) A Novel RSRP-Based E-CID Positioning for LTE Networks. In: *2017 13th International Wireless Communications and Mobile Computing Conference (IWCMC)*, pp. 1689–1692.
- [35] Nowak T., Hartmann M., Thielecke J., Hadaschik N. & Mutschler C. (2018) Super-Resolution in RSS-Based Direction-of-Arrival Estimation. In: *2018 International Conference on Indoor Positioning and Indoor Navigation (IPIN)*, pp. 1–8.
- [36] 3GPP (September 2022), 5G; Service Requirements for the 5G System. TS 22.261 version 17.11.0 Release 17.
- [37] Chaloupka Z. (2017) Technology and Standardization Gaps for High Accuracy Positioning in 5g. *IEEE Communications Standards Magazine* 1, pp. 59–65.
- [38] 3GPP (March 2019), Study on NR Positioning Support. TS 38.855 version 16.0.0 Release 16.
- [39] Schmidt R. (1986) Multiple Emitter Location and Signal Parameter Estimation. *IEEE Transactions on Antennas and Propagation* 34, pp. 276–280.
- [40] Roy R. & Kailath T. (1989) ESPRIT- Estimation of Signal Parameters via Rotational Invariance Techniques. *IEEE Transactions on Acoustics, Speech, and Signal Processing* 37, pp. 984–995.
- [41] 3GPP (April 2022), 5G; Study on Channel Model for Frequencies from 0.5 to 100 GHz. TR 38.901 version 17.4.0 Release 17.
- [42] Lagarias J.C., Reeds J.A., Wright M.H. & Wright P.E. (1998) Convergence properties of the nelder–mead simplex method in low dimensions. *SIAM Journal on Optimization* 9, pp. 112–147.
- [43] 3GPP (January 2023), 5G;NR;Physical Channels and Modulation. TS 38.211 version 17.4.0 Release 17.
- [44] 3GPP (January 2023), 5G; NR; Physical Layer Procedures for Data. TS 38.214 version 17.4.0 Release 17.

- [45] Wang S., Guan K., He D., Li G., Lin X., Ai B. & Zhong Z. (2018) Doppler Shift and Coherence Time of 5G Vehicular Channels at 3.5 GHz. In: *2018 IEEE International Symposium on Antennas and Propagation & USNC/URSI National Radio Science Meeting*, pp. 2005–2006.
- [46] He D., Ai B., Guan K., Zhong Z., Tian L. & Dou J. (2017) Channel Analysis for Millimeter-Wave Railway Communications in Urban Environment. In: *2017 XXXII Ind General Assembly and Scientific Symposium of the International Union of Radio Science (URSI GASS)*, pp. 1–4.
- [47] Goldsmith A. (2005) *Wireless Communications*. Cambridge University Press.
- [48] Rangan S., Rappaport T.S. & Erkip E. (2014) Millimeter-Wave Cellular Wireless Networks: Potentials and Challenges. *Proceedings of the IEEE* 102, pp. 366–385.
- [49] 3GPP (January 2022), 5G; NR; Multiplexing and Channel Coding. TS 38.212 version 17.4.0 Release 17.
- [50] McKinnon K.I.M. (1998) Convergence of the Nelder–Mead Simplex Method to a Nonstationary Point. *SIAM Journal on Optimization* 9, pp. 148–158.
- [51] Kennedy J. & Eberhart R. (1995) Particle Swarm Optimization. In: *Proceedings of ICNN'95 - International Conference on Neural Networks*, volume 4, pp. 1942–1948 vol.4.
- [52] Mezura-Montes E. & Coello Coello C.A. (2011) Constraint-handling in nature-inspired numerical optimization: Past, present and future. *Swarm and Evolutionary Computation* 1, pp. 173–194.
- [53] Pedersen M.E.H. (2010) *Good Parameters for Particle Swarm Optimization*. Luxembourg: Hvass Laboratories.
- [54] Brown W. & Crane R. (1969) Conjugate linear filtering. *IEEE Transactions on Information Theory* 15, pp. 462–465.

## 10 APPENDICES

- Appendix 1 Overview of widely linear operators
- Appendix 2 Quasiconvexity of the objective function
- Appendix 3 Adapting the blind IQI estimator
- Appendix 4 Derivation of the gradient of the objective function

## Appendix 1 Overview of Widely Linear operators

One of the first documented applications of the idea of Widely Linear (WL) filtering seems to be by Brown and Crane [54], while the terminology itself was introduced by Picinbono and Chevalier [22] in a context of mean square estimation as an extension of the commonplace linear filtering. WL filtering is relevant in the context of complex *improper* random processes, where improper means that a random process  $x(t)$  is correlated with its complex conjugate, i.e.  $\mathbb{E}\{x(t_0)x(t_1)\} \neq 0$  for some  $t_0$  and  $t_1$ . A detailed exploration of the concepts of proper and improper signal processing, including WL filtering, is presented in [23]. The explanation presented in this appendix is taken directly from this reference.

Let  $\Omega$  be the sample space of a random vector  $\mathbf{x} : \Omega \rightarrow \mathbb{C}^n$ , and let  $\mathbf{x}^*$  denote the complex conjugate of  $\mathbf{x}$ . Also let  $\mathbf{H}_1$  and  $\mathbf{H}_2 \in \mathbb{C}^{m \times n}$ , then we say  $\mathbf{H}(\mathbf{x}) = \mathbf{H}_1\mathbf{x} + \mathbf{H}_2\mathbf{x}^*$  is a WL operator, also called a *linear-conjugate-linear* operator. Clearly the set of (strictly) linear operators are a subset of the WL operators with  $\mathbf{H}_2 = \mathbf{0}$ . A typical representation of WL operators uses the so called *augmented matrix*  $\mathbf{H}_e$ , which satisfies

$$\begin{bmatrix} \mathbf{y} \\ \mathbf{y}^* \end{bmatrix} = \begin{bmatrix} \mathbf{H}_1 & \mathbf{H}_2 \\ \mathbf{H}_2^* & \mathbf{H}_1^* \end{bmatrix} \begin{bmatrix} \mathbf{x} \\ \mathbf{x}^* \end{bmatrix} \rightarrow \mathbf{y}_e = \mathbf{H}_e \mathbf{x}_e \quad (10.1)$$

This is a convenient representation of WL operators. Denote the set of all matrices with the above *augmented matrix* structure as  $\mathbb{W}^{m \times n}$ , then, for  $m = n$ ,  $\mathbb{W}^{n \times n}$  is a matrix algebra over the real numbers, closed under addition, multiplication, inversion, and multiplication by a real scalar.

Regarding estimation, the WL-MMSE estimator is a WL operator that minimizes the mean square error between the estimated zero-mean signal  $\hat{\mathbf{x}}_{WL} = \mathbf{W}_1\mathbf{y} + \mathbf{W}_2\mathbf{y}^*$ , computed from the zero-mean measurements  $\mathbf{y}$ , and the ground truth value of  $\mathbf{x}$ , i.e. the WL-MMSE estimator minimizes  $\varepsilon_{WL} = \mathbb{E}\{\|\hat{\mathbf{x}}_{WL}^{opt} - \mathbf{x}\|^2\}$ . The WL-MMSE estimator can be derived in similar fashion to the linear MMSE estimator, leading to the *augmented* Wiener-Hopf equations

$$\mathbf{W}_e^{opt} = \mathbf{R}_{\mathbf{xy},e} \mathbf{R}_{\mathbf{yy},e}^{-1} \quad (10.2)$$

where

$$\mathbf{R}_{\mathbf{xy},e} = \mathbb{E}\{\mathbf{x}_e \mathbf{y}_e^H\} = \mathbb{E}\left\{ \begin{bmatrix} \mathbf{x} \\ \mathbf{x}^* \end{bmatrix} \begin{bmatrix} \mathbf{y}^H & \mathbf{y}^T \end{bmatrix} \right\} = \begin{bmatrix} \mathbf{R}_{\mathbf{xy}} & \mathbf{Q}_{\mathbf{xy}} \\ \mathbf{Q}_{\mathbf{xy}}^* & \mathbf{R}_{\mathbf{xy}}^* \end{bmatrix} \quad (10.3)$$

$$\mathbf{R}_{\mathbf{yy},e} = \mathbb{E}\{\mathbf{y}_e \mathbf{y}_e^H\} = \mathbb{E}\left\{ \begin{bmatrix} \mathbf{y} \\ \mathbf{y}^* \end{bmatrix} \begin{bmatrix} \mathbf{y}^H & \mathbf{y}^T \end{bmatrix} \right\} = \begin{bmatrix} \mathbf{R}_{\mathbf{yy}} & \mathbf{Q}_{\mathbf{yy}} \\ \mathbf{Q}_{\mathbf{yy}}^* & \mathbf{R}_{\mathbf{yy}}^* \end{bmatrix} \quad (10.4)$$

The WL-MMSE estimate is given by

$$\begin{bmatrix} \hat{\mathbf{x}} \\ \hat{\mathbf{x}}^* \end{bmatrix} = \mathbf{W}_e^{opt} \begin{bmatrix} \mathbf{y} \\ \mathbf{y}^* \end{bmatrix}. \quad (10.5)$$

Clearly the linear MMSE estimator is a suboptimal estimator in a WL context, which satisfies

$$\mathbf{W}_e^L = \begin{bmatrix} \mathbf{R}_{\mathbf{xy}} \mathbf{R}_{\mathbf{yy}}^{-1} & \mathbf{0} \\ \mathbf{0} & \mathbf{R}_{\mathbf{xy}}^* \mathbf{R}_{\mathbf{yy}}^{-*} \end{bmatrix}, \quad (10.6)$$

completely ignoring any information associated with the complementary covariance matrices  $\mathbf{Q}_{\mathbf{yy}}$  and  $\mathbf{Q}_{\mathbf{xy}}$ , which are assumed to be zero in the linear MMSE estimator. It is possible to show that the WL-MMSE estimator is always at least as good as the linear MMSE estimator.

## Appendix 2 Quasiconvexity of the objective function

Showing that  $\gamma$  is convex on some regions, and determining the specific conditions for finding these regions is a very complicated task. We will instead try showing that  $\gamma$  is quasiconvex, i.e., that its sublevel sets are convex, within some domain. First we write the sublevel sets

$$\mathcal{S}_\eta = \left\{ (\hat{\epsilon}_r, \hat{\psi}_r) : \gamma(\hat{\epsilon}_r, \hat{\psi}_r) \leq \eta, \text{ and } -1 < \hat{\epsilon}_r < 1, -\frac{\pi}{2} < \hat{\psi}_r < \frac{\pi}{2} \right\}. \quad (10.7)$$

We restrict the variables to the domains  $-1 < \hat{\epsilon}_r < 1$  and  $-\frac{\pi}{2} < \hat{\psi}_r < \frac{\pi}{2}$  for practical reasons, since IQI is a phase and amplitude imbalance in the IQ demodulator LO signals,  $\epsilon$  and  $\psi_r$  are typically near 0. In that perspective, the chosen domain may even be said to be too large, the parameters should in no real situation be even close to border of the intervals. Similarly, the true values  $\epsilon_r$  and  $\psi_r$  are also restricted to these intervals.

We proceed with expanding the expression

$$\frac{1}{2} + \frac{\epsilon_r^2 + 2\epsilon_r - 2(\epsilon_r + 1)(\hat{\epsilon}_r + 1)}{2(\hat{\epsilon}_r^2 + 2\hat{\epsilon}_r + 2)} \cos(\hat{\psi}_r - \psi_r) \leq \eta, \quad (10.8)$$

which becomes a second degree polynomial in  $\hat{\epsilon}_r$ :

$$a\hat{\epsilon}_r^2 + b\hat{\epsilon}_r + c \geq 0 \quad (10.9)$$

$$a(\eta) = (2\eta - 1) \quad (10.10)$$

$$b(\Delta\psi_r, \eta) = (2(2\eta - 1) + 2(\epsilon_r + 1) \cos(\Delta\psi_r)) \quad (10.11)$$

$$c(\Delta\psi_r, \eta) = 2(2\eta - 1) + 2(\eta + 1) \cos(\Delta\psi_r) - \epsilon_r^2 - 2\epsilon_r, \quad (10.12)$$

where  $\Delta\psi_r = \hat{\psi}_r - \psi_r$ . For  $0 \leq \eta < \frac{1}{2}$  this polynomial is concave on  $\hat{\epsilon}_r$ , and under these conditions, we have a set in  $\hat{\epsilon}_r$  that satisfies the inequality in (10.9) equal to  $[r_1(\Delta\psi_r, \eta), r_2(\Delta\psi_r, \eta)]$  where

$$r_{1,2}(\Delta\psi_r, \eta) = \frac{-b(\Delta\psi_r, \eta) \pm \sqrt{b(\Delta\psi_r, \eta)^2 - 4a(\eta)c(\Delta\psi_r, \eta)}}{2a(\eta)}, \quad (10.13)$$

when the roots exist. For  $\eta > \frac{1}{2}$ , then the solution set becomes disjoint:  $\hat{\epsilon}_r \in (-\infty, r_2(\Delta\psi_r, \eta)] \cup [r_1(\Delta\psi_r, \eta), \infty)$ , but in that case, only one of the sets  $(-\infty, r_2(\Delta\psi_r, \eta)]$  or  $[r_1(\Delta\psi_r, \eta), \infty)$  will have a non-empty intersection with  $(-1, 1) \times (-\frac{\pi}{2}, \frac{\pi}{2})$ , thus it suffices to analyse the convexity of this set. We will only focus on showing conditions for quasiconvexity on the  $0 \leq \eta < \frac{1}{2}$  interval. The reasoning for  $\eta \geq \frac{1}{2}$  is similar and can be done in a straightforward way with the same methods that will be presented.

Similarly, a set in  $\Delta\psi_r$  is defined such that

$$b(\Delta\psi_r, \eta)^2 - 4a(\eta)c(\Delta\psi_r, \eta) \geq 0 \quad (10.14)$$

because  $\hat{\epsilon}_r$  must be real-valued. This set in  $\Delta\psi_r$  is given by

$$\Delta\psi_r \in [\Delta\psi_{r,min}(\eta), \Delta\psi_{r,max}(\eta)] \quad (10.15)$$

$$\Delta\psi_{r,min}(\eta) = -\arccos(p_1(\eta)), \quad \Delta\psi_{r,max}(\eta) = \arccos(p_1(\eta)) \quad (10.16)$$

$$p(\eta)_{1,2} = \cos(\Delta\psi_{r,max/min}(\eta)) = \pm \sqrt{\frac{(\epsilon_r + 1)^2 - 2\eta(\epsilon_r^2 + 2(\epsilon_r - \eta) + 2)}{(\epsilon_r + 1)^2}} \quad (10.17)$$

The  $p(\eta)_2$  branch (negative sign for the square root) is outside the range of interest, but it meets with the  $p_1(\eta)$  branch when  $\cos(\Delta\psi_{r,max/min}(\eta)) = 0$ , which is satisfied for

$$\eta = \frac{(\epsilon_r + 1)^2}{2} \quad (10.18)$$

This means that the two regions are disjoint in  $\Delta\psi_r$  for some  $\hat{\epsilon}_r$  up until the level is  $\eta = \frac{(\epsilon_r+1)^2}{2}$ . Naturally, these disjoint regions are a mere product of the periodicity in  $\Delta\psi_r$ , however, we only care about the principal branch centered around  $\Delta\psi_r = 0$ . It can also be shown that the condition  $0 \leq \eta \leq \frac{(\epsilon_r+1)^2}{2}$  guarantees that  $b(\Delta\psi_r, \eta)^2 - 4a(\eta)c(\Delta\psi_r, \eta) \geq 0$ , when  $0 \leq \eta \leq 1/2$ . For  $\eta > 1/2$ ,  $b(\Delta\psi_r, \eta)^2 - 4a(\eta)c(\Delta\psi_r, \eta) \geq 0$  when  $\eta \geq \frac{(\epsilon_r+1)^2}{2}$ . By substituting  $\eta = 0$  in (10.17) and in (10.13), we get a sublevel set equal to the single point  $(\epsilon_r, \psi_r)$ , confirming that  $\gamma$  has an unique minimum at the true value of the IQI parameters.

For  $0 \leq \eta < \frac{1}{2}$ , the sublevel sets are then given by

$$\mathcal{S}_\eta = \left\{ (\hat{\epsilon}_r, \hat{\psi}_r) : \hat{\epsilon}_r \in [r_1(\Delta\psi_r, \eta), r_2(\Delta\psi_r, \eta)] \text{ for} \right. \\ \left. \Delta\psi_r \in [\Delta\psi_{r,min}, \Delta\psi_{r,max}], \text{ and } -1 < \hat{\epsilon}_r < 1, -\frac{\pi}{2} < \hat{\psi}_r < \frac{\pi}{2} \right\}. \quad (10.19)$$

From this formulation of the sublevel sets we can see that they are in fact the intersection of the epigraph of  $r_1(\Delta\psi_r, \eta)$  with the hypograph of  $r_2(\Delta\psi_r, \eta)$ , for  $\Delta\psi_r \in [\Delta\psi_{r,min}(\eta), \Delta\psi_{r,max}(\eta)]$ . We want to find out whether these sublevel sets are convex and under which conditions on  $\eta$  this happens. If the epigraph of  $r_1(\Delta\psi_r, \eta)$  and the hypograph of  $r_2(\Delta\psi_r, \eta)$  are convex, then the sublevel set is convex, because it is an intersection of convex sets.

Writing down the expression for  $r_1(\Delta\psi_r, \eta)$  with the dependence on  $\Delta\psi_r$  and  $\eta$  being suppressed for cleanliness of notation, and manipulating it

$$r_1 = \frac{-b + \sqrt{b^2 - 4ac}}{2a} \quad (10.20)$$

$$\frac{-b}{2a} = - \left( 2 + \frac{\epsilon_r + 1}{2\eta - 1} \cos(\Delta\psi_r) \right) \quad (10.21)$$

$$\sqrt{b^2 - 4ac} = \sqrt{4(\epsilon_r + 1)^2 \cos^2(\Delta\psi_r) - 4(2\eta - 1)(2\eta - (\epsilon_r + 1)^2)} \quad (10.22)$$

$$= 2(\epsilon_r + 1) \sqrt{\cos^2(\Delta\psi_r) + (2\eta - 1) \left( 1 - \frac{2\eta}{(\epsilon_r + 1)^2} \right)} \quad (10.23)$$

$$\frac{\sqrt{b^2 - 4ac}}{2a} = \frac{\epsilon_r + 1}{2\eta - 1} \sqrt{\cos^2(\Delta\psi_r) + (2\eta - 1) \left( 1 - \frac{2\eta}{(\epsilon_r + 1)^2} \right)} \quad (10.24)$$

And finally

$$r_1 = -2 - \frac{\epsilon_r + 1}{2\eta - 1} \left( \cos(\Delta\psi_r) - \sqrt{\cos^2(\Delta\psi_r) + K} \right) \quad (10.25)$$

$$K = (2\eta - 1) \left( 1 - \frac{2\eta}{(\epsilon_r + 1)^2} \right) \quad (10.26)$$

Because, for  $0 \leq \eta < \frac{1}{2}$ ,  $(2\eta - 1)$  is a negative constant, to show convexity of  $r_1$  is equivalent to show convexity of the term inside the parenthesis, which we'll call  $\zeta(\Delta\psi_r)$ . The second derivative of  $\zeta$  with respect to  $\Delta\psi_r$  is

$$\frac{\partial^2 \zeta}{\partial \Delta\psi_r^2}(\Delta\psi_r) = -\cos(\Delta\psi_r) + \frac{\cos^2(\Delta\psi_r)}{\sqrt{\cos^2(\Delta\psi_r) + K}} + \frac{\sin^2(2\Delta\psi_r)}{(\sqrt{\cos^2(\Delta\psi_r) + K})^3} - \frac{\sin^2(\Delta\psi_r)}{\sqrt{\cos^2(\Delta\psi_r) + K}} \quad (10.27)$$

It can be shown that, for  $K \leq 0$ ,  $\frac{\partial^2 \zeta}{\partial \Delta\psi_r^2} \geq 0 \forall \Delta\psi_r$  such that  $\sqrt{\cos^2(\Delta\psi_r) + K} \in \mathbb{R}$  which is equivalent to say that  $r_1$  is convex in  $\Delta\psi_r \in [\Delta\psi_{r,min}, \Delta\psi_{r,max}]$  when  $K \leq 0$ . This is done by noticing that, under these conditions, the following inequalities hold

$$\frac{\cos^2(\Delta\psi_r)}{\sqrt{\cos^2(\Delta\psi_r) + K}} \geq \cos(\Delta\psi_r) \quad (10.28)$$

$$\frac{\sin^2(2\Delta\psi_r)}{(\sqrt{\cos^2(\Delta\psi_r) + K})^3} \geq \frac{\sin^2(\Delta\psi_r)}{\sqrt{\cos^2(\Delta\psi_r) + K}} \quad (10.29)$$

Thus, the second derivative is always non-negative under the stated conditions. Let us now understand the implications of  $K \leq 0$ . Because  $(2\eta - 1)$  is negative, we can rewrite it as the condition  $\left(1 - \frac{2\eta}{(\epsilon_r+1)^2}\right) \geq 0$ , which is equivalent to  $\eta \leq \frac{(\epsilon_r+1)^2}{2}$ . This is the same condition for  $b^2 - 4ac \geq 0$ , we then conclude once again that  $\frac{\partial^2 \zeta}{\partial \Delta\psi_r^2} \geq 0 \forall \Delta\psi_r \in [\Delta\psi_{r,min}, \Delta\psi_{r,max}]$ , by the very definition of the  $[\Delta\psi_{r,min}, \Delta\psi_{r,max}]$  set.

The same can be done to show the concavity of  $r_2$ , which ends up reducing to showing that

$$\frac{\partial^2 \xi}{\partial \Delta\psi_r^2}(\Delta\psi_r) \leq 0 \quad (10.30)$$

$$\xi(\Delta\psi_r) = \left( \cos(\Delta\psi_r) + \sqrt{\cos^2(\Delta\psi_r) + K} \right) \quad (10.31)$$

Computing the second derivative, we get

$$\frac{\partial^2 \xi}{\partial \Delta\psi_r^2}(\Delta\psi_r) = -\cos(\Delta\psi_r) - \frac{\cos^2(\Delta\psi_r)}{\sqrt{\cos^2(\Delta\psi_r) + K}} - \frac{\sin^2(2\Delta\psi_r)}{(\sqrt{\cos^2(\Delta\psi_r) + K})^3} + \frac{\sin^2(\Delta\psi_r)}{\sqrt{\cos^2(\Delta\psi_r) + K}} \quad (10.32)$$

The first two terms are already non-positive for  $\Delta\psi_r \in \left[-\frac{\pi}{2}, \frac{\pi}{2}\right]$ , which is a superset of  $[\Delta\psi_{r,min}, \Delta\psi_{r,max}]$ . The sum of the third and fourth terms is non-positive as a consequence of the (10.29), which holds for  $K \leq 0$ . We then conclude that  $r_1$  and  $r_2$  are convex and concave, respectively, in  $\Delta\psi_r$ . Thus, the epigraph of  $r_1$  and the hypograph of  $r_2$  are convex, and so is their intersection. This intersection is the sublevel set for a particular value of  $\eta$ , which is convex as long as  $0 \leq \eta \leq \frac{(\epsilon_r+1)^2}{2}$  (we only showed this for  $0 \leq \eta < \frac{1}{2}$ , but convexity of the sublevel sets holds whenever the former inequality is satisfied). Violating this condition leads to sublevel sets which are not necessarily convex over the whole practical domain of  $\Delta\psi_r$ . Then we can safely state that  $\gamma$  is quasiconvex on the  $\Omega = \left\{(\hat{\epsilon}_r, \hat{\psi}_r) : \gamma(\hat{\epsilon}_r, \hat{\psi}_r) \leq \frac{(\epsilon_r+1)^2}{2}, -1 < \hat{\epsilon}_r < 1, -\frac{\pi}{2} < \hat{\psi}_r < \frac{\pi}{2}\right\}$  domain.

### Appendix 3 Adapting the blind IQI estimator

Here we detail the steps taken to adapt the estimator in [15] to the IQI model used in this thesis. The procedure relies on performing the same original derivation but assuming our model. We will now present this short derivation. Assume the transmitted signal  $\mathbf{x}(n) \sim \mathcal{CN}(\mathbf{0}, \sigma_x^2 \mathbf{I}, \mathbf{0})$ , i.e.,  $\mathbf{x}(n)$  is a complex white circularly symmetric Gaussian random variable. Further assume that  $\mathbf{x}(n)$ , for  $n = 1, 2, \dots, N$  is a WSS random process, then from (4.2) we can state that  $\mathbf{y}(n) \sim \mathcal{CN}(\mathbf{0}, \sigma_x^2 (\mathbf{\Theta}_A \mathbf{\Theta}_A^H + \mathbf{\Theta}_B \mathbf{\Theta}_B^H), 2\sigma_x^2 \mathbf{\Theta}_A \mathbf{\Theta}_B)$ . Because  $\mathbf{y}$  has diagonal covariance and complementary covariance matrices, we can match the diagonal elements of the sample covariance and complementary covariance matrices to the theoretical expressions, yielding

$$\sum_{n=0}^{N-1} y_k(n) y_k^*(n) = \sigma_x^2 (|\alpha_k|^2 + |\beta_k|^2) = \frac{1 + m_k^2}{2} \sigma_x^2 \quad (10.33)$$

$$\Re \left\{ \sum_{n=0}^{N-1} y_k(n) y_k(n) \right\} = \frac{1 - m_k^2}{2} \sigma_x^2 \quad (10.34)$$

$$\Im \left\{ \sum_{n=0}^{N-1} y_k(n) y_k(n) \right\} = -\sigma_x^2 m_k \sin(\psi_k), \quad (10.35)$$

where  $m_k = 1 + \epsilon_k$  and  $\psi_k$  are the IQI coefficients for the  $k$ th antenna. Solving for  $m_k$  in (10.33) and (10.34) we get

$$m_k = \sqrt{\frac{\sum_{n=0}^{N-1} y_k(n) y_k^*(n) - \Re \left\{ \sum_{n=0}^{N-1} y_k(n) y_k(n) \right\}}{\sum_{n=0}^{N-1} y_k(n) y_k^*(n) + \Re \left\{ \sum_{n=0}^{N-1} y_k(n) y_k(n) \right\}}}. \quad (10.36)$$

Using (10.33), (10.34), (10.35), and (10.36) we can solve for  $\psi_k$  in similar fashion to get

$$\psi_k = \sin^{-1} \left( \frac{\Im \left\{ \sum_{n=0}^{N-1} y_k(n) y_k(n) \right\} (1 + m_k^2)}{2m_k \sum_{n=0}^{N-1} y_k(n) y_k^*(n)} \right). \quad (10.37)$$

The expressions (10.36) and (10.37) are the resulting blind estimates.

#### Appendix 4 Derivation of the gradient of the objective function

From (5.16), we compute the derivatives

$$\frac{\partial f}{\partial \hat{\epsilon}_r} = \sum_{k=-K}^K \sum_{m=0}^{N_s-1} \frac{\partial}{\partial \hat{\epsilon}_r} \left( \|\mathbf{e}_{k,m}(\hat{\epsilon}_r, \hat{\psi}_r)\|^2 \right) = \sum_{k=-K}^K \sum_{m=0}^{N_s-1} 2\Re \left\{ \mathbf{e}_{k,m}^*(\hat{\epsilon}_r, \hat{\psi}_r) \frac{\partial}{\partial \hat{\epsilon}_r} \left( \mathbf{e}_{k,m}(\hat{\epsilon}_r, \hat{\psi}_r) \right) \right\} \quad (10.38)$$

$$\frac{\partial f}{\partial \hat{\psi}_r} = \sum_{k=-K}^K \sum_{m=0}^{N_s-1} \frac{\partial}{\partial \hat{\psi}_r} \left( \|\mathbf{e}_{k,m}(\hat{\epsilon}_r, \hat{\psi}_r)\|^2 \right) = \sum_{k=-K}^K \sum_{m=0}^{N_s-1} 2\Re \left\{ \mathbf{e}_{k,m}^*(\hat{\epsilon}_r, \hat{\psi}_r) \frac{\partial}{\partial \hat{\psi}_r} \left( \mathbf{e}_{k,m}(\hat{\epsilon}_r, \hat{\psi}_r) \right) \right\}. \quad (10.39)$$

From (5.17), we expand the matrix products and get

$$\begin{aligned} \frac{\partial}{\partial \hat{\epsilon}_r} \left( \mathbf{e}_{k,m}(\hat{\epsilon}_r, \hat{\psi}_r) \right) &= -\frac{\partial}{\partial \hat{\epsilon}_r} \left( \frac{|\hat{\alpha}_r|^2 \tilde{\mathbf{g}}_{1,k} + \hat{\alpha}_r \hat{\beta}_r \tilde{\mathbf{g}}_{2,-k}^*}{|\hat{\alpha}_r|^2 + |\hat{\beta}_r|^2} \right) s_k(m) \\ &\quad - \frac{\partial}{\partial \hat{\epsilon}_r} \left( \frac{\hat{\alpha}_r \hat{\beta}_r \tilde{\mathbf{g}}_{1,-k}^* + |\hat{\beta}_r|^2 \tilde{\mathbf{g}}_{2,k}}{|\hat{\alpha}_r|^2 + |\hat{\beta}_r|^2} \right) s_{-k}^*(m) \end{aligned} \quad (10.40)$$

$$\begin{aligned} \frac{\partial}{\partial \hat{\psi}_r} \left( \mathbf{e}_{k,m}(\hat{\epsilon}_r, \hat{\psi}_r) \right) &= -\frac{\partial}{\partial \hat{\psi}_r} \left( \frac{|\hat{\alpha}_r|^2 \tilde{\mathbf{g}}_{1,k} + \hat{\alpha}_r \hat{\beta}_r \tilde{\mathbf{g}}_{2,-k}^*}{|\hat{\alpha}_r|^2 + |\hat{\beta}_r|^2} \right) s_k(m) \\ &\quad - \frac{\partial}{\partial \hat{\psi}_r} \left( \frac{\hat{\alpha}_r \hat{\beta}_r \tilde{\mathbf{g}}_{1,-k}^* + |\hat{\beta}_r|^2 \tilde{\mathbf{g}}_{2,k}}{|\hat{\alpha}_r|^2 + |\hat{\beta}_r|^2} \right) s_{-k}^*(m), \end{aligned} \quad (10.41)$$

with each term's derivative in  $\hat{\epsilon}_r$  being

$$\frac{\partial}{\partial \hat{\epsilon}_r} \left( \frac{|\alpha_r|^2}{|\hat{\alpha}_r|^2 + |\hat{\beta}_r|^2} \right) = -\frac{\partial}{\partial \hat{\epsilon}_r} \left( \frac{|\beta_r|^2}{|\hat{\alpha}_r|^2 + |\hat{\beta}_r|^2} \right) = -\frac{\hat{\epsilon}_r(\hat{\epsilon}_r + 2)}{(\hat{\epsilon}_r^2 + 2\hat{\epsilon}_r + 2)^2} \cos(\hat{\psi}_r) \quad (10.42)$$

$$\frac{\partial}{\partial \hat{\epsilon}_r} \left( \frac{\alpha_r \beta_r}{|\hat{\alpha}_r|^2 + |\hat{\beta}_r|^2} \right) = \frac{-2(\hat{\epsilon}_r + 1) + j\hat{\epsilon}_r(\hat{\epsilon}_r + 2)}{(\hat{\epsilon}_r^2 + 2\hat{\epsilon}_r + 2)^2} \sin(\hat{\psi}_r), \quad (10.43)$$

and the derivatives in  $\hat{\psi}_r$  being

$$\frac{\partial}{\partial \hat{\psi}_r} \left( \frac{|\alpha_r|^2}{|\hat{\alpha}_r|^2 + |\hat{\beta}_r|^2} \right) = -\frac{\partial}{\partial \hat{\psi}_r} \left( \frac{|\beta_r|^2}{|\hat{\alpha}_r|^2 + |\hat{\beta}_r|^2} \right) = -\frac{\hat{\epsilon}_r + 1}{\hat{\epsilon}_r^2 + 2\hat{\epsilon}_r + 2} \sin(\hat{\psi}_r) \quad (10.44)$$

$$\frac{\partial}{\partial \hat{\psi}_r} \left( \frac{\alpha_r \beta_r}{|\hat{\alpha}_r|^2 + |\hat{\beta}_r|^2} \right) = -j \frac{\hat{\epsilon}_r + 1}{\hat{\epsilon}_r^2 + 2\hat{\epsilon}_r + 2} \cos(\hat{\psi}_r). \quad (10.45)$$

Substituting the derivatives back into (10.38) and (10.39) concludes our derivation of the gradient of  $f$ .